OUKA
The University of Osaka
Institutional Knowledge Archive

Title	Molecular and cellular function analysis of DNA polymerase X involved in DNA repair
Author(s)	Nakane, Shuhei
Citation	大阪大学, 2012, 博士論文
Version Type	VoR
URL	https://hdl.handle.net/11094/577
rights	
Note	

The University of Osaka Institutional Knowledge Archive : OUKA

https://ir.library.osaka-u.ac.jp/

The University of Osaka

Molecular and cellular function analysis of DNA polymerase X involved in DNA repair

（DNA 修復系で働く DNA ポリメラーゼ X の分子機能・細胞機能解析）

Doctoral Thesis

Shuhei Nakane

Department of Biological Sciences, Graduate School of Science

Osaka University

2012

CONTENTS

ABBREVIATIONS

AP	apurinic/apyrimidinic
AS	ammonium sulfate
BER	base excision repair
BRCT	BRCA1 (breast-cancer-susceptibility protein) C-terminus
CBB	Coomassie Brilliant Blue
CD	circular dichroism
ddGTP	dideoxyguanosine 5'-triphosphate
dNMP	deoxyribonucleotide monophosphate
dNTP	deoxyribonucleotide 5'-triphosphate
drPolX	PolX from *Deinococcus radiodurans*
DSBR	double strand break repair
dsDNA	double-stranded DNA
EMSA	electrophoretic mobility shift assay
EndoIV	endonuclease IV
HIS2	histidinol phosphatase domain-2
k_{cat}	catalytic rate constant
K_d	dissociation constant
K_m	Michaelis constant
KPi	potassium phosphate
LigA	DNA ligase A
LP	long-patch
MALDI-TOF-MS	matrix-assisted laser desorption/ionization time-of-flight mass spectrometry
MutM	formamidopyrimidine DNA glycosylase
NMP	ribonucleotide monophosphate
NTP	ribonucleotide 5'-triphosphate
PHP	polymerase and histidinol phosphatase
PMF	peptide mass fingerprinting
PolI	DNA polymerase I
PolIII	DNA polymerase III
PolX	DNA polymerase X
POLXc	PolX core

PPi	inorganic pyrophosphate
RT	reverse transcriptase
SN	single-nucleotide
ssDNA	single-stranded DNA
TdT	terminal deoxynucleotidyl transferase
TLS	translesion synthesis
Tm	melting temperature
ttPolX	PolX from *Thermus thermophilus*
1-nt	single-nucleotide
3'-PUA	3'-phospho-α,β-unsaturated aldehyde
5'-dRP	5'-deoxyribose phosphate
8-oxo-dGTP	8-oxo-deoxyguanosine triphosphate

ABSTRACT

Single-nucleotide (1-nt) gaps in DNA can arise during various DNA processing events, particularly during base excision repair (BER). These lesions are repaired by the X-family DNA polymerases (PolXs) with high gap-filling activity. Some PolXs can bind productively to deoxyribonucleotides (dNTPs) in the absence of DNA and fill these 1-nt gaps. Although PolXs play a crucial role in efficient gap filling, currently, little is known about the kinetic and structural details of their productive dNTP binding. Here, I show that *Thermus thermophilus* HB8 PolX (ttPolX) has a strong binding affinity for Mg^{2+}-dNTPs in the absence of DNA, and that it follows a Theorell-Chance (hit-and-run) mechanism, with nucleotide binding as the first step. Comparison of the crystal structures of ttPolX in a binary complex, with dGTP, and in a ternary complex, with 1-nt gapped DNA and dideoxyguanosine 5'-triphosphate (ddGTP), revealed that the conformation of the incoming nucleotide depended on whether or not DNA was present. Furthermore, the Lys-263 residue located between two guanosine conformations was essential for the strong binding affinity of the enzyme. The ability to bind to either *syn*-dNTP or *anti*-dNTP and the involvement of a Theorell-Chance mechanism are key aspects of the strong nucleotide-binding and efficient gap-filling activities of PolXs. Furthermore, many bacterial PolXs have a polymerase and a histidinol phosphatase (PHP) domain at their C-termini, in addition to a PolX core (POLXc) domain, and possess 3'-5' exonuclease activity. I found that the PHP domain of ttPolX functions as three types of phosphoesterases, including a 3'-5' exonuclease, an apurinic/apyrimidinic (AP) endonuclease, and a 3'-phosphatase. The phosphoesterase and gap-filling activities described above are required for BER. Partial reconstitution of BER using *T. thermophilus* HB8 cell lysates revealed that the majority of the AP endonuclease and 3'-phosphatase activities are attributable to the phosphoesterase, endonuclease IV (EndoIV). However, ttPolX had sufficient 3'-phosphatase activity in EndoIV-deficient cells, indicating complementation. Furthermore, ttPolX was found to be the only efficient gap-filling DNA polymerase in the cell. These results indicate that ttPolX is a multifunctional enzyme that is specialized in BER.

INTRODUCTION

DNA polymerases are generally classified into seven families, the A, B, C, D, X, Y and reverse transcriptase ones (Rothwell and Waksman, 2005) (Fig. 1A). In these seven families, the study of X-family DNA polymerases (PolXs) is advanced in eukaryotes, especially in mammals. Mammalian PolXs are further classified into six members: DNA polymerase β (Polβ), μ (Polμ), λ (Polλ), σ1 (Polσ1) and σ2 (Polσ2), and terminal deoxynucleotidyl transferase (TdT) (Ramadan *et al.*, 2004). Polβ exhibits Mg^{2+}-dependent DNA/RNA polymerase activity in a DNA-template-dependent manner (Bergoglio *et al.*, 2003) and is involved in base excision repair (BER) (Srivastava *et al.*, 1998). Polλ exhibits Mg^{2+}/Mn^{2+}-dependent DNA polymerase activity in a DNA-template-dependent/independent manner (Garcia *et al.*, 2002; Ramadan *et al.*, 2003) and is involved in DNA double-strand break repair (DSBR) (Capp *et al.*, 2006). Polμ exhibits Mg^{2+}/Mn^{2+}/Co^{2+}-dependent DNA/RNA polymerase activity in a DNA-template-dependent/independent manner (Nick *et al.*, 2003; Dominguez *et al.*, 2000) and is involved in DSBR (Capp *et al.*, 2007) and V(D)J recombination (Bertocci *et al.*, 2003). TdT can incorporate nucleotides at 3'-OH in a template-independent manner (Boule *et al.*, 2001) and is involved in V(D)J recombination. The Polσs are involved in sister-chromatid cohesion (Carson *et al.*, 2001). Thus, mammalian PolXs are involved in DNA repair and other DNA processing pathways.

DNA is altered and damaged by various endogenous and exogenous reactions (Morita *et al.*, 2010, Gates, 2009). With regard to endogenous reactions, DNA is damaged by deamination, depurination, depyrimidination, reactive oxygen species and DNA replication errors. With regard to exogenous reactions, DNA is susceptible to damage by agents such as UV radiation and alkylating compounds. The lesions caused by endogenous and exogenous reactive species can be repaired through the BER pathway, which is probably the most frequently used DNA repair pathway in the cell (Morita *et al.*, 2010). Damaged bases are specifically recognized by various DNA glycosylases to initiate BER. Monofunctional DNA glycosylases catalyze the hydrolysis of N-glycosyl bonds and generate an apurinic/apyrimidinic (AP) site. Bi- and trifunctional DNA glycosylases have AP lyase activity via a β- or β/δ-elimination mechanism using an ε amino group of a lysine residue or α-imino group in addition to DNA glycosylase activity. AP sites are targeted by both AP endonuclease and AP lyase. AP endonuclease nicks an AP site through a hydrolytic reaction to generate a 3'-OH and 5'-deoxyribosephosphate (dRP). This 5' block is removed by

deoxyribophosphodiesterase (dRPase) or dRP lyase using hydrolytic or lyase (β-elimination) mechanisms, respectively. When the AP lyase incises an AP site, it produces 3'-phospho-α,β-unsaturated aldehyde (by β-elimination) or 3'-phosphate (by β/δ-elimination) and 5'-phosphate. These 3'-blocking groups must be removed by 3'-phosphoesterase to allow DNA polymerase activity. Single-nucleotide (1-nt) gaps typically remain after AP-site processing. Failure to deal with these gaps can cause serious damage to the DNA, such as strand breaks. Rapid and efficient filling of these gaps is carried out by PolXs. After 1-nt gaps are filled by PolXs or other DNA polymerases, the resulting nick is sealed by DNA ligase.

The African swine fever virus (ASFV) PolX is a highly distributive DNA polymerase (Oliveros *et al.* 1997) and follows an ordered Bi Bi mechanism with a nucleotide as the first substrate (Kumar *et al.* 2008). This means that ASFV PolX can form a productive complex with a nucleotide in the absence of DNA and can, thereby, provide an effective means for filling 1-nt gaps. TdT, a mammalian PolX (Boule *et al.* 2001), follows a random Bi Bi mechanism (Deibel *et al.* 1980); thus, it can also form a productive binary complex with a nucleotide. To date, however, the mechanism and order of binding and release of substrates and products have not been fully elucidated for these PolXs. By contrast with these DNA polymerases, the ordered Bi Bi mechanism with DNA as the first substrate is a conserved reaction mechanism for other DNA polymerases, especially replicative polymerases with high processivity. For example, the A-family DNA polymerase I (PolI) of *Escherichia coli* binds to DNA prior to binding to Mg^{2+}-deoxyribonucleotides (dNTPs) (McClure *et al.* 1975); PolI has low affinity for Mg^{2+}-dNTPs in the absence of DNA (Muise *et al.* 1985). Although PolI can bind to a nucleotide in the absence of DNA, this binary complex is nonproductive and must be dissociated before binding to DNA (Bryant *et al.* 1983). Polβ, a mammalian PolXs involved in base excision repair, has also been shown to follow an ordered Bi Bi mechanism with DNA as the first substrate, although these studies used primer/template and ~14-nt gapped DNA, which may not be the most appropriate substrates for PolXs (Tanabe *et al.* 1979; Wang *et al.* 1982). These differences in reaction mechanism among polymerases suggest the possibility that productive dNTP binding in the absence of DNA is responsible for the high activity of some PolXs, such as ASFV PolX, for filling 1-nt gaps.

The crystal structures of a few DNA polymerases in binary complexes with a nucleotide have been reported, for example, the Klenow fragment of *E. coli* PolI with dCTP (Beese *et al.* 1993), *Thermus aquaticus* PolI with dCTP (Li *et al.* 1998), and Polβ with dATP

(Sawaya *et al.* 1994). These binary structures lacked metal ions and the nucleotides had different binding positions and conformations compared to ternary complexes, which suggest nonproductive binding. These observations on crystal structures are consistent with a polymerase mechanism of ordered Bi Bi with DNA as the first substrate. With respect to the crystal structure of TdT in binary complex with Co^{2+}-dideoxyadenosine 5'-triphosphate (ddATP), the conformation and location of ddATP are similar to nucleotides in the ternary complexes of other PolXs (Delarue *et al.* 2002). However, it is uncertain whether this binary complex structure is productive or not because the TdT reaction proceeds via a random Bi Bi mechanism (Deibel *et al.* 1980). To date, the structure of a productive binary complex of dNTP and DNA polymerase with an ordered Bi Bi mechanism has not been elucidated.

Eukaryotic PolXs are composed of mainly two domains, a PolX core (POLXc) domain at the C-terminus and a BRCA1 (breast-cancer-susceptibility protein) C-terminal (BRCT) domain at the N-terminus (Fig. 1B). However, Polβ consists of only a POLXc domain, and Polσs have no POLXc or BRCT domain (Aravind *et al.*, 1999). The POLXc domain possesses polymerase activity and contains two helix-hairpin-helix motifs, which are responsible for sequence-nonspecific DNA binding (Beard *et al.*, 2006a). On the other hand, the BRCT domain interacts with other proteins and/or DNA and joins the Ku-XRCC4-DNA ligase IV-DNA complex for DSBR (Bork *et al.*, 1997; Ma *et al.*, 2004). Therefore, although all PolXs are single-subunit enzymes, their domain architecture permits them to exhibit multiple biochemical activities.

The recent completion of many bacterial genome sequences revealed the presence of genes encoding PolXs. Sequence analysis of bacterial PolXs revealed that no bacterial PolXs have a BRCT domain, and that many of them have a polymerase and histidinol phosphatase (PHP) domain at their C-termini in addition to a POLXc domain (Ramadan *et al.*, 2004). The PHP domain (also called the histidinol phosphatase domain-2 (HIS2) domain) is conserved in three taxonomic domains, especially in almost all bacteria. The PHP domain is associated with several proteins such as DNA polymerases or exists as a stand-alone PHP domain protein (Aravind *et al.*, 1998). The crystal structures of several proteins containing a PHP domain were determined to have a distorted $(\beta\alpha)_7$ barrel fold (Teplyakov *et al.*, 2003; Lamers *et al.*, 2006; Bailey *et al.*, 2006; Omi *et al*., 2007). The PHP domain of the DNA polymerase III (PolIII) α subunit from *T. aquaticus* possesses a trinuclear metal site (Bailey *et al.*, 2006), which is composed of conserved residues including histidine and aspartate ones.

The PHP domain exhibits sequence and structural similarity to those of enzymes belonging to the metal-dependent amidohydrolase superfamily (Aravind *et al.*, 1998), but exhibits no similarity to the BRCT domain in mammalian PolXs. Thus, bacterial PolXs have a completely different domain structure from eukaryotic PolXs.

It has been reported that bacterial PolXs are similar to eukaryotic PolXs, except for additional activities derived from the PHP domain. The biochemical analysis of PolX from *Deinococcus radiodurans* (drPolX), a well-known extremophile exhibiting high resistance to desiccation and ionizing radiation, showed that drPolX has Mg^{2+}/Mn^{2+}-dependent DNA polymerase and Mn^{2+}-dependent 3'-5' exonuclease activities (Lecointe *et al.*, 2004; Blasius *et al.*, 2006). The finding of the 3'-5' exonuclease activity was unexpected because the other PolXs examined so far lack this activity. The fact that the PHP domain is missing in mammalian PolXs raises the possibility that the PHP domain is needed for 3'-5' exonuclease activity. The crystal structure analysis of drPolX showed the overall structure and active site of the POLXc domain was similar to eukaryotic PolXs, indicating similar activity. This observation is consistent with the reports that bsPolX has strong gap-filling activity and drPolX has dRP lyase activity (Banos *et al.*, 2008a; Khairnar *et al*., 2009); these activities are required for BER. Furthermore, bsPolX has AP endonuclease activity located in the PHP domain, which is also required for BER (Banos *et al.*, 2010). As expected from these activities, drPolX were indicated to be involved in BER *in vivo*; drPolX could complement of disruption of DNA glycosylases in *E. coli* (Khairnar *et al*., 2009). It was also reported that disruption of drPolX gene resulted in a significant delay in DSBR and in an increased sensitivity to γ-irradiation (Lecointe *et al.*, 2004; Bentchikou *et al*., 2007). However, it should be noted that compared to in other bacteria, the intracellular concentration of Mn^{2+} in *D. radiodurans* is very high, which is supposed to be important for the radioresistance inherent to this bacterium (Daly *et al.*, 2004), and this bacterium might use peculiar molecular mechanisms in response to DNA damage (Zahradka *et al.*, 2006). Therefore, bacterial PolXs are likely involved in BER similar to some eukaryotic PolXs. However, the molecular function of the PHP domain, especially in BER, has little known.

The extremely thermophilic eubacterium, *Thermus thermophilus* HB8 is a promising model organism for DNA repair, as evidenced by the ongoing Whole Cell Project on *T. thermophilus* HB8 (Yokoyama *et al*., 2000; Morita *et al*., 2010). *T. thermophilus* HB8 has a relatively small genome size (2.2 Mbp), and its intracellular biological systems are thought to consist of minimal essential components. Furthermore, proteins from *T. thermophilus* HB8

are extremely thermostable and suitable for physicochemical and crystallographic analyses (Iino *et al*., 2008). *T. thermophilus* HB8 has only three DNA polymerases annotated at present; PolIII α subunit (TTHA0180) involved in DNA replication, PolI (ttPolI, TTHA1054) involved in DNA replication and repair and PolX (ttPolX, TTHA1150) possibly involved in DNA repair (Fig. 1A). Although ttPolI has been thought to be major DNA repair DNA polymerase, ttPolX is also expected to have DNA repair function. Moreover, the existence of the PHP domain associated with ttPolX is expected to provide additional functions to ttPolX.

In this study, I performed structural and functional domain analysis of ttPolX. Steady-state kinetic experiments showed that ttPolX follows a Theorell-Chance mechanism, which is thought to be advantage for filling 1-nt gaps. I determined the crystal structures of the reaction intermediates during 1-nt gap filling. I found that ttPolX had several activities required for BER, including 3'-phosphatase activity which has not been reported in other PolXs. My observations on mechanism and structures suggest a model for how ttPolX achieves efficient filling of 1-nt gaps in BER pathway.

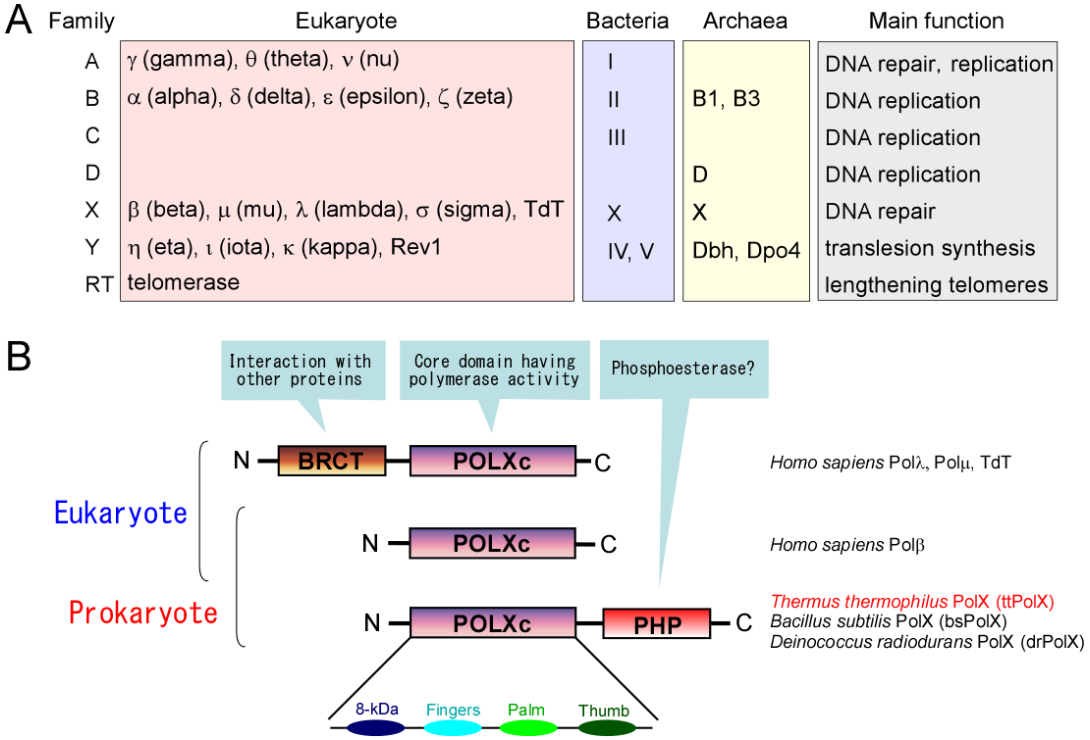

Figure 1. DNA polymerase family and domain organization of PolXs. (A) Seven families of DNA polymerases and functions in three domains of life. (B) Domain structures predicted by sequence motif analysis of representative PolXs. The accession numbers are as follows: NP_037406 for hsPolλ; NP_037416 for hsPolμ; NP_004079 for hsTdT; NP_002681 for hsPolβ, YP_144416 for ttPolX; NP_390737 for bsPolX and NP_294190 for drPolX. The POLXc domain is further divided into four subdomains; 8-kDa, Fingers, Palm and Thumb subdomains. The abbreviations are as follows: BRCT, BRCA1 C-terminal domain; POLXc, PolX core domain; PHP, polymerase and histidinol phosphatase domain.

MATERIALS AND METHODS

Materials

The DNA-modifying enzymes, including restriction enzymes and LA Taq polymerase, were from Takara Bio Inc., Shiga, Japan. The yeast extract and polypeptone were from Nihon Pharmaceutical Co., Tokyo, Japan. The dNTPs and ribonucleotide 5'-triphosphates (NTPs) were from Sigma, St. Louis, USA. The DNA oligomers were synthesized by BEX Co., Tokyo, Japan. All other reagents used were of the highest grade commercially available.

Cloning and overexpression

Sequence analysis of the *T. thermophilus* HB8 genome (DDBJ/EMBL/GenBank AB107660) revealed one ORF, TTHA1150, encoding a protein which belongs to the PolX family. Using this sequence information, I synthesized two primers for amplification of the *ttha1150* gene by PCR. The gene fragment amplified by PCR using LA Taq polymerase was ligated into the pT7Blue T-vector (Novagen, Wisconsin, USA) by TA cloning and confirmed by sequencing. Using the NdeI and BamHI sites, the fragment bearing the target gene was ligated into pET-11a (Novagen, Wisconsin, USA). *Escherichia coli* Rosetta2(DE3)pLysS cells transformed with the resulting plasmid were cultured at 37°C to 1×10^8 cells/ml in 1.5 l LB medium containing 50 μg/ml ampicillin. The cells were then incubated for 5 h in the presence of 50 μg/ml isopropyl-β-D-thiogalactopyranoside, harvested by centrifugation and stored at -20°C. The domains of the POLXc (1-379), POLXc (1-316), PHP (339-575) and PHP (336-575) were amplified from the pT7Blue plasmid containing the *ttha1150* gene by PCR using KOD DNA polymerase (Toyobo, Osaka, Japan) and ligated into the pET-15b (POLXc (1-379) and PHP (339-575)), pET-11a (POLXc (1-316)) and pET-21a (PHP (336-575)) expression vectors (Novagen, Wisconsin, USA). The primer sets used for the POLXc (1-379) were 5'-TATACATATGCGTAACCAGGAGCTCGCCCGGATC-3' and 5'-TATAAGATCTTATTACCGCACCGCCGGGGAG-3', for the POLXc (1-316) were 5'-TATACATATGCGTAACCAGGAGCTCGCCCGGATC-3' and 5'-TATAGATCTTATTAGTCCTCCCGGAGGGGGGGC-3', for the PHP (339-575) were 5'-TATGAATTCCATATGGGTGACCTCCAGGTCCACTCC-3' and 5'-TATGGATCCTTATTAAACGCCACGACGGGCTTTGAG-3', and for the PHP (336-575) were 5'-GAGATATACATATGCAGGTCAAGGGGGACCTCCAG-3' and 5'-TATATATATGCGGCCGCAACGCCACGACGGGCTTTG-3'. ttPolX mutants of K263A, K263D, Q342A, H344A, D349A, H374A, E413A, H440A, H468A, D529A and

H531A were generated by means of the inverse PCR method using the pET-11a/tt*polx* plasmid as a template and the following primers: 5'-CGGCCCACTCCATCCGCCTTC-3' (K263A, forward), 5'-ACGCCCACTCCATCCGCCTTC-3' (K263D, forward) and 5'-CGCTCCCCGTGAGGTACTGGAGG-3' (K263A and K263D, reverse); 5'-TCGCGGTCCACTCCACCTACTCC-3' (Q342A, forward), 5'-GGTCCCCCTTGACCTGAGGAAGCTC-3' (Q342A, reverse); 5'-GTCGCGTCCACCTACTCCGACG-3' (H344A, forward), 5'-CTGGAGGTCCCCCTTGACCTGAGG-3' (H344A, reverse); 5'-GCCGGCCAGAACACCTTGGAGG-3' (D349A, forward), 5'-GGAGTAGGTGGAGTGGACCTGGAGG-3' (D349A, reverse); 5'-GCCTCTCCAGCAGTGCGGGTG-3' (H374A, forward), 5'-GTCGGTCACGGCGAGGTAGCG-3' (H374A, reverse); 5'-GCAGTGGACATCCACCCCGACG-3' (E413A, forward), 5'-GGCACCGGCGAGGAGGTAGG-3' (E413A, reverse); 5'-GCCTCCCGCTTCAACCTCCCCAAGA-3' (H440A, forward), 5'-GACGGAAACCAAAACCAGGTCCAGCTCC-3' (H440A, reverse); 5'-GCCCCCACGGCGAGGCTTTTG-3' (H468A, forward), 5'-GGCGAGGACGTGGACGAAGGG-3' (H468A, reverse); 5'-GCAGCACACCAGACCGACCACC-3' (D529A, forward), 5'-CGTGGAGAGGCTGATCCAAAGCCCCATC-3' (D529A, reverse); 5'-GCACAAACCGACCACCTCCGCTTC-3' (H531A, forward), 5'-TGCGTCGGTGGAGAGGCTGATCC-3' (H531A, reverse). PCR was performed using KOD -Plus- Ver. 2 DNA polymerase (Toyobo, Osaka, Japan) and low amount of the template plasmid (< 1 ng). The targeted fragments were electrophoresed and purified from the gel. Purified fragments were mixed with DpnI, T4 polynucleotide kinase and ATP in the T4 DNA ligase buffer. After incubation at 37°C for 30 min, the solution was mixed with T4 DNA ligase and incubated at 16°C for overnight. The self-ligated plasmids were amplified using *E. coli* DH5α. Overexpression of the domains and mutants were performed similar to those of the wild-type ttPolX.

For expression of selenomethionyl ttPolX, *E. coli* B834(DE3) cells carrying pET-11a/tt*polX* and pRARE (Novagen, Wisconsin, USA) were cultured in LB medium at 37°C to a density of 1×10^8 cells/ml. Cells were harvested, resuspended in LeMaster medium (LeMaster *et al.*, 1985) (containing L-selenomethionine) and lactose and cultured at

37°C for 24 h. I obtained 1.5 g (wet weight) of cells expressing selenomethionyl ttPolX, and 1 mg of purified selenomethionyl ttPolX.

Protein purification

All the following procedures were carried out at room temperature (RT) unless stated otherwise. Frozen cells expressing ttPolX were thawed, suspended in 20 mM Tris-HCl and 100 mM KCl and 1 mM EDTA, pH 8.5, and then disrupted by sonication on ice. The lysate was incubated at 60°C for 10 min and centrifuged (38,900 × *g*) for 20 min at 4°C. Ammonium sulfate (AS) was added to the resulting supernatant to a final concentration of 1.5 M. Then the solution was centrifuged (38,900 × *g* for 30 min at 4ºC), and the resulting supernatant was applied to a TOYOPEARL Phenyl-650 M column (Tosoh, Tokyo, Japan) and proteins were eluted with a linear gradient of 1.5-0 M AS in 20 mM Tris-HCl (pH 8.5). The fractions containing ttPolX were applied to a TOYOPEARL SuperQ-650 M column equilibrated with 20 mM Tris-HCl, pH 8.5, and proteins were eluted with a linear gradient of 0-0.5 M KCl. The fractions containing ttPolX were then applied to a hydroxyapatite column (Bio-Rad, California, USA) equilibrated with 10 mM sodium phosphate, pH 7.0, and eluted with a linear gradient of 10-500 mM sodium phosphate (pH 7.0). The fractions containing the ttPolX were collected and concentrated with a Vivaspin concentrator (molecular weight 30,000 cut-off). The concentrated solution was applied to a Superdex 200 HR 10/30 column (GE Healthcare UK Ltd., England) equilibrated with 20 mM Tris-HCl and 100 mM KCl, pH 8.5, and eluted with the same buffer using an ÄKTA explorer system (GE Healthcare UK Ltd., England). The fractions containing the ttPolX were concentrated and stored at 4°C or -80°C after liquid nitrogen freezing. Frozen cells expressing the N-His-tagged POLXc (1-379) were thawed, suspended in binding buffer (20 mM Tris-HCl, 500 mM NaCl and 5 mM imidazole, pH 7.9), and then disrupted by sonication on ice. The lysate was centrifuged (38,900 × *g*) for 30 min at 4°C. The resulting supernatant was applied to a His·Bind Resin column (Novagen, Wisconsin, USA) equilibrated with binding buffer and proteins were eluted with a linear gradient of 5-1,000 mM imidazole. The fractions containing the POLXc (1-379) were collected and AS was added to a final concentration of 0.8 M. Then the solution was applied to a TOYOPEARL Butyl column (Tosoh, Tokyo, Japan) equilibrated with 20 mM glycine and 0.8 M AS, pH 7.0, and eluted with a linear gradient of equilibration buffer to 20 mM glycine, pH 9.0. The fractions containing the POLXc (1-379) were collected, concentrated and applied to a Superdex 75 HR 10/30 column (GE Healthcare UK

Ltd., England). The purified POLXc (1-379) was stored in 20 mM Tris-HCl and 100 mM KCl, pH 9.1, at 4ºC. Purification of the N-His-tagged PHP (339-575) was performed in a similar way to for the POLXc (1-379) but with the use of a TOYOPEARL Phenyl column not a TOYOPEARL Butyl one, with equilibration buffer comprising 20 mM Tris-HCl and 1 M AS, pH 7.4, and elution with a linear gradient of equilibration buffer to 20 mM Tris-HCl, pH 8.5. For purification of the POLXc (1-316), cells were disrupted by sonication in a buffer containing 10 mM potassium phosphate (KPi) and 1mM EDTA, pH 7.0, and then the supernatant was purified by following purification steps: heat treatment (60°C, for 10 min), SP Sepharose column (0-500 mM KCl in 10 mM Kpi [pH 7.0]), hydroxyapatite column (10-500 mM NaPi, pH 7.0), TOYOPEARL Phenyl-650 M (1-0 M AS in 20 mM Tris-HCl (pH 7.5)) and Superdex 75 HR 10/30 column (10 mM HEPES-NaOH and 100 mM KCl, pH 7.5). For purification of the C-His-tagged PHP (336-575), cells were disrupted by sonication in a buffer containing by 20 mM Kpi and 500 mM KCl, pH 8.0, and then the supernatant was applied to a His·Bind Resin column and washed by 20 mM Kpi, 500 mM KCl and 50 mM imidazole, pH 8.0. The protein was eluted with a linear gradient of 20-500 mM imidazole, and further purified by Superdex 75 HR 10/30 column (20 mM Tris-HCl, 100 mM KCl, pH 8.0). After each step, fractions were analyzed by SDS-PAGE. The purification of selenomethionyl ttPolX and the mutants were performed similar to those of the wild-type ttPolX. The concentration of the purified protein was determined by using a molar extinction coefficient at 278 nm calculated according to the formula of Kuramitsu *et al.* (Kuramitsu *et al.*, 1990). The calculated molar extinction coefficients of ttPolX, POLXc (1-379), POLXc (1-316), PHP (339-575) and PHP (336-575) were 66,885, 29,190, 19,005, 47,880 and 47,880 $M^{-1}cm^{-1}$, respectively. I identified the purified protein as a ttPolX by means of peptide mass fingerprinting (PMF) involving matrix-assisted laser desorption/ionization time-of-flight mass spectrometry (MALDI-TOF MS). Briefly, I measured a mass spectrum of the peptide mixture resulting from the digestion of a protein by trypsin and compared it to the database containing the theoretical mass spectra of tryptic peptide mixtures from each protein encoded in *T. thermophilus* HB8 genome. By statistical comparison between experimentally determined and theoretical mass spectra, I identified each purified protein as a target protein.

Limited proteolysis

ttPolX (10 μM) was incubated with trypsin (0-100 nM) in buffer comprising 20 mM Tris-HCl,

pH 8.0, at 25°C or with thermolysin (0-100 nM) in buffer comprising 20 mM Tris-HCl and 10 mM $CaCl_2$, pH 7.8, at 37ºC. After incubation for 1 h, samples were analyzed by 12.5% SDS-PAGE. The N-terminal sequences of peptide fragments were determined using a protein sequencer (Procise HT, Applied Biosystems, California, USA)

DNA/RNA polymerase assays

The sequences of the oligonucleotides were 5'-ATGACAACTAAAGCAACACCC-3' (21F), 5'-ATGACAACTAAAGCAACACCCG-3' (22F), 5'-GTCATAGCTGTTTCCTGTGTGAAATTGTTATCCGCTCACAATTCCACACAACATACGAGCCG-3' (62F), 5'-CACTGGCGGTCGTTCTATCGGGTGTTGCTTTAGTTGTCAT-3' (40T), 5'-ATAGAACGACCGCCAGTG-3' (18G), 5'-phosphorylated 18G (P18G), 5'-ATGACAACTAACGCAACACCC-3' (12C21), 5'-ATGACAACTAAIGCAACACCC-3' (12I21, I = deoxyinosine), 5'-ATGACAACTAAXGCAACACCC-3' (12X21, X = deoxyxanthine), 5'-r(AUGACAACUAAAGCAACACCC)-3' (21RNA), and 5'-GGGTGTTGC-3' (9P). Reaction mixtures comprised 20 mM Tris-HCl, 20 mM KCl, 10 μM dNTPs or NTPs, 5 mM $MgCl_2$ or 1 mM $MnCl_2$, 1 μM enzyme and 10 nM oligonucleotides, pH 8.0, at 37ºC. The assays were performed with 21F/40T (primer/template), 21F/40T/18G (1-nt gap), 21F/40T/P18G (5'-phosphorylated 1-nt gap), 9P/21F (primer/template), 9P/12C21 (primer/template), 9P/12I21 (primer/template), 9P/12X21 (primer/template), or 9P/21RNA (primer/template). Each primer was radiolabeled of the 5'-end using [γ-^{32}P] ATP and T4 polynucleotide kinase, and purified by ethanol precipitation. The oligonucleotides were mixed in equimolar and heated at 95°C for 2 min, and cooled gradually for the annealing. The reaction mixtures were incubated for 30 min at 37ºC unless stated otherwise and the reactions were stopped by the addition of 2 × denaturing dye (5 mM EDTA, 80% deionized formamide, 10 mM NaOH, 0.1% bromophenol blue and 0.1% xylene cyanol), followed by analysis by denaturing PAGE. The gel contained 8 M urea, and electrophoresis was performed with 1 × TBE buffer (89 mM Tris-borate and 2 mM EDTA). The DNA was visualized and analyzed by autoradiography using a Bio-imaging analyzer BAS2500 (Fuji Film, Tokyo, Japan).

For the kinetic analyses, oligonucleotides were mixed in the 21F:40T ratio of 1:1.2 (primer/template) or the 21F or 22F:40T:P18G ratio of 1:1.2:1.5 (1-nt gap and nick). Mixed oligonucleotides in buffer containing 1 mM Tris-HCl (pH 7.5), 0.1 mM EDTA (pH 8.0) and 100 mM KCl were heated at 95°C for 2 min and cooled gradually to allow annealing. For

1-nt gap-filling assay, a reaction mixture typically composed of 50 mM Tris-HCl, 100 mM KCl, 10 mM $MgCl_2$, 100 μg/ml bovine serum albumin (BSA), 0.00625-10 μM dGTP and 2-500 nM annealed 1-nt gapped DNA, pH 7.5 at 37°C. The reaction was initiated by adding 0.5-20 nM ttPolX wild-type or mutants. The samples were analyzed by 20% (w/v) denaturing PAGE (8 M urea) and visualized by autoradiography using BAS2500. For inhibition assay, dCTP (mismatched substrate), inorganic pyrophosphate (PPi) (Sigma-Aldrich, MO, USA) and nicked DNA were used as inhibitors. The apparent rate constant k_{app} (= $v_0/[E]_0$) was plotted against [S] and [I], and fitted to the following equations using Igor 4.03 (Wave metrics, USA):

$$k_{app} = k_{cat}[S]/(K_m+[S]) \quad \text{(no inhibition)} \quad (1)$$

$$k_{app} = k_{cat}[S]/((1+[I]/K_i)K_m+[S]) \quad \text{(competitive inhibition)} \quad (2)$$

$$k_{app} = k_{cat}[S]/((1+[I]/K_i)K_m+(1+[I]/K_i')[S]) \quad \text{(mixed inhibition)} \quad (3)$$

where v_0, $[E]_0$, [S], [I], k_{cat}, and K_m are initial velocity, total enzyme concentration, free substrate concentration, free inhibitor concentration, catalytic rate constant and Michaelis constant, respectively. K_i and K_i' are inhibition constants for binding to different enzyme species.

Surface plasmon resonance

Surface plasmon resonance (SPR) analysis was performed at 25°C using a Biacore3000 (GE Healthcare UK Ltd, England). ttPolX was diluted with 10 mM acetate (pH 6.0) to 0.1 mg/ml and immobilized on a CM4 sensor chip by amine coupling followed by blocking with ethanolamine hydrochloride. Approximately 7,000-10,000 resonance units (RU) of ttPolXs were immobilized. Since dNTPs have low molecular weight (~ 500) and are difficult to detect, as much ttPolX as possible was immobilized. Control cells were also blocked by ethanolamine hydrochloride in a similar manner to ttPolX cells to reduce nonspecific electrostatic binding. The running buffer was composed of 10 mM HEPES-NaOH, 100 mM KCl and 10 mM $MgCl_2$ or $CaCl_2$, pH 7.5, and was filtered and degassed. The concentrations of nucleotides were determined by extinction coefficients (Struhl, 2001). Each nucleotide diluted with running buffer was injected over ttPolX at flow rates of 30-100 μl/min. After binding for 2.5-5 min, ttPolX-nucleotide complexes were dissociated using running buffer without nucleotides, followed by flowing running buffer without metal ions.

Experiments with ttPolI were performed in the same manner as for ttPolX. I failed in our attempts to measure the kinetic parameters of binding because the level of immobilization was too high. Therefore, the dissociation constant (K_d) was calculated by fitting the average RU of the steady state (R_{eq}) to the following equation using Igor 4.03 (Wave metrics, OR, USA):

$$R_{eq} = R_{max}\,[S]/([S] + K_d) \qquad (4)$$

where R_{eq} and R_{max} corresponds to [ES] and $[E]_0$, respectively, and [S] is free concentration of nucleotides. The observed R_{max} was much lower than the theoretical R_{max} (= immobilized ttPolX (RU) × binding ratio (= 1) ×molecular weight (MW) of nucleotide/MW of ttPolX) because ttPolX was probably inactivated either by the immobilization buffer (10 mM acetate, pH 6.0) or by immobilization at more than two points. Another possibility is that immobilization at the POLXc domain inhibited nucleotide binding. I purified and immobilized the POLXc (1-316), and obtained a barely discernable SPR response upon flow of Mg^{2+}-dGTP.

Crystal structure analysis

Native or selenomethionyl ttPolX with dGTP were crystallized by the hanging-drop vapor-diffusion method with seeding. Drops (1 μl) of 5 mg/ml ttPolX containing 1 mM dGTP were mixed with 1 μl of crystallization solution containing 0.2 M potassium chloride, 0.01 M calcium chloride, 0.005 M sodium cacodylate (pH 6.0) and 5% or 10% polyethylene glycol 4,000 (v/v), and equilibrated against 0.15 ml of the reservoir solution at 20°C. A few days later, highly clustered crystals were broken up and diluted with the reservoir solution. Protein solutions with dGTP were mixed with the seed solution and crystallized as above. The crystals were grown at 20°C for about 9 months (native ttPolX) or a few days (selenomethionyl ttPolX) to obtain large crystals. Crystallization of the Lys-263 mutants was performed similarly to the wild-type but without seeding. For crystallization of the ternary complex of ttPolX with 1-nt gapped DNA and dideoxyguanosine 5'-triphosphate (ddGTP), a DNA 28-mer (pGCCGTTTTCGGCCCGACTGTTTTCAGTC) was self-annealed in 10 mM Tris-HCl (pH 7.5), 100 mM KCl and 15 mM $MgCl_2$ using a thermal cycler by heating for 10 min at 90°C and cooling to 4°C (1°C/min). Annealed 2-nt gapped loop DNA (200 μM) was incubated with ttPolX (100 μM) and ddGTP (1 mM) (GE Healthcare UK Ltd.,

England) at 20°C for overnight to make 1-nt gapped DNA. The resultant mixture (1 μl) was mixed with 1 μl 15% PEG1500 (v/v) and crystallized as above. For crystallization of the ttPolX with primer/template and ddGTP complex, template (CGGCCATACTG) and primer (CAGTAT) were mixed in a 1:1 ratio in 40 mM Tris-HCl (pH 7.5) and 10 mM $MgCl_2$ and annealed using a thermal cycler as above. The annealed primer/template DNA was mixed with ttPolX and ddGTP, resulting in 200 μM DNA, 100 μM (6.4 mg/ml) ttPolX and 1 mM ddGTP. After incubation at 20°C overnight, the solution was mixed with 50 mM Tris-HCl (pH 8.5), 25 mM $MgSO_4 \cdot 7H_2O$ and 1.8 M ammonium sulfate and crystallized as above. For cryoprotection, drops (2 μl) containing the crystals were mixed with 5 μl of crystallization solution containing 22.5% ethylene glycol (v/v), and then 5 μl of mixed solution was removed. This manipulation was repeated at least three times, and then the crystals were flash-frozen in a liquid nitrogen stream (-180°C). Selenium multiple-wavelength anomalous dispersion data and other single-wavelength diffraction data were collected at beamline BL26B2 (Ueno *et al.*, 2004; Ueno *et al.*, 2005; Ueno *et al.*, 2006; Okazaki *et al.*, 2008) at SPring-8 (Hyogo, Japan). The data were processed by the HKL2000 program package (Otwinowski *et al.*, 1997). Seven of ten selenium sites were determined with the program SOLVE (Terwilliger *et al*., 1999). The resulting phases were improved with the program RESOLVE (Terwilliger *et al.*, 2000; Terwilliger *et al*., 2003), followed by automatic model tracing with the program ARP/wARP (Langer *et al*., 2008). Model refinement was carried out initially for the selenomethionyl ttPolX diffraction data and continued for the native ttPolX diffraction data using programs CCP4 suite, XtalView/X-fit, Coot, CNS and Refmac5 (Bailey *et al*., 1994; McRee *et al*., 1999; Emsley *et al*., 2004; Brunger *et al*., 1998; Brunger, 2007; Vagin *et al*., 2004). The occupancy of *syn* and *anti* conformations of dGTP was refined by a program of Phenix (Adams *et al*., 2010). The stereochemistry of the structure was checked using the program PROCHECK (Laskowski *et al*., 1993). Data collection and refinement statistics are shown in Table 5.

Electrophoretic mobility shift assay

Reaction mixtures comprised 20 mM Tris-HCl, 20 mM KCl, 2 mM EDTA, protein and oligonucleotides, pH 8.0, at 37ºC. The oligonucleotides used were 5'-ATGACAACTAAAGCAACACCCGATAGAACGACCGCCAGTG-3' (40C), 21F, 40T, 18G, and P18G. The assays were performed with 40T (single-stranded DNA, ssDNA), 40T/40C (double-stranded DNA, dsDNA), 21F/40T/18G (1-nt gapped DNA), or

21F/40T/P18G (5'-phosphorylated 1-nt gapped DNA). In electrophoretic mobility shift assay (EMSA), the oligonucleotide of 40T was 5'-radiolabeled and the annealing condition was as described above except for adding three times higher concentration of the oligonucleotides of 18G and P18G to anneal perfectly. The reaction mixtures were incubated for 30 min at 37ºC and then mixed with 5 × native dye (5 mM EDTA, 50% glycerol and 0.05% bromophenol blue). The mixtures were loaded onto a 5% polyacrylamide gel, electrophoresed in TBE buffer and analyzed by autoradiography.

When multiple molecules of an enzyme bind to a substrate, the apparent dissociation constant (K_d^{app}) can be represented by the following equation:

$$nE + S \overset{K_d^{app}}{\rightleftharpoons} EnS \quad (5)$$

$$K_d^{app} = [E]^n[S]/[E_nS] \quad (6)$$

where E is the free enzyme, n the number of binding enzyme, S the free DNA, E_nS the enzyme-DNA complex. Since the substrates were mixed with a large excess of enzyme, the following postulations were applied.

$$[E]_0 = [E] \quad (7)$$

$$[S]_0 = [S] + [E_nS] \quad (8)$$

where $[E]_0$ is the concentration of total enzyme and $[S]_0$ the concentration of total DNA. Based on equations 5-7, $[E_nS]$ is represented as a function of $[E]_0$.

$$[E_nS] = [E]_0^n[S]_0/([E]_0^n + K_d^{app}) \quad (9)$$

The K_d^{app} value was calculated by fitting the data to equation 4 using Igor 4.03 (Wave Metrics).

dRP lyase assay

dRP lyase assay was performed according to the method of Beard *et al.* (Beard *et al.*, 2006b), except for using enzymes from *T. thermophilus* HB8: uracil DNA glycosylase A (UDGA) (TTHA0718) and endonuclease IV (TTHA0834). The sequences of the oligonucleotides were 5'-TTGCATGCCTGCAGGTGGACTCTAGAGGATCC-3' (32F) and

5’-GGATCCTCTAGAGTC(dU)ACCTGCAGGCATGCAA-3’ (32U).

Exonuclease assays

Reaction mixtures comprised 20 mM Tris-HCl, 20 mM KCl, 1 mM $MnCl_2$, 1 μM enzyme and 10 nM 5’-labeled oligonucleotides, pH 8.1, at 37ºC. The oligonucleotides used were 21F, 5’-GGGTGTTGCTTTAGTTGTCAT-3’ (21R), 5’-GTTGCTTTAGTTGTCAT-3’ (17R), 5’-TATCGGGTGTTGCTTTAGTTGTCAT-3’ (25R) and 5’-ATGACAACTAAAGCAACACCT-3’ (21F-T). The assays were performed with 21F (single strand), 21F/21R (double strand), 21F/17R (overhanging end), 21F/25R (recessed end) and 21F-T/25R (mismatched end). The annealing condition was as described above. The reaction mixtures were incubated for 30 min at 37ºC and analyzed as described above. For determination of kinetic parameters, 50 nM ttPolX or 200 nM domain mixture (200 nM POLXc (1-379) and 200 nM PHP (339-575)) was incubated in reaction mixtures comprising 20 mM Tris-HCl, 20 mM KCl, 1 mM $MnCl_2$, 10 nM 3’-labeled 21F, with or without 10 μM dNTPs and 6.25-12800 nM unlabeled oligonucleotides, 22F (5’-ATGACAACTAAAGCAACACCCA-3’), pH 8.1, at 37ºC. Radiolabeling at the 3’-end was performed using terminal deoxynucleotidyl transferase (Promega, Wisconsin, USA) and [α-^{32}P] cordycepin 5’-triphosphate (PerkinElmer Inc., Massachusetts, USA). Kinetic parameters were calculated by fitting the data to the Michaelis-Menten equation using Igor 4.03 (Wave Metrics, Oregon, USA).

Fourier transform ion cyclotron resonance mass spectrometer for exonuclease assay

To determine the polarity and products of exonuclease activity accurately, a reaction mixture containing 50 mM Tris-HCl, 20 mM KCl, 1 mM $MnCl_2$, 100 μM 21F ssDNA, and 1 μM or 10 μM ttPolX, pH 7.5 was incubated at 68°C for 1 and 10 min. The reaction was stopped by 50 mM EDTA and heat treatment at 95 °C for 10 min and then kept on ice. Each reaction product was extracted by using C18 ZipTip (Millipore, MA, USA) with ion-pairing agent, dibutylammonium formate (DBAF), pH 8.0 to eliminate any contaminants and salts. First, C18 ZipTip was equilibrated with 4 mM DBAF after activation by using 100% acetonitrile. The reactant was introduced into the equilibrated C18 ZipTip several times and then washed with pure water. The reaction products that bound to C18 resin with DBAF were eluted with 50% acetonitrile. The resulting solutions were introduced into a solariX, Fourier transform

ion cyclotron resonance (FT-ICR) mass spectrometer shielded with 9.4 T superconducting magnets (Bruker Daltonics Inc., MA, USA) by electrospray ionization under negative mode with 2 μl/min flow rate, 4000 V capillary voltage and –500 voltage spray shield. For data acquisition at solariX FT-ICR MS, a free induction decay was set to 1 M size and mass detection range was set from 200 to 3,000 *m*/*z*. One hundred spectra for each reaction product were combined to obtain average spectra. Mass analyses of all samples were carried out under the same condition. The obtained mass results were charge deconvoluted by DataAnalysis software (version 4.0, Bruker Daltonics Inc., MA, USA) for quantitative and comparative analysis of the enzyme products

Size exclusion chromatography

The oligomeric state of ttPolX, the domains and domain mixture in solution was assessed by size exclusion chromatography on Superdex 75 HR 10/30 column. A sample contained 20 mM Tris-HCl and 100 mM KCl with or without 10 μM dNTPs, and a protein, pH 8.5, at 25°C. The protein was eluted with the same buffer. The apparent molecular weight was estimated using molecular weight marker proteins (Sigma-Aldrich, MO, USA).

Inductively coupled plasma atomic emission spectrometry

The metal contents of purified ttPolX were determined with a CIROS CCD inductively coupled plasma-atomic emission spectrometry (ICP-AES) instrument (Rigaku, Tokyo, Japan). Stock solutions of ttPolX were diluted with 20 mM Tris-HCl (pH 8.5 at 25°C) and 100 mM KCl to a concentration of 3.5-9.3 μM. Various solution concentrations of the metals Mg, Ca, Mn, Fe, Co, Ni and Zn were used for constructing standard curves. Based on each standard curve, the metal contents of ttPolX were determined. Three ttPolX samples purified on different dates were measured.

AP endonuclease assay

The oligonucleotides of 21F and 5'-GGGTGTTGCXTTAGTTGTCAT-3' (X = tetrahydrofuran, THF; stabilized AP site analog) were annealed at the ratio of 1:1.2. The oligonucleotide containing THF was 5'-labeled by using T4 polynucleotide kinase and [γ-^{32}P] ATP. Reaction mixtures containing 50 mM Tris-HCl, 20 mM KCl, 1 mM $MnCl_2$ or 5 mM $MgCl_2$, 1 μM enzyme and 10 nM DNA, pH 7.5 were incubated at 37°C for 30 min. The reactions were stopped by the addition of 2 × denaturing dye (50 mM EDTA, 90% deionized

formamide, 10 mM NaOH, 0.1% bromophenol blue and 0.1% xylene cyanol) and analyzed by 20% denaturing gel (8 M urea) and autoradiography.

3'-phosphatase assay

The oligonucleotide of 3'-phosphorylated 21F (21F-P) was 5'-labeled using T4 polynucleotide kinase (3'-phosphatase minus) (New England Biolabs, MA, USA) and [γ-^{32}P] ATP. The oligonucleotides were mixed in the 21F-P:40T ratio of 1:1.2 (primer/template) or in the 21F-P:40T:P18G ratio of 1:1.2:1.5 (1-nt gap), in a buffer containing 1 mM Tris-HCl (pH 7.5), 0.1 mM EDTA (pH 8.0) and 100 mM KCl, after which they were heated at 95°C for 2 min and cooled gradually to allow annealing.

For the kinetic assay, the reaction mixtures were typically composed of 50 mM Tris-HCl, 100 mM KCl, 1 mM $MnCl_2$, 100 μg/ml BSA and 3'-phosphorylated DNA substrate, pH 7.5 at 25°C. The following concentrations of DNAs were used: 260-16,000 nM ssDNA (wild-type and H531A mutant of ttPolX), 35-810 nM primer/template DNA (Wild-type and H531A mutant of ttPolX), 5-125 nM 1-nt gapped DNA (ttPolX), 2.5-35 nM 1-nt gapped DNA (H531A), 5-320 nM 1-nt gapped DNA (endonuclease IV from *T. thermophilus* HB8, ttEndoIV), and 5-160 nM 1-nt gapped DNA (ttPolX and ttEndoIV with $MgCl_2$ [and dGTP]). The reactions were initiated by adding 5-20 nM ttPolX (for ssDNA), 100-400 nM H531A (for ssDNA), 10 nM ttPolX (for primer/template DNA), 20 nM H531A (for primer/template DNA), 2-2.5 nM ttPolX (for 1-nt gapped DNA), 2 nM H531A (for 1-nt gapped DNA) and 1 nM ttEndoIV (for 1-nt gapped DNA). The reaction was analyzed assuming the following of equations:

$$\mathrm{E} + \mathrm{S} \overset{K_S}{\Leftrightarrow} ES \overset{k_{cat}}{\longrightarrow} E + P \qquad (10)$$

Assuming that the reaction proceeds under rapid equilibrium, K_s is defined as follows,

$$K_s = [E][S]/[ES] = K_m \qquad (11)$$

The total concentrations of enzyme ($[E]_0$) and DNA substrate ($[S]_0$) are related to their respective free concentrations ([E] and [S]) as follows:

$$[E]_0 = [E] + [ES] \qquad (12)$$

$[S]_0 = [S] + [ES]$ (13)

The Michaelis-Menten equation corrected free substrate concentration is obtained from equations 10-13,

$$k_{app} = \frac{k_{cat}}{1+\frac{2K_m}{(S_0-E_0-K_m)+\sqrt{(E_0-S_0+K_m)^2+4K_mS_0}}} \quad (14)$$

The apparent rate constant k_{app} (= $v_0/[E]_0$) was plotted against [S], and fitted to equation (14) using Igor 4.03 (Wave Metrics, Oregon, USA).

For single-turnover analysis under saturating enzyme conditions ([E] > [S] >> K_m), the reaction mixture containing 1 μM of the ttPolX wild-type or H531A mutant, 0.25 μM 1-nt gapped DNA with 3'-phosphate, 50 mM Tris-HCl, 100 mM KCl, 100 μg/ml BSA, 1 mM $MnCl_2$, pH 7.5 was incubated at 25°C. The reaction was stopped at each time point and, aliquots of the reaction mixtures were removed. The data were fitted to equation (15) using Igor 4.03 (Wave Metrics, Oregon, USA):

$$\%\ \text{product} = A(1 - e^{-kt}) \quad (15)$$

where A is the amplitude, *k* is the rate constant and *t* is the reaction time.

For the stoichiometric assay, the reaction mixtures were typically composed of 50 mM Tris-HCl, 100 mM KCl, 1 mM $MnCl_2$, 100 μg/ml BSA, and 2 μM 3'-phosphorylated DNA (primer/template or 1-nt gap), pH 7.5 at 25°C. The reactions were initiated by adding 0.5-8 μM H531A. The reactions were stopped by adding a 2-fold volume of denaturing dye (50 mM EDTA, 90% deionized formamide, 10 mM NaOH, 0.1% bromophenol blue, and 0.1% xylene cyanol), analyzed by 15% or 20% (w/v) denaturing PAGE (8 M urea) and visualized by autoradiography using BAS2500.

Crosslinking reactions

The buffer of the ttPolX stock solution was replaced by HEPES buffer (50 mM HEPES and 100 mM KCl, pH 7.5 at 25°C) to remove Tris. ttPolX (10 μM) was mixed with various concentrations of the 2-nt gapped 28-mer loop DNA used for crystallization and 500 μM of ddGTP in HEPES buffer with 10 mM $MgCl_2$. All samples except the controls (Fig. 33,

lanes 2 and 10) were mixed with 63 or 33 nM 5'-^{32}P end-labeled loop DNA using T4 polynucleotide kinase. The samples were incubated overnight at 25°C to produce 1-nt gapped DNA. Then, 5 μl of the ttPolX, 1-nt gapped DNA, ddGTP ternary complex was mixed with 2.5 μl of 25 mM dimethyl pimelimidate·2HCl (DMP) (Thermo Fisher Scientific, MA, USA) or 1 mM glutaraldehyde in 200 mM triethanolamine (pH 8.9) and crosslinked for 1 h or 10 min at 25°C. The crosslinking reactions were stopped by addition of 1 M Tris-HCl (pH 7.5). Crosslinked samples were mixed with SDS-PAGE sample buffer and boiled, followed by analyzed by 7.5% SDS-PAGE, Coomassie Brilliant Blue (CBB)-staining and autoradiography.

Gene disruption of *ttpolI*, *ttpolX* and *ttendoIV*

The *ttpolI* (*ttha1054*), *ttpolX* (*ttha1150*) and *ttendoIV* (*ttha0834*) null mutants of *T. thermophilus* HB8 (Δ*ttpolI*, Δ*ttpolX* and Δ*ttendoIV*) were generated by substituting the target gene with the thermostable kanamycin-resistance gene, *HTK* (Hoseki *et al*., 1999) and/or thermostable hygromycin-B kinase, *Hyg*^{r} (Ooga *et al*., 2009), through homologous recombination as previously described (Hashimoto *et al*., 2001). The plasmids for gene disruptions were derivatives of the pGEM-T Easy (*HTK*) (Promega) and pHG305 (*Hyg*^{r}) vectors, constructed by inserting *HTK* or *Hyg*^{r}, respectively, flanked by approximately 500-bp upstream and downstream sequences of each gene. Gene disruptions were confirmed by PCR amplification using the isolated genomic DNAs as templates (Fig. 39). Disappearance of expression of the enzymes was confirmed by Western blotting (Fig. 40).

Culture conditions for *T. thermophilus* HB8

T. thermophilus HB8 was grown at 70°C in TR medium: 0.4% (w/v) tryptone (Difco Laboratories, Detroit, MI, USA); 0.2% (w/v) yeast extract (Oriental Yeast, Tokyo, Japan); and 0.1% (w/v) NaCl (pH 7.5) (adjusted with NaOH). To prepare TT plates, 1.5% (w/v) gellan gum (Wako, Osaka, Japan), 1.5 mM $CaCl_2$, and 1.5 mM $MgCl_2$ were added to the TR medium. Wild-type and disruptants were grown at 70°C on TT plates containing appropriate antibiotics; 50 μg/ml kanamycin or 50 μg/ml kanamycin and 20 μg/ml hygromycin-B. After incubation for 24-48 h, each colony was inoculated into 5 ml TR medium and incubated at 70°C for 9-13 h. Log phase cells (OD_{600} ~ 0.5) were inoculated into 100 ml TR medium to OD_{600} = 0.01 and OD_{600} was monitored every 1 hour.

Preparation of whole cell extracts (WCEs) and immunodepleted (ID) cell lysates

Wild-type and disruptant cells in stationary phase (10 h in Fig. 41A) were collected and resuspended in PBS (10 mM KPi and 150 mM NaCl, pH 7.4) and 1 mM EDTA, or 10 mM Tris-HCl, 100 mM KCl, and 1 mM EDTA, pH 7.5, and sonicated on ice. The lysates obtained from wild-type cells were used as ID samples. Ten microliters of rabbit serum containing each antibody were mixed with 190 μl of bind/wash buffer and 50 μl of Dynabeads Protein A (Veritas, Tokyo, Japan) and rotated at RT for 10 min. The beads were washed three times, mixed with the lysate, and again rotated at RT for 10 min. The supernatant was collected and dialyzed against 2 l of PBS and 0.1 mM EDTA, pH 7.4, or 10 mM Tris-HCl, 100 mM KCl and 0.1 mM EDTA, pH 7.5, by using a dialysis membrane (size 8; MW cutoff, 14 kDa) (Wako, Osaka, Japanl). After dialysis at 4°C for 2 h, the dialysis buffer was replaced by fresh buffer, after which the dialysis was continued overnight. The cellular lysates obtained wild-type and disruptant cells were dialyzed as above and used as WCEs. Protein concentration was determined by the Bradford protein assay kit (Bio-Rad, California, USA).

Immunoprecipitation (IP) and pull-down assay

For the IP, approximately 20 g (wet weight) of *T. thermophilus* HB8 cells in the stationary phase were suspended in 200 ml PBS, after which they were sonicated, and centrifuged (38,900 × *g*) at 4°C for 30 min. The resulting supernatant (40 ml) was mixed with a Protein A HP Spin Trap column (GE Healthcare UK Ltd., England) that was crosslinked to each antibody by DMP (Thermo Fisher Scientific, MA, USA) according to the manufacturer's protocol, and the mixture was gently shaken at RT for 1 h. The resin was washed seven times with PBS + 2 M urea and eluted three times with 0.1 M glycine buffer (pH 2.7) + 2 M urea. The eluted samples were 2-fold diluted with 0.1 M NH_4HCO_3 and first incubated with 5 mM dithiothreitol (DTT) at RT for 1 h, and then with 10 mM iodoacetamide at RT for 1 h in the dark. After removal of iodoacetamide by 10 mM DTT, samples were digested overnight with 1/100-fold weight of trypsin in 50 mM NH_4HCO_3 at 37°C. The digested peptides were purified by using the C18 ZipTip column (Millipore, MA, USA) and then freeze-dried. The dried peptides were further digested overnight with 1/50-fold weight of trypsin in 50 mM NH_4HCO_3 at 37°C and stored at -20°C until use. The samples were filtered by a 0.22-μm membrane and analyzed by nLC-micrOTOF-QII MS system (Bruker

Daltonics Inc., MA, USA). The interacting proteins were identified by the MASCOT MS/MS ion search program (Matrix Science, MA, USA) using the following parameters: missed cleavage, 1; precursor mass tolerance (peptide tolerance), 50-100 ppm; MS/MS tolerance, 0.1-0.4 Da; peptide charge, 1+, 2+, and 3+; instrument, ESI-QUAD-TOF; variable modification, deamidation (N, Q), oxidation (M) and pyro-glu (Q, E).

For the pull-down assay, Protein A resin, which was crosslinked to an anti-ttPolX antibody, was bound to recombinant ttPolX with or without crosslinking by DMP. Approximately 20 g (wet weight) of *T. thermophilus* HB8 cells were suspended in PBS, 1 mM EDTA, benzonase (10 U/ml; Merck, darmstadt, Germany) and a protease inhibitor cocktail (Nacalai Tesque, Kyoto, Japan) at a final volume of 30 ml. The suspension was sonicated and ultracentrifuged (439,830 × *g*, 4°C for 2 h). The supernatants were pre-cleared with Protein A resin without the anti-ttPolX antibody using rotation at 4°C for 2 h. The precleared resin was removed by centrifugation and by filtration using a 0.22-μm membrane, and the supernatant was mixed with the ttPolX or control columns and incubated overnight using rotation at 4°C. The columns were washed 10 times with PBS, and the interacting proteins were eluted by 0.1 M glycine buffer (pH 2.8) + 2 M urea. The eluted solutions were freeze-dried and suspended in PBS. Urea in the samples was removed by using Vivaspin columns (10 kDa cutoff; GE Healthcare UK Ltd., England). The samples were then concentrated to 10 μl and mixed with 5 μl of SDS-PAGE sample buffer. After heating at 100°C for 10 min, the samples were analyzed by SDS-PAGE. The protein bands on the SDS-PAGE gels were identified by PMF using the ultraflex MALDI-TOF-MS system (Bruker Daltonics Inc., MA, USA).

RESULTS

I. Protein preparation

Preparation of ttPolX and its derivatives

The sequence of *ttha1150* encodes ttPolX of 575 amino acid residues. ttPolX has a calculated molecular mass of 64 kDa with a theoretical isoelectric point of 6.3. I overexpressed ttPolX in *E. coli* and purified the protein to homogeneity by means of heat treatment and four column chromatography steps (Fig. 2) (see Materials and Methods). Approximately 20 mg of ttPolX was obtained from 10 g of cells. Size exclusion chromatography was performed to investigate the oligomeric state of ttPolX. The apparent molecular mass corresponding to the peak was estimated to be 48 kDa (data not shown), which was less than the mass calculated from the sequence (64 kDa). This result indicates that ttPolX exists in a monomeric state in solution. The far-UV CD spectrum showed negative double maxima at 209 and 222 nm, characteristic of an alpha-helical structure (data not shown). Based on the ellipticity at 222 nm, the melting temperature (Tm) of ttPolX was shown to be 75ºC (data not shown).

The deletion and site-directed mutants of ttPolX were designed and purified as in Materials and Methods. POLXc (1-379) and PHP (339-575) were designed by limited proteolysis described in the next section. POLXc (1-316), PHP (336-575), Lys-263 mutants and active site mutants of the PHP domain were designed by multiple sequence alignments of bacterial PolXs (Banos *et al*., 2008a; Banos *et al*., 2008b) (see Fig. 12 and 27) and crystal structure of ttPolX (see Fig.11A). The Tm estimated from the CD spectrum of the POLXc (1-379), POLXc (1-316), PHP (339-575) and PHP (336-575) were 70, 75, 50 and 58 ºC respectively.

Limited proteolysis of ttPolX

To reveal the organization of the structural domains of ttPolX, I performed limited proteolysis of the purified ttPolX using trypsin and thermolysin. Under mild conditions, endoproteases are expected to preferentially hydrolyze a protein at the sites exposed to the solvent, which are often within interdomain linker regions. As shown in Fig. 3A, treatment of ttPolX (64 kDa) with trypsin or thermolysin mainly produced two fragments of 42 and 25 kDa. Peptide sequence analysis revealed that trypsin and thermolysin cleaved ttPolX at the same position. The N-terminal sequence of the 42 kDa fragment was MRNQELARIF, which agreed with N-terminal residues 1-10 of ttPolX. The N-terminal sequence of the 25 kDa fragment was

VAGGPSPEEA, which agreed with residues 380-389. The calculated molecular masses of the fragments comprising residues of 1-379 and 380-575 were close to 42 and 25 kDa, respectively. In addition, there was further evidence to locate the position of the interdomain linker region. The purified ttPolX was degraded into two fragments of 44 kDa and 25 kDa after cold storage in 20 mM Tris-HCl and 100 mM KCl, pH 9.1, at 4ºC for half a year (Fig. 3B). The N-terminal sequences of these 44 kDa and 25 kDa fragments were MRNQELA (residues 1-7) and GGPSPEE (residues 382-388), respectively. These results indicated that residues around 380 comprised the interdomain region of ttPolX. The notion that ttPolX is composed of mainly two structural domains is in agreement with the prediction based on sequence motif analysis (Fig. 1). Based on the results of limited proteolysis, I prepared the N-terminal and C-terminal domains as separate protein fragments. The His-tagged N-terminal fragment, corresponding to residues 1-379, was successfully overexpressed in *E. coli* and purified (Fig. 2). However, the C-terminal fragment, corresponding to residues 380-575, with or without a His-tag, was hardly overexpressed and could not be purified. Then, I compared the amino acid sequences of the C-terminal regions of ttPolX and *E. coli* YcdX. YcdX is a hypothetical protein comprising a PHP domain alone and its crystal structure has already been determined (Teplyakov *et al.*, 2003). Several charged residues conserved among PHP domain sequences are coordinated to bound metal ions and thus assumed to be catalytically important residues. Sequence alignment revealed that these residues are well conserved in the C-terminal regions of ttPolX and YcdX (Fig. 3C). This alignment showed that the C-terminal domain obtained by limited proteolysis lacks the putative four residues of catalytic importance. Therefore, I reevaluated that the C-terminal domain comprises residues 339-575 of ttPolX and constructed an expression plasmid containing this region. As a consequence, I succeeded in overexpression and purification of this fragment (Fig. 2). In this study, I used these N-terminal (1-379) and C-terminal domains (339-575) to identify functional domains and called them the POLXc (1-379) and PHP (339-575), respectively.

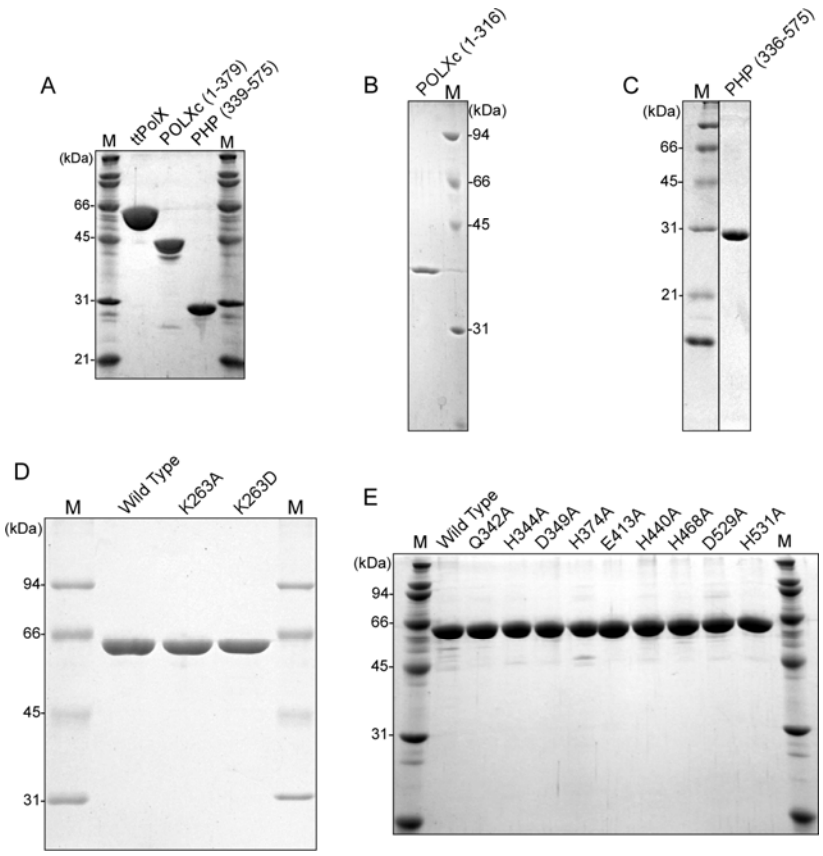

Figure 2. Purified ttPolX and its derivatives used in this study. The purified proteins were analyzed by SDS-PAGE and stained with Coomassie Brilliant Blue (CBB). M represents molecular weight markers. (A-C) ttPolX and its domains. (D) Site-directed mutants of the POLXc domain. (E) Site-directed mutants of the PHP domain active-site residues. The theoretical molecular weights of ttPolX and the domains were 64, 44 (His-POLXc (1-379)), 29 (His-PHP (339-575)), 35 (POLXc (1-316)) and 28 (PHP-His (336-575)) kDa, respectively.

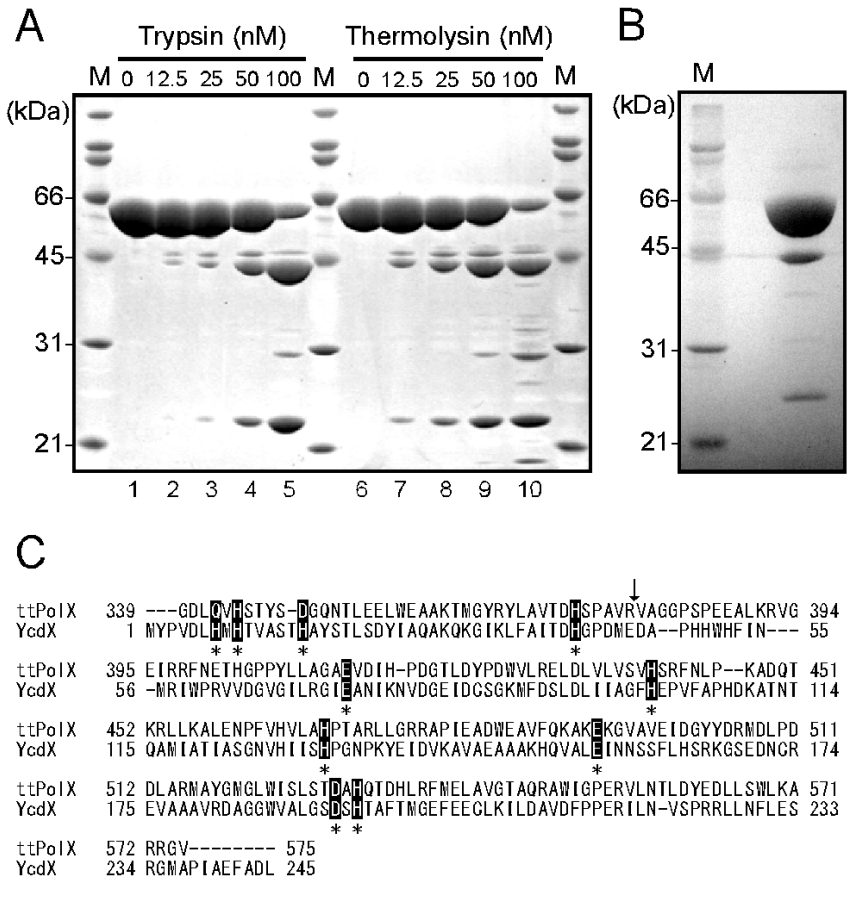

Figure 3. The organization of structural domains of ttPolX. M represents molecular weight markers. (A) ttPolX (10 μM) was digested with trypsin or thermolysin under mild conditions and then analyzed by 12.5% SDS-PAGE and stained with CBB. (B) ttPolX degraded after cold storage at 4ºC for half a year was analyzed by 12% SDS-PAGE and blotted onto a PVDF membrane for peptide sequence analysis, and stained with CBB. (C) Sequence alignment of ttPolX and *E. coli* YcdX. The accession number of YcdX is NP_415552. Stars indicate putative catalytically important residues for binding to metal ions in the YcdX crystal structure (Teplyakov *et al.*, 2003). The arrow indicates the cleaved position on ttPolX with trypsin and thermolysin. The alignment was performed with ClustalW2 (Larkin *et al.*, 2007).

II. The molecular and functional analysis of the POLXc domain

The polymerase activity of full-length ttPolX

I found that ttPolX had Mg^{2+}-dependent 5'-3' DNA/RNA polymerase and Mn^{2+}-dependent 3'-5' exonuclease activities (Fig. 4). Note that the RNA polymerase activity is defined as DNA primer/template-dependent NMP polymerization activity here. In the polymerase assay, I observed that the 5'-labeled primer (21F) binding to the template (40T) was extended in the 5'-3' direction by ttPolX in the presence of Mg^{2+} (Fig. 4A). I also performed polymerase assay with Mn^{2+} because several PolXs are known to have Mn^{2+}-dependent polymerase activity (Garcia-Diaz et al., 2002; Nick McElhinny et al., 2003; Lecointe et al., 2004); however, degradation of the primer was observed (Fig. 4A, lane 2). Similar degradation was observed for ssDNA with Mn^{2+} but not with Mg^{2+} (Fig. 4A, lanes 3 and 4). Such Mn^{2+}-dependent nuclease activity prevented us from determining whether ttPolX had Mn^{2+}-dependent DNA polymerase activity or not. After 240 min, the primer was extended up to the template length of a 40-mer (Fig. 4B, lanes 1-6). Fig. 4B also shows that ttPolX was able to insert not only deoxyribonucleotide monophosphates (dNMPs) but also ribonucleotide monophosphates (NMPs) (Fig. 4B, lanes 7-12). This indicated that ttPolX was able to synthesize RNA against the DNA template, although the RNA polymerase activity was lower than the DNA polymerase activity.

To estimate the ability of ttPolX to discriminate bases, I examined what kinds of nucleotide ttPolX can insert opposite the template base, dC. When one kind of canonical dNTP or NTP was added to the reaction mixture for the polymerase assay, ttPolX inserted only dGMP and GMP next to the 3'-OH of the primer (21F), indicating that ttPolX preferentially inserted complementary nucleotides for canonical nucleotides (Fig. 4C, lanes 1-10). I further examined the incorporation of guanine nucleotide derivatives opposite dC, XTP, dITP, ITP and 8-oxo-deoxyguanosine triphosphate (8-oxo-dGTP) being used as substrates. ttPolX inserted 8-oxo-dGMP, and slightly inserted dIMP and IMP (Fig. 4C, lanes 11-14). The observation that ttPolX inserted dGMP, GMP and 8-oxo-dGMP opposite dC indicated that ttPolX synthesizes DNA following the rule of Watson-Crick base-pairing.

ttPolX was unable to insert nucleotides opposite noncanonical bases or RNA. I measured the translesion synthesis (TLS) activity of ttPolX using oligonucleotides 9P/12I21 (containing inosine) and 9P/12X21 (containing xanthine), and reverse transcriptase (RT) activity using 9P/21RNA. Because of the low Tm of the 9P primer (Tm = 30ºC), I performed the polymerase assay using 9P/21F and 9P/12C21 as a control experiment for

confirmation of primer annealing. With the use of 9P/12I21, 9P/12X21 or 9P/21RNA, ttPolX inserted neither dNMPs nor NMPs opposite dI (12I21), dX (12X21), or A (21RNA) of the template (Fig. 4D, lanes 5-10). These results suggest that ttPolX exhibits no TLS or RT activity in the presence of Mg^{2+}. It should be noted that extension of the primer was hardly observed with 9P/21F and dNTPs as substrates (Fig. 4D, lane 2). The first inserted bases were dT and dG for 9P/21F and 9P/2C21, respectively. When dTTP was the only available nucleotide, ttPolX was able to insert dTMP even with 9P/21F (Fig. 4D, lane 1). These results suggest that ttPolX likely prefers dG to dT.

ttPolX retained DNA polymerase activity at high temperature (Fig. 4E). The optimum growth temperature of *T. thermophilus* is 65-72°C (Oshima *et al.*, 1974). Therefore, many enzymes from *T. thermophilus* are known to exhibit high activity at high temperature. As expected from the optimum growth temperature, ttPolX had higher DNA polymerase activity at 70°C than 37°C (Fig. 4E).

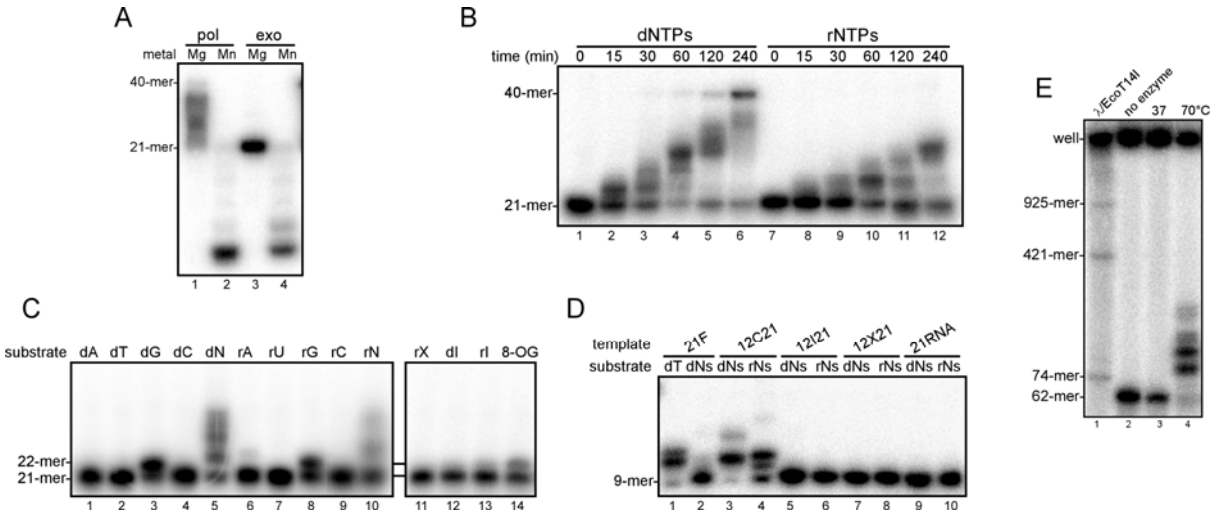

Figure 4. DNA/RNA polymerase activities of ttPolX. (A) Metal ion dependence of the activities in the presence of Mg^{2+} or Mn^{2+}. The reaction conditions for the polymerase assay using 21F/40T (pol) and the exonuclease assay using 21F (exo) are given under MATERIALS AND METHODS. (B) Time course analysis of the polymerase assay. (C) Single nucleotide insertion opposite dC in the polymerase assay. The substrates were in the triphosphate state and their concentrations were as follows: dG and rG, 1 μM; dNs and rNs, 10 μM; other nucleotides including damaged bases, 100 μM. Among the substrates, Ns, X, I and 8-OG stand for NTP mixtures, xanthine, inosine and 8-oxo-dGTP, respectively. (D) TLS and RT assays in the presence of Mg^{2+}, 10 μM dNTPs or NTPs, 1 μM ttPolX, 10 nM 5'-labeled primer (9P), and 10 nM each template (21F, 12C21, 12I21, 12X21, or 21RNA). (E) DNA polymerase activity at high temperature. Reaction mixtures were comprised of 50 mM Tris-HCl, 20 mM KCl, 10 mM $MgCl_2$, 100 μM dNTPs, 8.9 nM M13 ssDNA primed with 10 nM 5'-labeled 62F primer, and 1 μM ttPolX, pH 7.5. λ DNA digested with EcoT14I was used as a ladder marker. The reaction mixtures were incubated for 10 min (panel E), 30 min (panels A and C), 2 h (panel D) or as indicated in the figure (panels B) at 37ºC (panels A-D) or the indicated temperatures (panel E), and then analyzed by 15% (panel E), 18% (panels A, B and C) or 20% (panel D) denaturing PAGE (8 M urea) and autoradiography. In the figure, "d" and "r" represents deoxyribonucleotide and ribonucleotide, respectively.

The activities of the POLXc (1-379) domain

I found that the POLXc (1-379) had Mg^{2+}-dependent DNA polymerase activity but no 3'-5' exonuclease activity (Fig. 5A). Furthermore, I observed Mn^{2+}-dependent DNA polymerase activity for the POLXc (1-379) under the polymerase assay conditions (Fig. 5A, lane 2). This is probably because the POLXc (1-379) had no Mn^{2+}-dependent 3'-5' exonuclease activity (Fig. 5A, lane 4). The POLXc (1-379) exhibited no exonuclease activity in the presence of Mg^{2+} or Mn^{2+} (Fig. 5A, lanes 3 and 4). Time course analysis of the polymerase activity showed that the POLXc (1-379) had DNA/RNA polymerase activity dependent on both Mg^{2+} and Mn^{2+} (Fig. 5B). The Mg^{2+}-dependent polymerase reaction was faster than the Mn^{2+}-dependent activity in the presence of 5 mM Mg^{2+} or 1 mM Mn^{2+}. The POLXc (1-379) showed faster polymerase reaction with Mg^{2+} than that of ttPolX (see Figs. 4B and 5B). The POLXc (1-379) exhibited no polymerase activity with 5 mM Zn^{2+}, Ni^{2+}, Ca^{2+}, or Co^{2+}, or without a metal ion (data not shown).

I examined the ability of POLXc (1-379) to discriminate bases. In the presence of Mg^{2+} or Mn^{2+}, the POLXc (1-379) inserted dIMP, IMP and 8-oxo-dGMP opposite dC (Fig. 5C) as well as dGMP and GMP (data not shown). Although ttPolX showed such insertion with Mg^{2+}, the POLXc (1-379) seemed to produce more extended primers (22-mer) (see Figs. 4C and 5C). The POLXc (1-379) did not insert dNMP or NMP opposite A in the template of 21RNA or dX in 12X21, but inserted dNMPs opposite dI in the template of 12I21 in the presence of Mg^{2+} or Mn^{2+} (Fig. 5D), which was different from ttPolX (Fig. 4D). Thus, the POLXc (1-379) had lower ability to discriminate base-pairing than that of ttPolX.

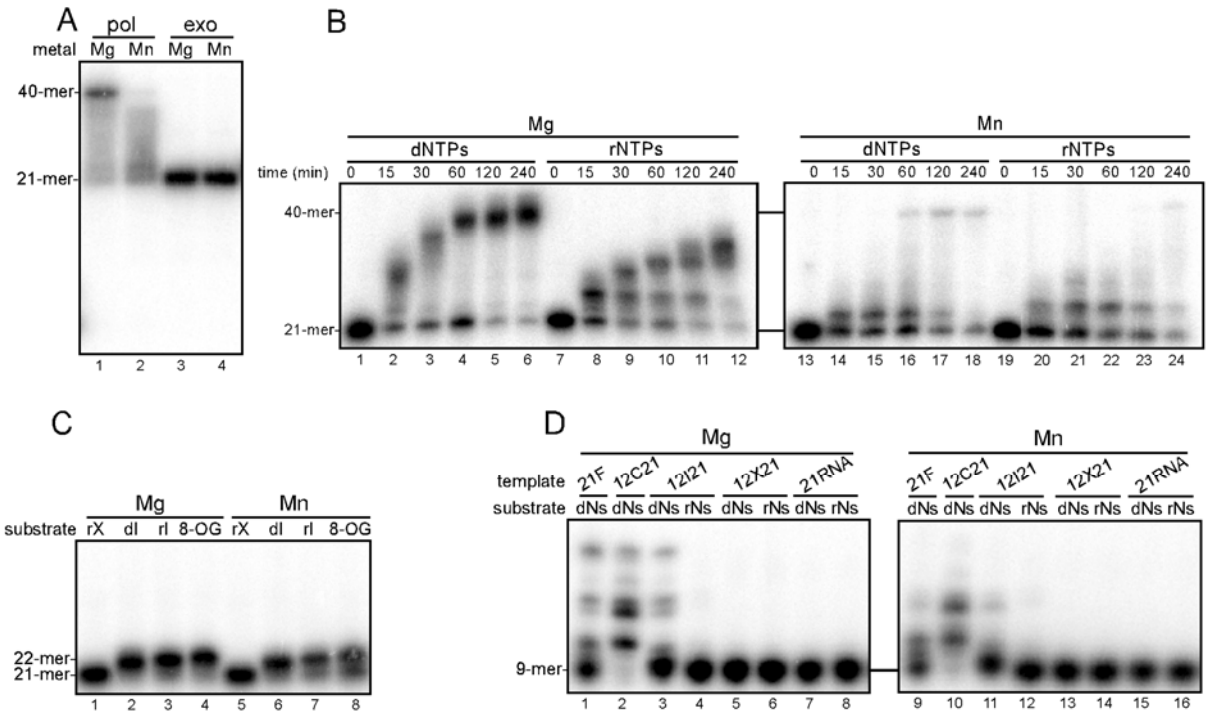

Figure 5. Mg^{2+}- and Mn^{2+}-dependent polymerase activity of the POLXc (1-379). The measurement conditions were the same as given in Fig. 4 except for the use of POLXc (1-379). In these assays, 5 mM $MgCl_2$ or 1 mM $MnCl_2$ was used as a cofactor. (A) Metal ion dependence of the activities. (B) Time course analysis of polymerase activity. (C) Single nucleotide insertion opposite dC. (D) TLS and RT assays.

Stimulation of polymerase activity by Zn^{2+} ions

Although the majority of DNA polymerases exhibit a Mg^{2+}- or Mn^{2+}-dependent DNA polymerase activity, it has been reported that the DNA polymerase from avian myeloblastosis virus has a Zn^{2+}-dependent DNA polymerase activity (Prabhudas *et al*., 1978). Hence, in the present study, the presence of a Zn^{2+}-dependent DNA polymerase activity in ttPolX was tested. I found that ttPolX had a high Zn^{2+}-dependent DNA polymerase activity (Fig. 6A), even in the presence of 100 mM KCl at pH 7.5, although ttPolX showed a higher Mg^{2+}-dependent DNA polymerase activity in the presence of 20 mM KCl at pH 8.0 than in the presence of 100 mM KCl or at pH 7.5 (Figs. 4 and 6A). Moreover, the DNA polymerase activity of ttPolX was further stimulated in the presence of both Mg^{2+} and Zn^{2+} ions (Fig. 6A). I speculated that the mechanism for stimulation of polymerase activity was located in the POLXc domain; however, the PHP domain was not involved, because I also observed Zn^{2+}-dependent stimulation of DNA polymerase activity in the presence of POLXc (1-316) (Fig. 6B). ttPolI also exhibited Zn^{2+}-dependent DNA polymerase activity; however, the activity was inhibited above 0.1 mM $ZnCl_2$ (Fig. 6C). Unlike ttPolX activity, the Mg^{2+}-dependent DNA polymerase activity of ttPolI was inhibited by Zn^{2+} ions (Fig. 6C).

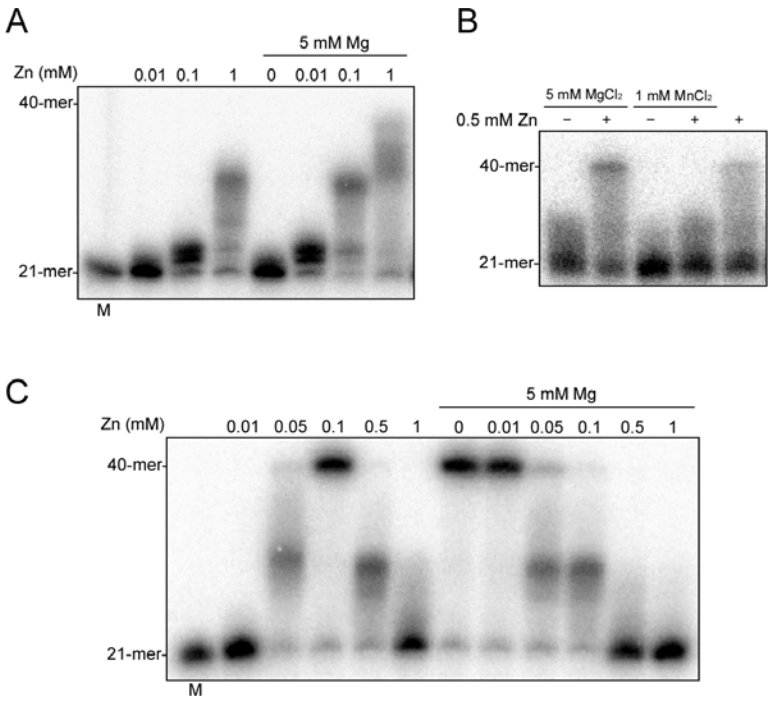

Figure 6. Zn^{2+}-dependent DNA polymerase activity of ttPolX and ttPolI. (A) Zn^{2+}-dependent DNA polymerase activity of ttPolX. Reaction mixtures containing 50 mM HEPES-NaOH, 100 mM KCl, metal ions, 100 μM dNTPs, 1 μM EDTA, 10 nM 21F/40T and 1 μM ttPolX, pH 7.5, were incubated at 37°C for 10 min. (B) Zn^{2+}-dependent DNA polymerase activity of POLXc (1-316). Reaction mixtures containing 50 mM Tris-HCl, 100 mM KCl, metal ions, 100 μM dNTPs, 5 μM EDTA 10 nM 21F/40T and 1 μM POLXc (1-316), pH 7.5, were incubated at 37°C for 10 min. (C) Zn^{2+}-dependent DNA polymerase activity of ttPolI. Reaction mixtures containing 50 mM HEPES-NaOH, 100 mM KCl, metal ions, 100 μM dNTPs, 1 μM EDTA, 10 nM 21F/40T and 100 nM ttPolI, pH 7.5, were incubated at 37°C for 30 s. The samples were analyzed by 20% denaturing PAGE (8 M urea) and autoradiography.

ttPolX has strong binding affinity for Mg^{2+}-dNTP in the absence of DNA

ttPolX is a highly distributive DNA polymerase which shows preferential activity for repair of 1-nt gaps over activity with primer/template DNA (Fig. 7). I found that ttPolX had little strand-displacement and misincorporation activities for 1-nt gapped DNA (Fig. 7B). SPR measurements showed ttPolX had strong affinity for Mg^{2+}-dNTP, regardless of the identity of the base (Fig. 8 and Table 1). The binding affinity of ttPolX for Mg-GTP was approximately two orders lower than for Mg^{2+}-dGTP. Compared to ttPolX, ttPolI showed much lower binding affinity for Mg^{2+}-dGTP (Table 1), which may reflect the substrate-binding order of each polymerase. The strong binding affinity of ttPolX for Mg^{2+}-dNTPs may be related to its ability to form a productive binary complex with Mg^{2+}-dNTPs in the absence of DNA.

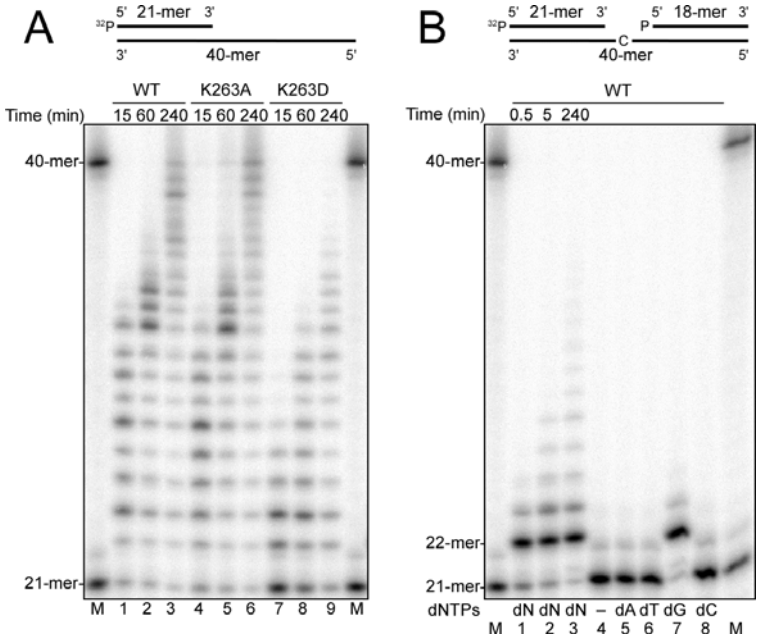

Figure. 7. DNA polymerase activity of ttPolX. (A) DNA polymerase activity for primer/template DNA. Reaction mixtures composed of 50 mM Tris-HCl, 20 mM KCl, 10 mM $MgCl_2$, 100 μg/ml BSA, 10 μM dNTPs, 10 nM primer/template DNA and 1 μM ttPolX (wild-type or mutants), pH 8.2 at 37°C were incubated for the indicated times. (B) DNA polymerase activity for 1-nt gapped DNA. Reaction mixtures composed of 50 mM Tris-HCl, 20 mM KCl, 10 mM $MgCl_2$, 100 μg/ml BSA, 10 μM dNTP, 10 nM 1-nt gapped DNA and 1 μM ttPolX wild-type, pH 8.2 at 37°C were incubated for the indicated times. Four dNTPs mixture (lanes 1-3) or single dNTP (lanes 5-8) were added to the reaction mixture. Lane 4 contained no dNTP. M represents marker lanes. The samples were analyzed by 20% (w/v) denaturing PAGE (8 M urea) and visualized by autoradiography using BAS2500.

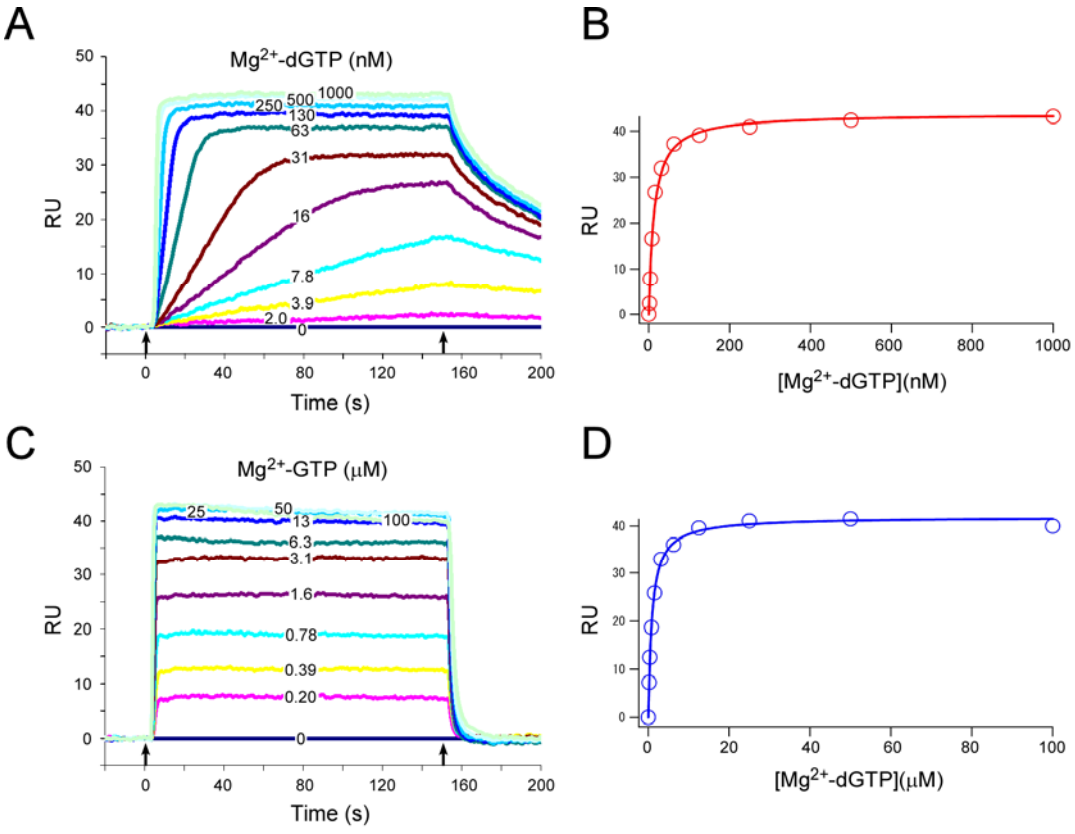

Figure 8. SPR analysis of the binding affinity of ttPolX and nucleotides. (A) SPR sensorgrams of the binding of Mg^{2+}-dGTP to ttPolX were obtained using the Biacore3000 system®. After equilibrating with running buffer, Mg^{2+}-dGTP was passed over the chip at a flow rate of 100 μl/min for 2.5 min (between arrowed points), followed by running buffer without dGTP, and then running buffer without Mg^{2+} to release nucleotides. (B) The averaged equilibrium points of RU were plotted against Mg^{2+}-dGTP concentrations and fitted using equation (4) (see *Materials and Methods*). (C) SPR sensorgrams of the binding of Mg^{2+}-GTP to ttPolX. (D) Averaged equilibrium points of RU were plotted against Mg^{2+}-GTP concentrations.

Table 1. Dissociation constants (K_d) of *T. thermophilus* DNA polymerases and nucleotides determined by SPR at 25°C.

		Analyte	n	K_d (nM)
ttPolX	Wild-type	Ca^{2+}-dGTP	4	26 ± 9.6
		Mg^{2+}-dGTP	6	12 ± 1.6
		Mg^{2+}-dCTP	5	6.6 ± 1.1
		Mg^{2+}-dATP	4	6.9 ± 1.1
		Mg^{2+}-dTTP	6	24 ± 1.8
		Mg^{2+}-GTP	3	1,100 ± 190
	K263A	Mg^{2+}-dGTP	4	58 ± 7.9
		Mg^{2+}-dCTP	4	25 ± 5.4
	K263D	Mg^{2+}-dGTP	4	260 ± 25
		Mg^{2+}-dCTP	4	220 ± 17
ttPolI		Mg^{2+}-dGTP	6	87,000 ± 18,000

Data represent the means of replicate experiments (n) ± standard deviation

Mechanism of 1-nt gap filling by ttPolX

To determine whether Mg^{2+}-dNTP-bound ttPolX was productive, I investigated the ttPolX reaction mechanism using steady-state kinetics with dead-end and product inhibition (Fig. 9; Tables 2, 3 and 4). First, the kinetic parameters for dGTP and DNA were determined in the absence of inhibitor (Figs. 9A and 9B; Table 2). The K_m value for dGTP (9.3 nM) (Table 2) was very low, as was the K_d value (12 nM) (Table 1). The K_m value for DNA (8.2 nM) was also low (Table 2) and was inconsistent with the K_d value (0.3 μM) obtained from an EMSA in the absence of dNTP (see Table 8). Second, I performed the kinetic analysis using dCTP as a dead-end inhibitor to identify the order of substrate binding. ttPolX showed similar binding characteristics to Mg^{2+}-dCTP and Mg^{2+}-dGTP (Table 1), but did not incorporate dCTP against a dC template (Fig. 7B). Therefore, dCTP was a good dead-end inhibitor. dCTP exhibited competitive inhibition for variable dGTP substrate (Fig. 9C) and had almost same K_i (14 nM) as K_m for dGTP (Table 2). Moreover, dCTP exhibited mixed inhibition for variable DNA substrate (Fig. 9D). These results suggested that dNTP was the first substrate to bind (Table 3) because S_1 and S_2 were able to be interpreted as dGTP and DNA in Table 3, respectively. The inhibition constants of dCTP for variable DNA substrate were high because the fixed dGTP concentration (10 μM) was high (Table 2). I could not distinguish between "dNTP-first" ordered Bi Bi and rapid equilibrium random Bi Bi mechanisms by the dead-end inhibition pattern using dCTP (Table 3). I therefore examined the effect of the product inhibitor PPi and found competitive inhibition for variable dGTP substrate (Fig. 9E) and mixed inhibition for variable DNA substrate with an unsaturated dGTP concentration (Fig. 9F). These results support a dNTP-first ordered Bi Bi mechanism (Table 2 and 4), namely, dGTP, DNA, and PPi correspond to S_1, S_2, and P_2 in Table 4, respectively.

Furthermore, the observation that PPi bound to ttPolX competitively with dGTP (Fig. 9E) indicated that PPi was released at the end of the reaction, a behavior pattern that differs from other DNA polymerases. Finally, I used the other product, nicked DNA, as the inhibitor (P_1) in order to further test the hypothesis of a dNTP-first ordered Bi Bi mechanism. Interestingly, nicked DNA exhibited mixed inhibition for variable dGTP substrate with an unsaturated DNA concentration (Fig. 9G) and competitive inhibition for variable DNA substrate (Fig. 9H and Table 2). This inhibition pattern is consistent with a Theorell-Chance mechanism (Table 4), which is a special type of ordered Bi Bi mechanism (Cleland *et al.*, 1963a). This reaction mechanism indicates that the steady-state concentrations of the ternary complexes were very low under the conditions used in the gap-filling assays with ttPolX, and that dNTP-bound ttPolX reacted with 1-nt gapped DNA in a "hit-and-run" fashion. This mechanism may be advantageous for filling 1-nt gaps.

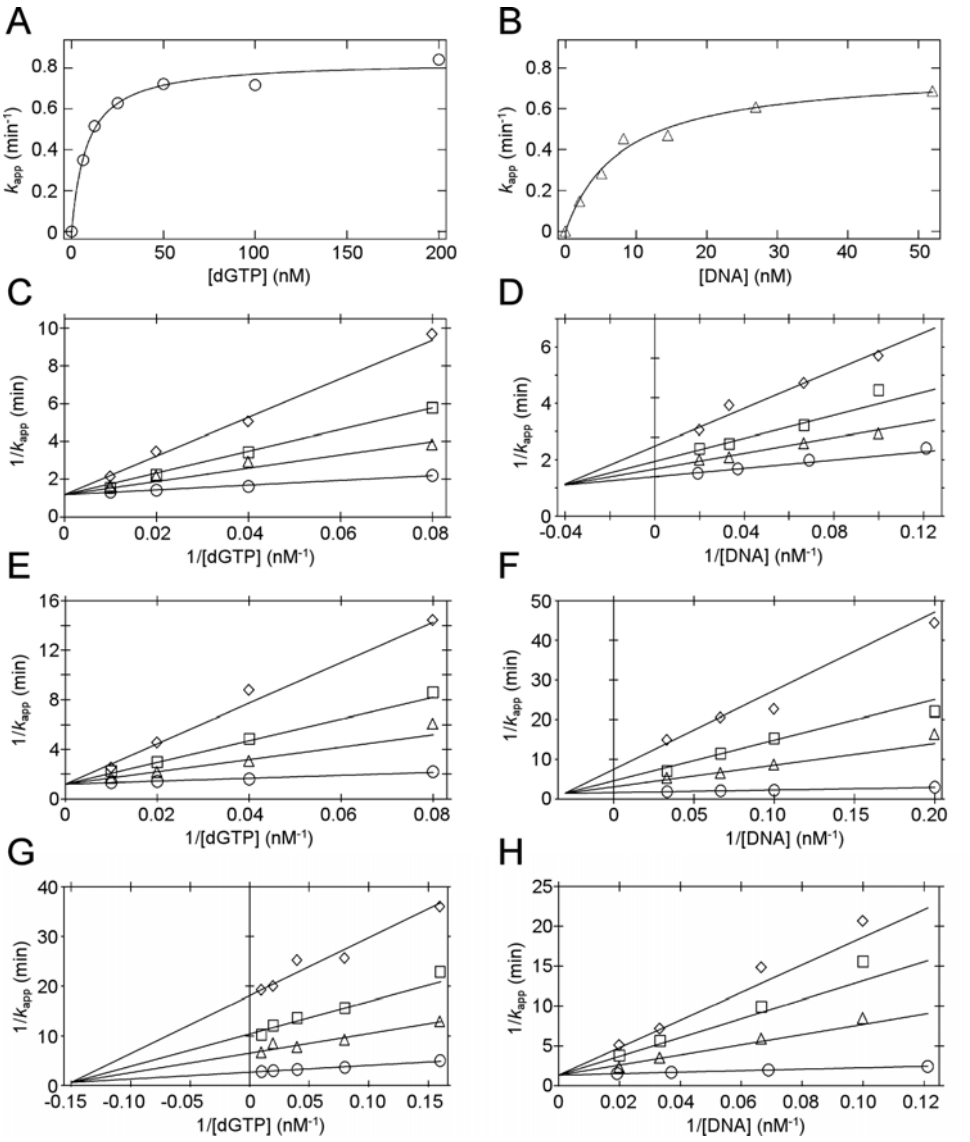

Figure 9. Dead-end and product inhibition of wild-type ttPolX during 1-nt gap filling with dGTP. Reaction mixtures were composed of 50 mM Tris-HCl, 100 mM KCl, 10 mM $MgCl_2$, 100 μg/ml BSA, dGTP, 1-nt gapped DNA and 0.5-1 nM ttPolX wild-type, pH 7.5 at 37°C. (A) Dependence of k_{app} on dGTP concentration using a fixed concentration of DNA (100 nM). The data were fitted with equation (1), as described in the *Materials and Methods*, to obtain the steady-state kinetic parameters of, k_{cat} and K_m. (B) Dependence of k_{app} on DNA concentration using a fixed concentration of dGTP (10 μM). (C) Double-reciprocal plots for dead-end inhibition assays performed using a fixed concentration of DNA (100 nM) and various concentrations of dGTP in the presence of 0 (○), 25 (△), 50 (□) and 100 (◇) nM dCTP as the mismatched substrate. (D) Double-reciprocal plots for dead-end inhibition assays performed using a fixed concentration of dGTP (10 μM) and various concentrations of DNA in the presence of 0 (○), 5 (△), 10 (□) and 20 (◇) μM dCTP. (E) Double-reciprocal plots for product inhibition assays with 100 nM DNA and various concentrations of dGTP in the presence of 0 (○), 50 (△), 100 (□) and 200 (◇) μM PPi. (F) Double-reciprocal plots for product inhibition assays performed using an unsaturated concentration of dGTP (12.5 nM) and various concentrations of DNA in the presence of 0 (○), 50 (△), 100 (□) and 200 (◇) μM PPi. (G) Double-reciprocal plots for product inhibition assays performed using an unsaturated concentration of DNA (10 nM) and various concentrations of dGTP in the presence of 0 (○), 1 (△), 2 (□) and 4 (◇) μM nicked DNA. (H) Double-reciprocal plots for product inhibition assays performed using 10 μM dGTP and various concentrations of DNA in the presence of 0 (○), 2 (△), 4 (□) and 6 (◇) μM nicked DNA.

Table 2. Inhibition patterns and steady-state kinetic parameters of wild-type ttPolX during 1-nt gap filling with dGTP.

Inhibitor	Variable substrate	Fixed substrate	Inhibition pattern	k_{cat} (min^{-1}) [a]	K_m (nM) [a]	K_i (μM) [a]	K_i' (μM) [a]
None	dGTP	DNA		0.83 ± 0.11[b]	9.3 ± 1.4[b]		
	DNA	dGTP		0.77 ± 0.078[c]	8.2 ± 0.31[c]		
dCTP	dGTP	DNA	Competitive	0.85 ± 0.034	11 ± 1.9	0.014 ± 0.0023	
	DNA	dGTP	Mixed	0.73 ± 0.017	6.3 ± 0.60	7.3 ± 1.3	24 ± 2.9
PPi	dGTP	DNA	Competitive	0.84 ± 0.022	10 ± 1.1	16 ± 1.5	
	DNA	dGTP (unsaturation)[d]	Mixed	0.62 ± 0.012	4.0 ± 0.31	6.8 ± 0.80	56 ± 9.6
Nicked DNA	dGTP	DNA (unsaturation)[d]	Mixed	0.37 ± 0.0054	5.1 ± 0.36	0.53 ± 0.095	0.69 ± 0.035
	DNA	dGTP	Competitive	0.76 ± 0.023	7.1 ± 0.84	0.35 ± 0.033	

[a]Errors associated with global fitting are shown as standard deviations.
[b]Means of 4 experiments ± standard deviations.
[c]Means of 5 experiments ± standard deviations.
[d]Unsaturated concentrations of substrates were determined by their K_m values.

Table 3. Identification of the reaction mechanism of a two-substrate enzyme by dead-end inhibition (Cleland, 1963b).

Mechanism	Enzyme species bound by inhibitor	Inhibition type for variable S_1	Inhibition type for variable S_2
Ordered Bi Bi	E	Competitive	Mixed
	ES_1	Uncompetitive	Competitive
Ping pong Bi Bi	E	Competitive	Uncompetitive
	ES_1	Uncompetitive	uncompetitive
Rapid equilibrium random	E	Competitive	Competitive
	$E+ES_1$	Mixed	Competitive
	$E+ES_2$	Competitive	Mixed

Table 4. Identification of the reaction mechanism of a two-substrate enzyme by product inhibition (Cleland, 1963a)**.**

Mechanism	Inhibitor	Variable substrate: S_1		Variable substrate: S_2	
		Unsaturated S_2	Saturated S_2	Unsaturated S_1	Saturated S_1
Ordered Bi Bi	P_1	Mixed	Uncompetitive	Mixed	Mixed
	P_2	Competitive	Competitive	Mixed	–[a]
Theorell-Chance	P_1	Mixed	–[a]	Competitive	Competitive
	P_2	Competitive	Competitive	Mixed	–[a]
Rapid equilibrium random Bi Bi	P_1	Competitive	–[a]	Competitive	–[a]
	P_2				
Ping pong Bi Bi	P_1	Mixed	–[a]	Competitive	Competitive
	P_2	Competitive	Competitive	Mixed	–[a]

[a]No inhibition

ttPolX can form both *syn*-dGTP and *anti*-dGTP binary complexes

Next, I investigated the implications of a Theorell-Chance mechanism on the crystal structures associated with ttPolX. I compared the crystal structures of ttPolX with Ca-dGTP at 1.4 Å (binary complex) against 1-nt gapped DNA and ddGTP at 2.7 Å (ternary complex) (Figs. 10, 11A and 11B; Table 5). These two complexes are thought to be the first and second intermediates of the ttPolX gap-filling reaction pathway. ttPolX has POLXc and PHP domains; these domains have also been identified in the crystal structure of *Deinococcus radiodurans* PolX (Leulliot *et al*., 2009). The POLXc domain has four subdomains: 8-kDa, fingers, palm and thumb (Figs. 11A, 11B and 12). Two Ca ions, derived from the crystallization reagent, were present in the polymerase active site of the binary complex (Fig. 13). The binding affinities for Ca-dGTP and Mg^{2+}-dGTP were similar despite the fact that Ca is not an active cofactor for the polymerase activity of ttPolX (Table 1). The 8-kDa subdomain bound to downstream DNA and 1-nt gapped DNA was bent (Fig. 11B, black arrow). These two binary and ternary complexes showed good superposition in the palm, thumb and PHP domains (Fig. 11C). The N-terminal 8-kDa and fingers subdomains were shifted by binding to DNA, implying N-terminal flexibility.

Comparison of the active sites in the binary and ternary complexes showed they have similar structures (Fig. 11D). The site for polymerase activity in ttPolX has three conserved Asp residues (D198, D200 and D243) and two metal ions, similar to Polβ (Fig. 14A), indicating that ttPolX has the standard two-metal-ion mechanism for polymerase activity. I found that dGTP conformations were different between the binary and ternary complexes (Fig. 11D). The spatial relationship between ribose and the nucleoside base can be

classified into *syn* or *anti* conformations. Under the IUPAC definition, the conformation is deemed to be *syn* when the N-glycosidic angle χ of the nucleoside is 0 ± 90° and to be *anti* when the angle is 180 ± 90°. I found an N-glycosidic angle of 77.17° for dGTP in the binary complex, i.e., a *syn* conformation. In contrast, the incoming ddGTP in the ternary complex was in the *anti* conformation, like all nucleotides in A- and B-DNA (Fig. 11D). This difference was also observed when I compared the binary complex of ttPolX with the ternary complexes of Polβ with 1-nt gapped DNA or with ttPolX with primer/template DNA (Fig. 14). Detailed analysis of the residual density map revealed that the dGTP in the binary complex was also in the *anti* conformation (Fig. 11E) and its glycosidic angle was similar to that of ddGTP (*anti*) in the ternary complex (Fig. 11D). Assuming that the crystallographic B-factors are the same in both *syn* and *anti* conformations of dGTP, occupancy of *syn* and *anti* conformations was approximately 0.64 and 0.36, respectively. Thus, the conformation of the nucleotides changed from *syn* to *anti* in the presence of DNA. It is possible that the binding to nucleotides in the *syn* conformation may be related to the strong and productive binding in the absence of DNA.

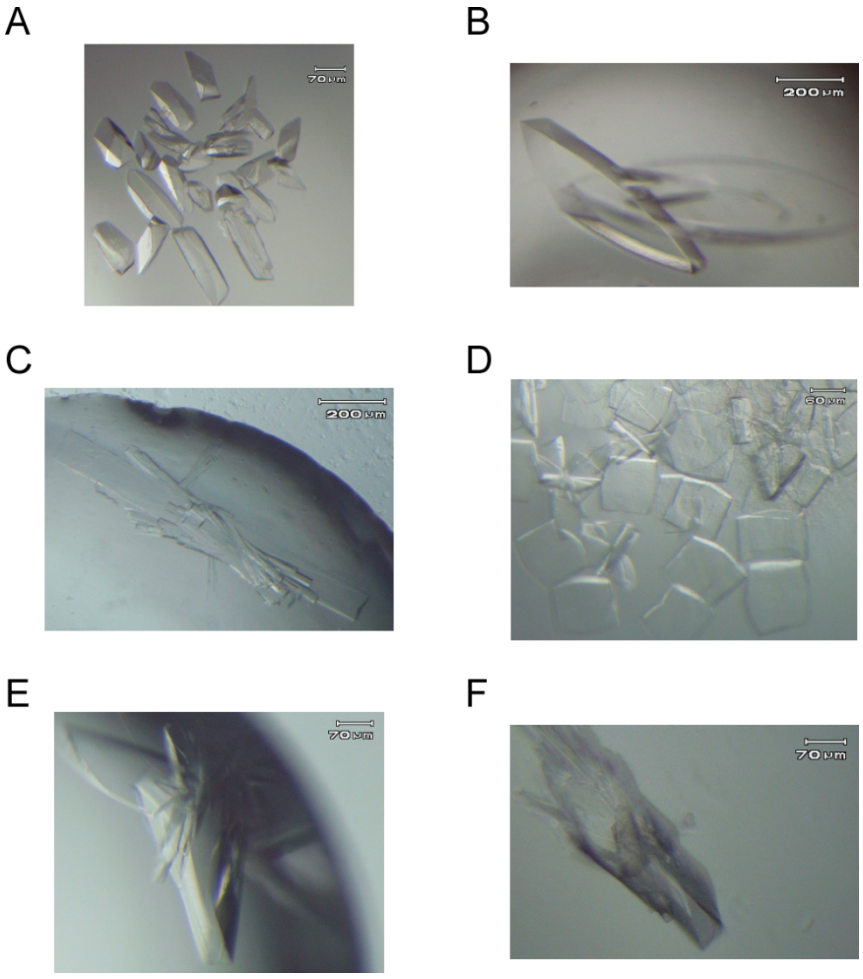

Figure 10. Crystals using for X-ray crystallography. (A) Selenomethionyl ttPolX complexed with Ca-dGTP. (B) Wild-type ttPolX complexed with Ca-dGTP. (C) Wild-type ttPolX complexed with primer/template DNA and Mg-ddGTP. (D) Wild-type ttPolX complexed with 1-nt gapped DNA and Mg-ddGTP. (E) K263A mutant complexed with Ca-dGTP. (F) K263D mutant complexed with Ca-dGTP. The scale bar is represented at the upper right.

Table 5. Data collection and refinement statistics

	Wild-type Ca-dGTP (binary complex)	SeMet (Ca-dGTP)		Primer /template DNA + ddGTP	1-nt gapped DNA + ddGTP (ternary complex)	K263A mutant (Ca-dGTP)	K263D mutant (Ca-dGTP)
Data collection[a]							
X-ray source	BL26B2 at SPring-8	BL26B2 at SPring-8		BL26B2 at SPring-8	BL26B2 at SPring-8	BL26B2 at SPring-8	BL26B2 at SPring-8
Space group	$P2_1$	$P2_1$		$P4_32_12$	$P2_12_12_1$	$P2_1$	$P2_1$
Cell dimensions							
a, b, c (Å)	69.2, 53.3, 84.9	68.6, 54.5, 85.0		80.2 80.2, 268.6	95.4 96.9 143.4	69.1, 53.2, 84.9	68.9, 53.2, 84.9
α, β, γ (°)	90.0, 107.5, 90.0	90.0, 105.2, 90.0		90.0, 90.0, 90.0	90.0 90.0 90.0	90.0, 107.7, 90.0	90.0, 107.7, 90.0
		Peak	*Inflection*				
Wavelength	1.000	0.9790	0.9793	1.000	1.000	1.000	1.000
Resolution (Å)	50-1.40 (1.42-1.40)	50-1.80 (1.86-1.80)	50-1.80 (1.86-1.80)	50-3.3 (3.42-3.3)	50-2.70 (2.75-2.70)	50-1.36 (1.38-1.36)	50-1.45 (1.48-1.45)
R_{merge}	0.043 (0.256)	0.079 (0.328)	0.077 (0.512)	0.065 (0.2)	0.136 (0.567)	0.044 (0.258)	0.040 (0.322)
$I/\sigma I$	52.2 (6.6)	34.3 (5.7)	31.7 (3.6)	36.7 (6.2)	15.6 (3.5)	26.6 (4.0)	29.1 (3.1)
Completeness (%)	98.5 (97.2)	99.7 (99.4)	99.7 (99.7)	99.3 (98.1)	100 (100)	99.6 (99.6)	99.7 (100)
Redundancy	7.5 (6.8)	7.1 (6.2)	6.9 (5.6)	11.5 (7.7)	7.4 (7.3)	3.7 (3.6)	3.7 (3.7)
Refinement							
Resolution (Å)	80.94-1.40			76.82-3.30	50.0-2.70	50.0-1.36	50-1.45
No. reflections	108638			13885	37064	118839	98308
R_{work} / R_{free}	0.162/0.188			0.256/0.319	0.241/0.293	0.171/0.198	0.175/0.205
No. atoms							
Protein	4531			4425	9001	4536	4539
DNA	0			346	1178	0	
Ligand/ion	39			42	66	38	37
Water	622			26	134	551	521
B-factors							
Protein	20.8			83.8	33.1	19.7	20.7
DNA				79.8	44.8		
Ligand/ion	18.2			80.0	15.1	15.9	16.7
Water	30.7			45.2	22.7	27.1	28.1
R.m.s deviations							
Bond lengths (Å)	0.011			0.014	0.006	0.010	0.012
Bond angles (°)	1.38			1.63	1.14	1.38	1.50
Ramachandran plot							
Most favored (%)	93.7			82.8	90	93.3	92.7
Additional allowed (%)	5.9			16.1	9.1	6.3	6.7
Generously allowed (%)	0.4			1	0.9	0.4	0.6
Disallowed (%)	0			0	0	0	0
PDB ID	3AU2			3AU6	3AUO	3B0X	3B0Y

[a]One crystal was used for each data set.

Values in parentheses are for the highest-resolution shell.

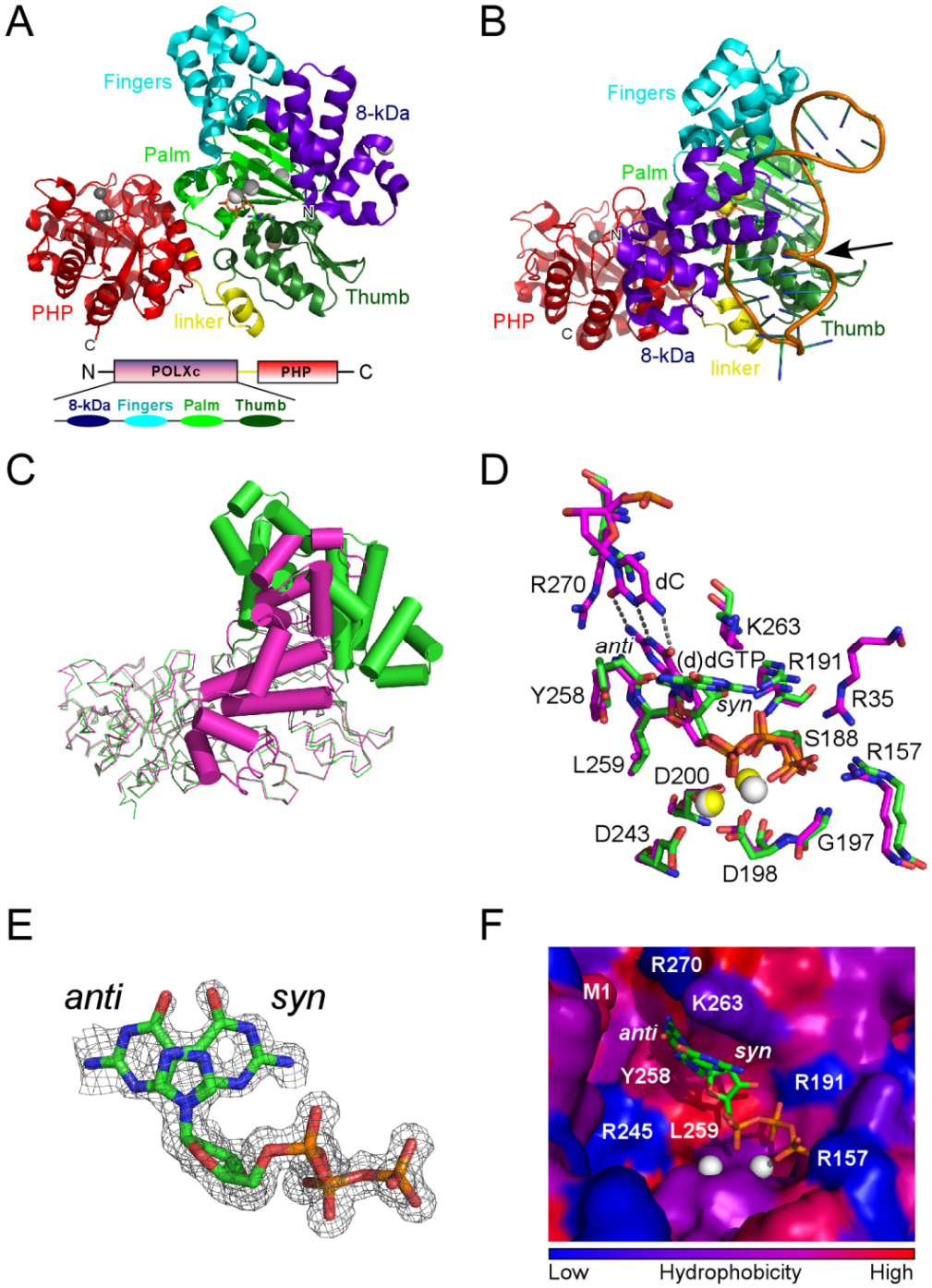

Figure 11. Overall and active site structures of the binary and ternary complexes. (A) The binary complex of ttPolX and Ca-dGTP has four POLXc subdomains [8-kDa (purple blue, residues 1-87), fingers (cyan, 88-157), palm (light green, 158-247), thumb (dark green, 248-316)], linker (yellow, 317-335) and PHP (red, 336-575) (see also Fig. 12). (B) The ternary complex of ttPolX with 1-nt gapped DNA and ddGTP. The black arrow indicates the template strand bend. (C) Superposition of the binary (green) and ternary (magenta) complexes of panels A and B. The DaliLite program (Holm *et al.*, 2000) was used to perform superposition of the palm and thumb subdomains. The cylinders in the 8-kDa and fingers subdomains represent α helices. (D) Superposition of the polymerase active site residues shown in panel C. (E) The F_{obs}-F_{calc} omit map of dGTP in the wild-type binary complex is contoured at 2 σ as a gray mesh. (F) Hydrophobicity and surface profiles of the active site of the binary complex. Red and blue indicate hydrophobic and hydrophilic regions, respectively. Amino acid hydrophobicity is colored in accordance with the normalized consensus hydrophobicity scale (Eisenberg *et al.*, 1984). White, yellow and gray spheres are Ca, Mg and Zn ions, respectively. *Syn* and *anti* conformations of dGTP in the binary complex are shown in superposition in panels E and F.

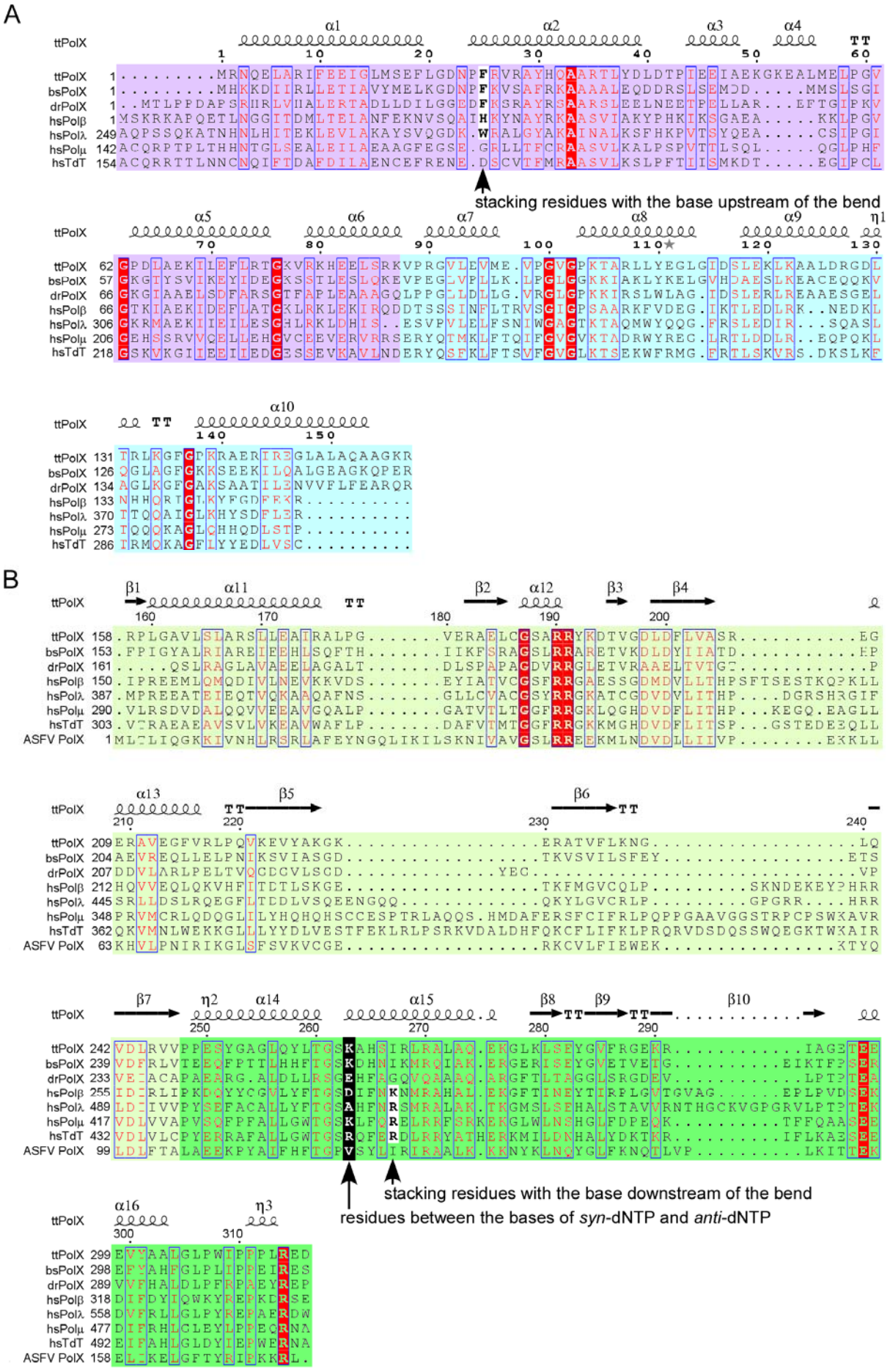
A
ttPolX
bsPolX
drPolX
hsPolβ
hsPolλ
hsPolμ
hsTdT
stacking residues with the base upstream of the bend
B
ASFV PolX
stacking residues with the base downstream of the bend
residues between the bases of syn-dNTP and anti-dNTP

Figure. 12. Sequence alignments of POLXc domains of representative PolXs. (A) Alignment of the 8-kDa and fingers subdomains. (B) Alignment of the palm and thumb subdomains. Residues in white and highlighted in black show the important residues for *syn-anti* equilibrium of the incoming nucleotide. Residues in black and highlighted in white show stacking residues around the bend. The abbreviations are as follows: ttPolX, *Thermus thermophilus* HB8 PolX; bsPolX, *Bacillus subtilis* PolX; drPolX, *Deinococcus radiodurans*; hsPolβ, *Homo sapiens* Polβ; hsPolλ, *H. sapiens* Polλ; hsPolμ, *H. sapiens* Polμ; hsTdT, *H. sapiens* terminal deoxynucleotidyl transferase; and ASFV PolX, African swine fever virus PolX. The sequence accession numbers are: YP_144416 for ttPolX, NP_390737 for bsPolX, NP_294190 for drPolX, NP_002681 for hsPolβ, NP_037406 for hsPolλ, NP_037416 for hsPolμ, NP_004079 for hsTdT, and NP_042790 for ASFV PolX. Sequence domains are highlighted using the same color scheme as in Figure 11. Multiple alignments were calculated by ClustalW2 (Chenna *et al*., 2003) and displayed by ESPript (Gouet *et al*., 2003). The represented secondary structure derives from the ttPolX binary complex. The notations in the figure are as follows: α, α-helix, β, β-sheet, TT, strict β-turn, and η, 3_{10} helix.

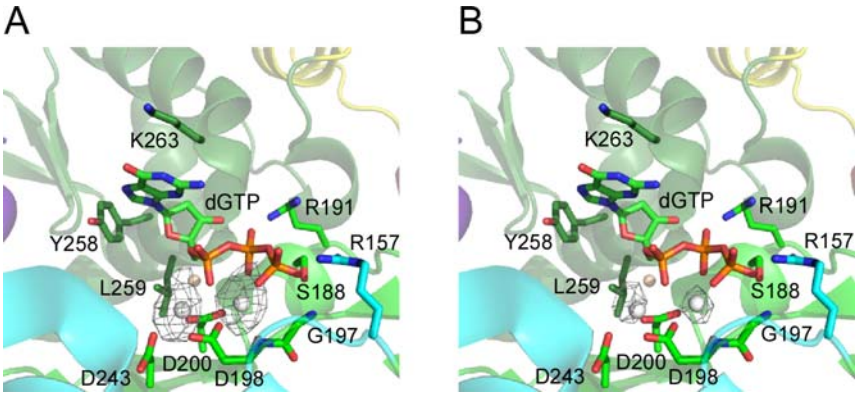

Figure 13. Ca sites in the POLXc domain active site of the binary complex. Electron density maps (anomalous difference Fourier maps) were generated from data collected at 1.8 Å (f'' is 1.7) (panel A) and 1 Å (f'' is 0.6) (panel B). All electron densities are contoured at 3 σ. White and light brown spheres are Ca and Cl ions, respectively.

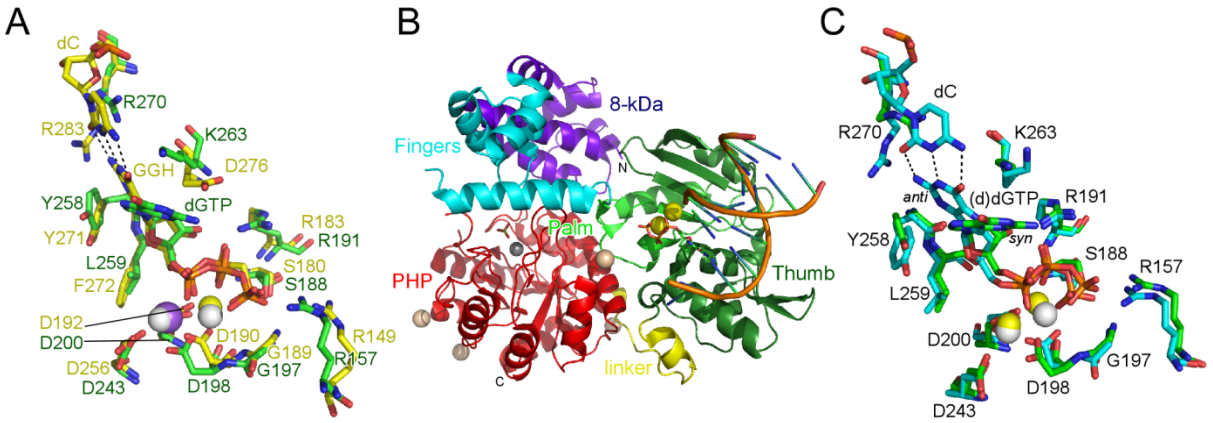

Figure. 14. Comparison of the polymerase active sites of the ttPolX binary complex and of ternary complexes. (A) Superposition of the polymerase active sites of the ttPolX binary complex (green) and the Polβ ternary complex (yellow). The structure of the Polβ ternary complex contains 1-nt gapped DNA and a dGTP analog, 2'-deoxyguanosine 5'-β,γ-methylene triphosphate (GGH) (Sucato *et al.*, 2007). The residues and residue numbers are shown as green (ttPolX binary complex) and yellow (Polβ). The DaliLite program (Holm *et al.*, 2000) was used to perform the structure superposition of palm and thumb subdomains. (B) Overall structure of ttPolX with primer/template DNA and ddGTP. In the illustrated complex, the N-terminal direction appears to be an artifact of crystallization due to binding between the 8-kDa subdomain and the next symmetric template 3'-end. (C) Superposition of the polymerase active sites of the ttPolX binary complex (green) and the complex with primer/template and ddGTP (cyan). White, yellow, gray, light brown and purple spheres are Ca, Mg, Zn, Cl and Na ions, respectively.

Lys-263 controls binding affinity and conformation of dGTP

Mutational studies indicated that Lys-263 was essential for the strong binding to Mg^{2+}-dNTPs (Table 1). Lys-263 is located between the bases of *syn*-dGTP and *anti*-dGTP and appears to stack with bases in the *syn* conformation (Figs. 11D and 11F). The K263A and K263D mutants had a 4- to 20-fold lower binding affinity, respectively, for Mg^{2+}-dNTP than the wild-type enzyme. The positive charge on the long side chain of Lys at this position may provide additional stabilization of Mg^{2+}-dNTPs compared to Ala. Lysine (or similar residue) is widely conserved at this position in ttPolX, for example, bacterial and archaeal PolXs, human DNA polymerase μ (Lys-438) and human TdT (Arg-453) (Banos *et al*., 2008a) (Fig. 12B). This conservation implies that strong binding to Mg^{2+}-dNTPs is a common strategy among PolXs. The observation that a negatively charged residue at this position (Asp-263 in the K263D mutant) weakened the binding affinity for Mg^{2+}-dNTPs is consistent with the mutation analysis of Polβ (Berg *et al*., 2001). Polβ has an Asp at this position and is thus different from other PolXs (Fig. 12B), although its other active site residues are similar to those of ttPolX (Fig. 14A). The residue at position 263 may control binding affinity for Mg^{2+}-dNTPs, and thus may provide different properties among PolXs with respect to processivity, selectivity and substrate-binding order.

I compared the ttPolX crystal structures of wild-type, K263A and K263D mutants in complex with Ca-dGTP (Table 5). The three structures were similar except for residue 263 and dGTP conformation (Fig. 15A). In the wild-type structure, Lys-263 had higher average B-factors (24.2 $Å^2$, side chain) than other active site residues, implying that Lys-263 did not prevent conformational change of dGTP (Figs. 11E and 11F). dGTP bound to K263A was in the *anti* conformation (Figs. 15A and 15B). dGTP bound to K263D appeared to be prevented from flipping by Asp-263, and was in the *syn* conformation (Figs. 15A and 15C). Moreover, Asp-263, together with Arg-270, stably held two water molecules (W1 and W2) (Fig. 16C). These two water molecules were also held by Arg-270 and main chain of Lys-263 in the wild-type (Fig. 16A), but there were fewer and longer hydrogen bonds between the wild-type and two water molecules (W1 and W2, hydrogen-bonding distances of 3.1. 3.0 and 2.9 Å) compared to K263D (hydrogen-bonding distances of 3.0, 2.9, 2.8 and 2.7 Å). K263A also had two water molecules; however, the hydrogen bond between W2 and ttPolX was absent in K263A (Fig. 16B). Furthermore, W3 in the wild-type and W1 in the K263D were close to *anti*-dGTP (Figs. 16A and 16C). These differences may affect the hydrophilic environment around *anti*-dGTP. The hydrophobic guanine moiety of *anti*-dGTP

may be rejected by the hydrophilic environment in the absence of DNA. When DNA was bound, the bound dNTP was in the *anti* conformation, Arg-270 was directed to the other side, and the water molecules held by Arg-270 were released (Fig. 11D). In the K263A structure, there was a weak hydrophilic environment around the *anti*-dGTP and no obvious interaction between Ala-263 and *syn*-dGTP (Fig. 16B). The *syn-anti* equilibrium may be biased towards *anti* in the K263A structure by these factors. Taken together, our observations indicate that Lys-263 may flexibly control the *syn-anti* equilibrium of dGTP bound to ttPolX.

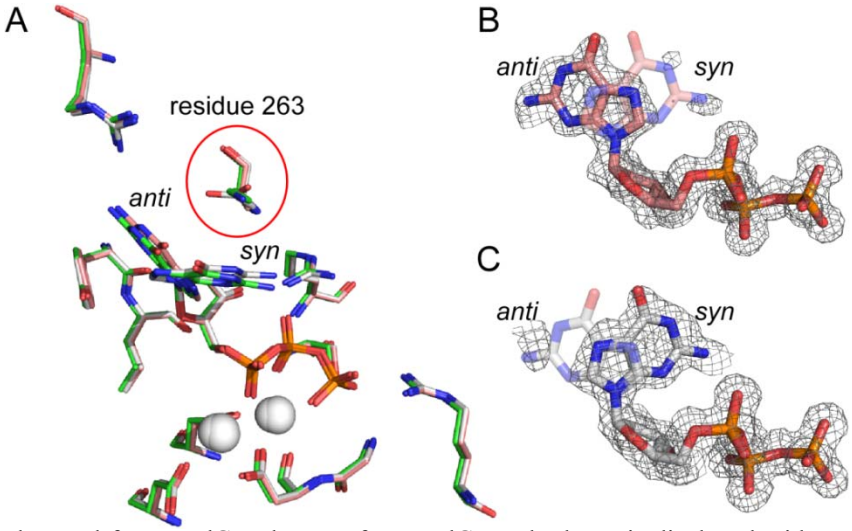

Figure 15. Structure of the polymerase active sites of Lys-263 mutants. (A) Superposition of the polymerase active site residues of the wild-type (green), K263A (pink) and K263D (white) binary complexes. dGTPs are shown as *syn* and *anti* (wild-type), *anti* (K263A) and *syn* (K263D) conformations. White spheres are Ca ions. (B) The F_{obs}-F_{calc} omit map of dGTP in the K263A structure is contoured at 2 σ as a gray mesh. Electron density was clearly observed for *anti*-dGTP but not for *syn*-dGTP; the latter is displayed with a semitransparent appearance. (C) The F_{obs}-F_{calc} omit map of dGTP in the K263D structure is contoured at 2 σ as a gray mesh. Electron density was clearly observed for *syn*-dGTP but not for *anti*-dGTP; the latter is displayed with a semitransparency appearance.

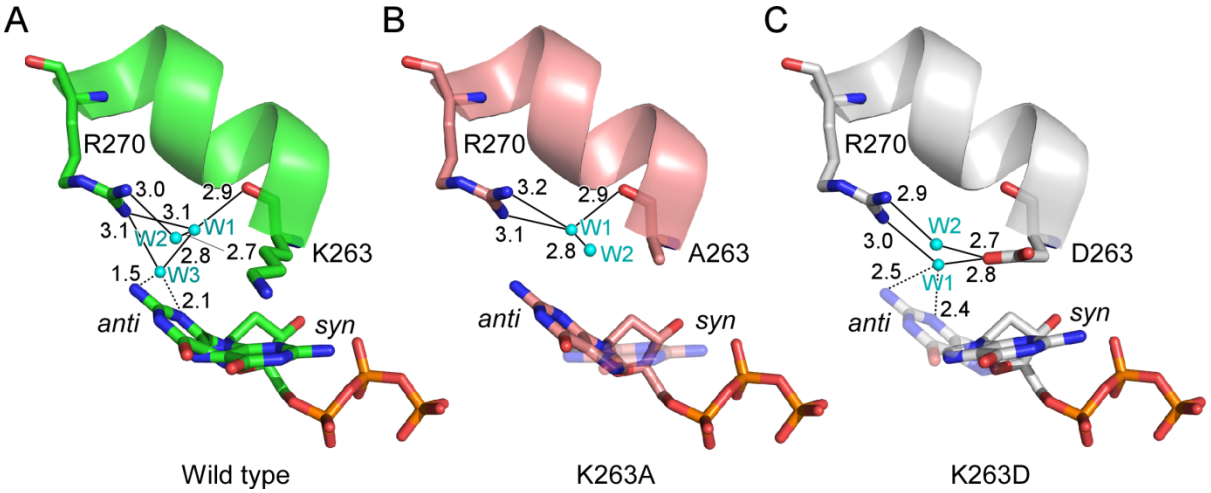

Figure 16. Arrangement of water molecules around *anti*-dGTPs. Three water molecules (W1, W2 and W3) are present around *anti*-dGTPs of wild-type (A), K263A (B) and K263D (C) structures; water molecules are shown in cyan. Solid lines represent hydrogen bonds within a 3.2 Å diameter around the water molecules. Dashed lines represent clashes (wild-type) or possible hydrogen bonds (K263D) with *anti*-dGTP. The numbers along the lines represent distances in Å. W3 can only be placed when *anti*-dGTP is not present, because the distance between W3 and *anti*-dGTP is otherwise too short (≤ 2.2 Å). *syn*-dGTP and *anti*-dGTP are shown as semitransparent in the K263A and K263D structures, respectively.

Influence of residue 263 on the kinetic mechanism for filling 1-nt gaps

Since Lys-263 mutants had a different binding strategy for dGTP and lower binding affinity than the wild-type (Fig. 16 and Table 1), I examined the reaction mechanism of the mutants (Figs. 17 and 18; Tables 6 and 7). Both K263A and K263D showed distributive polymerase activity similar to that of the wild-type (Fig. 7A). The K_m value for dGTP was increased in both mutants (K263A, 24 nM; K263D, 260 nM); however, the K_m for DNA of K263A (11 nM) was similar to that of the wild-type, whereas that of K263D was slightly increased (41 nM), indicating that residue 263 was not involved in DNA binding. The k_{cat} and K_m values for DNA of K263A (0.89 min^{-1} and 11 nM) were similar to those of the wild-type (0.77 min^{-1} and 8.2 nM) (Fig. 17; Tables 2 and 6). Thus, the *anti*-dGTP (Fig. 16B) did not prevent DNA binding and catalysis. The decrease of k_{cat} of K263D (0.48 min^{-1} for dGTP and 0.46 min^{-1} for DNA) (Fig. 18; Tables 2 and 7) may indicate that the conformational change of the incoming nucleotide from *syn* to *anti* was directly involved in the catalysis step. The kinetic differences between the wild-type and mutants suggest that the ability of Lys-263 to bind to both *syn*- and *anti*-dGTP contributed to the binding affinity for Mg^{2+}-dGTP without decreasing the k_{cat} value (Tables 2, 6 and 7).

The decreased binding affinity of the mutants for Mg^{2+}-dNTP raised the possibility that the substrate-binding order was altered by mutation of residue 263. However, dead-end and product inhibition assays revealed that the reaction mechanism for filling 1-nt gaps of the mutants was similar to that of the wild-type (Figs. 17 and 18; Tables 6 and 7). The K_i values of dCTP were increased in proportion to the K_m for dGTP, because ttPolX bound to Mg^{2+}-dCTP with almost the same affinity as to Mg^{2+}-dGTP (Table 1). The inhibition constants of the mutants for PPi and nicked DNA were similar to those of the wild-type (Tables 2, 6 and 7). Therefore, it was likely that residue 263 was involved in the interaction between ttPolX and the base of incoming nucleotide.

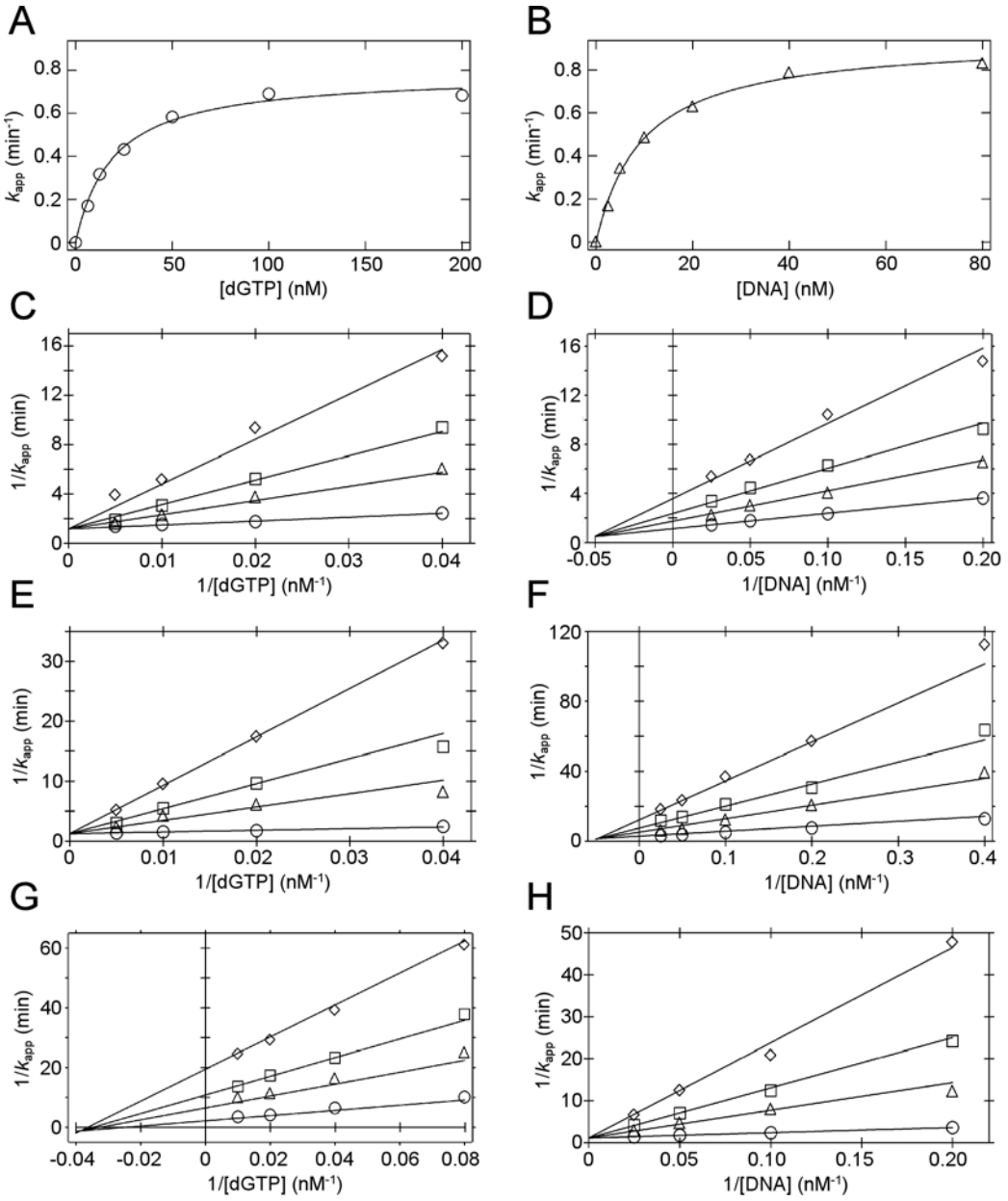

Figure 17. Dead-end and product inhibition of K263A during 1-nt gap filling with dGTP. Reaction mixtures were composed of 50 mM Tris-HCl, 100 mM KCl, 10 mM $MgCl_2$, 100 μg/ml BSA, dGTP, 1-nt gapped DNA, 0.5-2 nM K263A, pH 7.5 at 37°C. (A) Dependence of k_{app} on dGTP concentration using a fixed concentration of DNA (150 nM). The data was fitted with equation (1), as described in the *Materials and Methods*, to obtain the steady-state kinetic parameters of, k_{cat} and K_m. (B) Dependence of k_{app} on DNA concentration using a fixed concentration of dGTP (10 μM). (C) Double-reciprocal plots for dead-end inhibition assays performed using a fixed concentration of DNA (150 nM) and various concentrations of dGTP in the presence of 0 (○), 25 (△), 50 (□) and 100 (◇) nM dCTP, which is a mismatched substrate. (D) Double-reciprocal plots for dead-end inhibition assays performed using a fixed concentration of dGTP (10 μM) and various concentrations of DNA in the presence of 0 (○), 5 (△), 10 (□) and 20 (◇) μM dCTP. (E) Double-reciprocal plots for product inhibition assays performed using 150 nM DNA and various concentrations of dGTP in the presence of 0 (○), 50 (△), 100 (□) and 200 (◇) μM PPi. (F) Double-reciprocal plots for product inhibition assays performed using an unsaturated concentration of dGTP (25 nM) and various concentrations of DNA in the presence of 0 (○), 50 (△), 100 (□) and 200 (◇) μM PPi. (G) Double-reciprocal plots for product inhibition assays performed using an unsaturated concentration of DNA (10 nM) and various concentrations of dGTP in the presence of 0 (○), 1 (△), 2 (□) and 4 (◇) μM nicked DNA. (H) Double-reciprocal plots for product inhibition assays performed using 10 μM dGTP and various concentrations of DNA in the presence of 0 (○), 2 (△), 4 (□) and 6 (◇) μM nicked DNA.

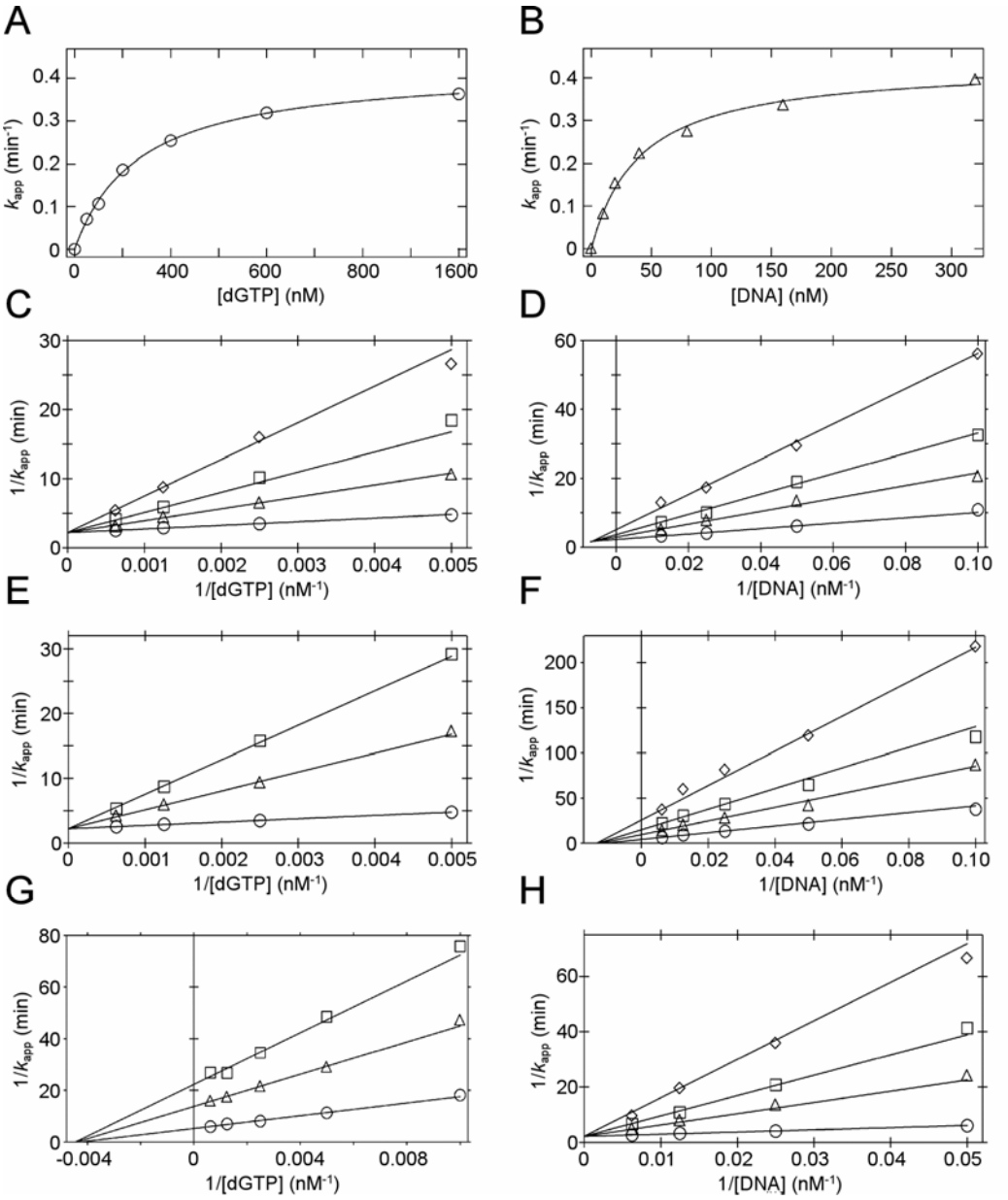

Figure 18. Dead-end and product inhibition of K263D during 1-nt gap filling with dGTP. Reaction mixtures were composed of 50 mM Tris-HCl, 100 mM KCl, 10 mM $MgCl_2$, 100 μg/ml BSA, dGTP, 1-nt gapped DNA, 1-20 nM K263D, pH 7.5 at 37°C. (A) Dependence of k_{app} on dGTP concentration using a fixed concentration of DNA (500 nM). The data was fitted with equation (1), as described in the *Materials and Methods*, to obtain the steady-state kinetic parameters, k_{cat} and K_m. (B) Dependence of k_{app} on DNA concentration using a fixed concentration of dGTP (10 μM). (C) Double-reciprocal plots for dead-end inhibition assays performed using a fixed concentration of DNA (500 nM) and various concentrations of dGTP in the presence of 0 (○), 25 (△), 50 (□) and 100 (◇) nM dCTP, which is a mismatched substrate. (D) Double-reciprocal plots for dead-end inhibition assays performed using a fixed concentration of dGTP (10 μM) and various concentrations of DNA in the presence of 0 (○), 5 (△), 10 (□) and 20 (◇) μM dCTP. (E) Double-reciprocal plots for product inhibition assays performed using 500 nM DNA and various concentrations of dGTP in the presence of 0 (○), 50 (△) and 100 (□) μM PPi. (F) Double-reciprocal plots for product inhibition assays performed using an unsaturated concentration of dGTP (200 nM) and various concentrations of DNA in the presence of 0 (○), 50 (△), 100 (□) and 200 (◇) μM PPi. (G) Double-reciprocal plots for product inhibition assays performed using an unsaturated concentration of DNA (40 nM) and various concentrations of dGTP in the presence of 0 (○), 2 (△) and 4 (□) μM nicked DNA. (H) Double-reciprocal plots for product inhibition assays performed using 10 μM dGTP and various concentrations of DNA in the presence of 0 (○), 2 (△), 4 (□) and 6 (◇) μM nicked DNA.

Table 6. Inhibition patterns and steady-state kinetic parameters of K263A during 1-nt gap filling with dGTP.

Inhibitor	Variable substrate	Fixed substrate	Inhibition pattern	k_{cat} (min^{-1}) [a]	K_m (nM) [a]	K_i (μM) [a]	K_i' (μM) [a]
None	dGTP	DNA		0.80 ± 0.062[b]	24 ± 5.3[b]		
	DNA	dGTP		0.89 ± 0.12[b]	11 ± 1.8[b]		
dCTP	dGTP	DNA	Competitive	0.86 ± 0.042	27 ± 5.0	0.038 ± 0.0061	
	DNA	dGTP	Mixed	0.89 ± 0.020	11 ± 0.68	5.2 ± 0.56	9.2 ± 0.82
PPi	dGTP	DNA	Competitive	0.81 ± 0.022	23 ± 2.5	15 ± 1.4	
	DNA	dGTP (unsaturation)[c]	Mixed	0.36 ± 0.0097	10 ± 0.73	15 ± 1.9	30 ± 3.5
Nicked DNA	dGTP	DNA (unsaturation)[c]	Mixed	0.46 ± 0.0076	40 ± 1.5	0.78 ± 0.075	0.51 ± 0.026
	DNA	dGTP	competitive	0.88 ± 0.010	11 ± 0.34	0.23 ± 0.057	

[a]Errors associated with global fitting are shown as standard deviations.
[b]Means of three experiments ± standard deviations.
[c]Unsaturated concentrations of substrates were determined from their K_m values.

Table 7. Inhibition patterns and steady-state kinetic parameters of K263D during 1-nt gap filling with dGTP.

Inhibitor	Variable substrate	Fixed substrate	Inhibition pattern	k_{cat} (min^{-1}) [a]	K_m (nM) [a]	K_i (μM) [a]	K_i' (μM) [a]
None	dGTP	DNA		0.48 ± 0.045[b]	260 ± 44[b]		
	DNA	dGTP		0.46 ± 0.046[b]	41 ± 4.1[b]		
dCTP	dGTP	DNA	Competitive	0.46 ± 0.085	240 ± 16	0.45 ± 0.026	
	DNA	dGTP	Mixed	0.45 ± 0.016	35 ± 2.8	7.3 ± 0.81	31 ± 8.0
PPi	dGTP	DNA	Competitive	0.44 ± 0.060	220 ± 11	10 ± 0.45	
	DNA	dGTP (unsaturation)[c]	Mixed	0.24 ± 0.0081	89 ± 6.0	24 ± 3.0	19 ± 2.0
Nicked DNA	dGTP	DNA (unsaturation)[c]	Mixed	0.19 ± 0.0027	240 ± 11	1.3 ± 0.16	1.2 ± 0.063
	DNA	dGTP	competitive	0.46 ± 0.010	36 ± 2.4	0.24 ± 0.013	

[a]Errors associated with global fitting are shown as standard deviations.
[b]Means of three experiments ± standard deviations.
[c]Unsaturated concentrations of substrates were determined from their K_m values.

DNA binding-residues of ttPolX

It is possible that other residues, in addition to residue 263, are involved in determining the substrate-binding order. Polβ has an Asp at the corresponding position to 263 of ttPolX and follows a DNA-first ordered Bi Bi mechanism (Wang *et al*., 1982). However, the K263D mutant of ttPolX retained the dNTP-first binding order (Table 7), although the binding affinity for Mg^{2+}-dNTP in the absence of DNA was much lower than that of wild-type (Table 1). This difference is consistent with a role for other residues also determining substrate-binding order through interaction with the incoming nucleotide or DNA. In ttPolX and Polβ, the residues interacting with the incoming nucleotides are similar except for residue 263 in ttPolX (Fig. 14A). Therefore, the residues involved in DNA-binding seem also to have a role in substrate-binding order in PolXs. The number of interactions between ttPolX and 1-nt gapped DNA was similar to other PolXs (Fig. 19A). However, the interaction around the template strand bend (Figs. 19A and 19B) differed (Figs. 19C and 19D). The Phe-25 in the 8-kDa subdomain has a stacking interaction with dC-12, which is upstream of the bend in the template strand (Figs. 19A and 19C). This stacking residue is conserved in many bacterial and archaeal PolXs (Fig. 12A and Fig. 1 of Banos *et al.,* 2008a). An aromatic residue is also found at this position in *H. sapiens* Polβ (hsPolβ) (His-34) (Fig. 19D) and hsPolλ (Trp-274), but not in hsPolμ (Gly-174) or hsTdT (Asp-186) (Fig. 12). Eukaryotic PolXs also have stacking interactions with the base downstream of the bend (Fig. 19D); e.g., hsPolβ Lys-280, hsPolλ Arg-514, hsPolμ Arg-442 and hsTdT Arg-457. However, this stacking residue is not conserved in ttPolX (Ile-267) (Fig. 19C), bacterial and archaeal PolXs (Fig. 12B) (Banos *et al.,* 2008a). hsPolβ and hsPolλ have two stacking residues near the bend position, however, hsPolμ, hsTdT, and bacterial and archaeal PolXs have only one stacking residue. This difference may be related to the affinity for gapped DNA, substrate-binding order and efficiency of filling gaps larger than two nucleotides (Garcia-Diaz *et al.*, 2009).

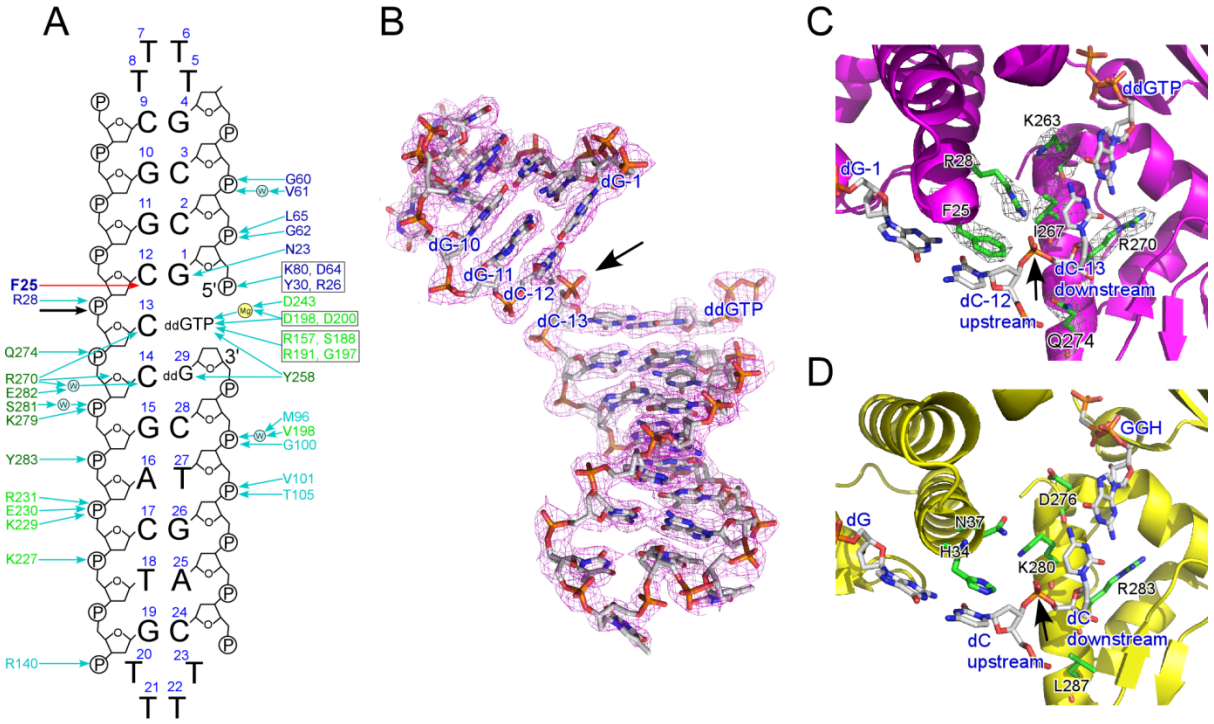

Figure 19. DNA-binding residues of the ttPolX ternary complex with 1-nt gapped DNA. (A) Interaction between ttPolX, gapped DNA and ddGTP. Residue numbers are colored as in Figure 11B. Cyan arrows indicate hydrogen bonds (≤ 3.2 Å); red arrows indicate nonbonded interactions; W, water molecules; P, DNA backbone phosphates; and Mg, magnesium ion. DNA residue numbers are shown in blue. (B) 1-nt gapped DNA and ddGTP. A 2Fo-Fc electron density map contoured at 1σ is shown in magenta. (C) The DNA-interacting residues of ttPolX ternary complex with 1-nt gapped DNA around the template strand bend. DNA residues and protein residues are shown as white and green, respectively. A 2Fo-Fc electron density map contoured at 1σ is shown in gray. (D) The DNA-interacting residues of the Polβ ternary complex with 1-nt gapped DNA (Sucato *et al.*, 2007) around the template strand bend. Black arrows in panels A, B, C and D indicate the template strand bend.

DNA-binding abilities of ttPolX and its domains

I examined the DNA-binding abilities of ttPolX and its domains by means of EMSA. I used four DNAs of different structures: ssDNA, dsDNA, 1-nt gapped DNA and 5'-phosphorylated 1-nt gapped DNA. ttPolX and the POLXc (1-379) were able to bind to all DNA substrates but exhibited different binding properties for the four DNA structures (Figs. 20A and 20B; Table 8). ttPolX showed stronger binding ability as to gapped DNAs than ssDNA and dsDNA. The POLXc (1-379) showed weaker binding ability as to all DNA substrates than ttPolX (Figs. 20A and 20B). Additionally, the POLXc (1-379) showed no significant difference in binding ability between gapped DNA and non-gapped DNA. It should be mentioned that the binding curves were sigmoidal (Fig. 20B). Assuming multiple molecules of a protein bind to DNA, I determined K_d^{app} and n (the number of bound protein) (see MATERIALS AND METHODS). The PHP (339-575) was unable to bind to all of the DNA structures, even though the concentration of PHP (339-575) was 6.5 μM (Figs. 20A and 20B).

I observed more than two shifted bands in some lanes for ttPolX and the POLXc (1-379). The appearance of multiple shifted bands and the n values suggest that more than two molecules of ttPolX or the POLXc (1-379) bound to a DNA. There was almost no difference between the binding abilities as to 5'-phosphorylated and unphosphorylated 1-nt gapped DNA (Figs. 20A and 20B; Table 8). Fig. 20C shows that putative residues which recognize 5'-phosphate are conserved in various PolXs.

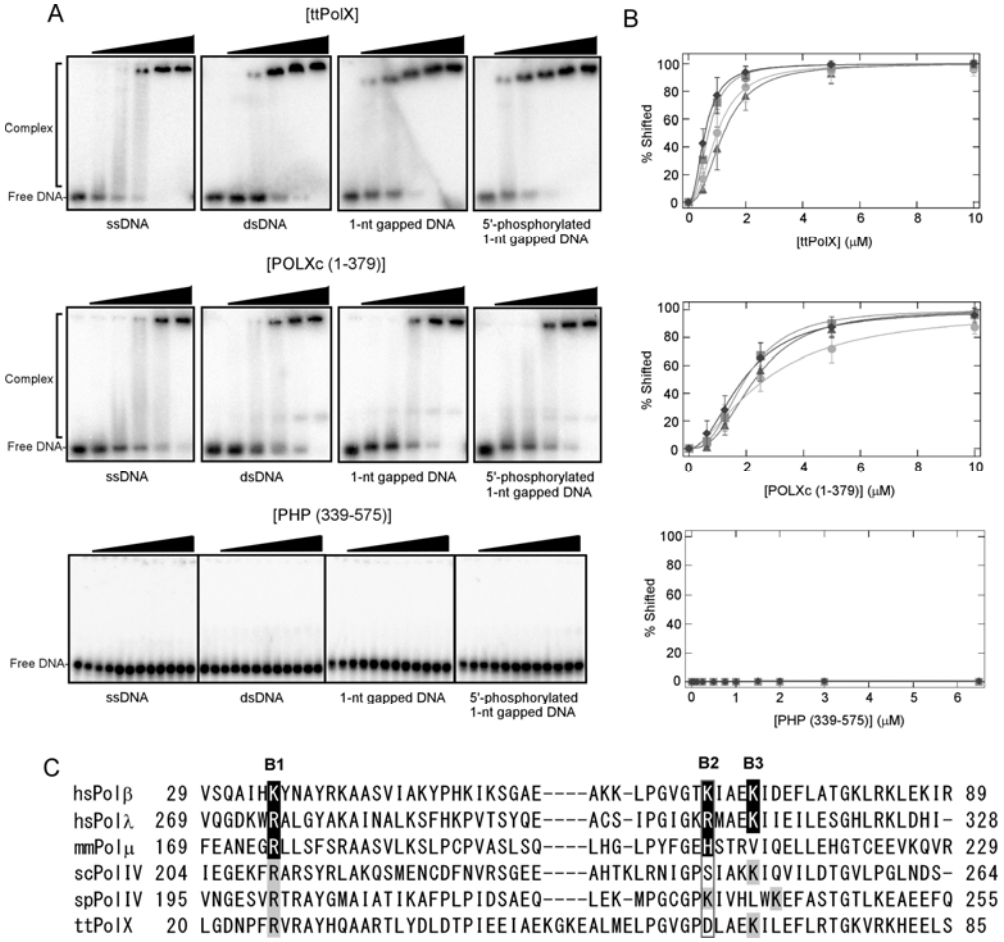

Figure 20. EMSA of ttPolX, and the POLXc (1-379) and PHP (339-575) against four kinds of DNA. (A) Proteins were mixed with 10 nM each DNA and then analyzed by 5% PAGE. The concentrations of ttPolX were 0, 0.5, 1, 2, 5 and 10 μM. The concentrations of the POLXc (1-379) were 0, 0.625, 1.25, 2.5, 5 and 10 μM. The concentrations of the PHP (339-575) were 0, 0.01, 0.0625, 0.125, 0.25, 0.5, 0.75, 1, 1.5, 2, 3 and 6.5 μM. (B) The percentage of the protein-DNA complex was determined and plotted against the protein concentration. The symbols were as follows: circles, ssDNA; squares, dsDNA; triangles, 1-nt gapped DNA; diamonds, 5'-phosphorylated 1-nt gapped DNA. The data were fitted with equation (9) using Igor 4.03. Data represent the means for four or five independent experiments ± standard deviation. (C) Sequence alignment of the POLXc domain regions of PolXs. White letters in black boxes indicate putative residues interacting with 5'-phosphate in the crystal structures of hsPolβ (PDB ID: 2fms), hsPolλ (PDB ID: 1xsn), and mmPolμ (PDB ID: 2ihm). The residues with a gray background are putative residues interacting with 5'-phosphate predicted from the alignment. B1, B2 and B3 represent the positions of the basic amino acid residues. The alignment was performed with ClustalW2 (Larkin *et al.*, 2007). The accession numbers were as follows: NP_002681 for *H. sapiens* Polβ (hsPolβ); NP_037406 for *H. sapiens* Polλ (hsPolλ); NP_059097 for *Mus musculus* Polμ (mmPolμ); NP_009940 for *Saccharomyces cerevisiae* PolIV (scPolIV); NP_592977 for *Schizosaccharomyces pombe* PolIV (spPolIV); and YP_144416 for *T. thermophilus* HB8 PolX (ttPolX).

Table 8. Comparison of DNA-binding abilities of ttPolX and its domains

	ssDNA		dsDNA		1-nt gapped DNA		5'-phosphorylated 1-nt gapped DNA	
	K_d^{app} (μM)	n	K_d^{app} (μM)	n	K_d^{app} (μM)	n	K_d^{app} (μM)	n
ttPolX	1.2 ± 0.70	2.4 ± 0.74	1.2 ± 0.70	2.5 ± 0.57	0.39 ± 0.15	2.3 ± 0.46	0.30 ± 0.18	2.4 ± 1.0
POLXc (1-379)	5.5 ± 1.7	1.7 ± 0.29	9.3 ± 3.8	2.6 ± 0.23	6.5 ± 2.5	2.5 ± 0.65	4.8 ± 2.5	2.3 ± 1.0
PHP (339-575)	N.D.	N.D.	N.D.	N.D.	N.D.	N.D.	N.D.	N.D.

K_d^{app}, dissociation constant; n, number of binding enzyme; N.D., not detected.
[a]Data represent the means for five independent experiments ± standard deviation.
[b]Data represent the means for four independent experiments ± standard deviation.

dRP lyase activity

It is generally accepted that the 5'-dRP group is removed from a BER intermediate by dRP lyase activity through a β-elimination mechanism (Deterding *et al.*, 2000) The 5'-dRP is generated after 5'-side of incision of AP site by AP endonuclease (Fig. 21A, 48). The β-elimination reaction proceeds via a Schiff base intermediate, and the ε-amino group of Lys-72 of hsPolβ (at B3 position, Fig. 20C) was identified as the nucleophile (Deterding *et al.*, 2000). ttPolX has the corresponding Lys at B3 position (Fig. 20C), and actually exhibited a dRP lyase activity (Fig. 21B). ttPolX could remove a 5'-dRP group without metal ion as an activator. Therefore, the observed removal of dRP by ttPolX was thought to proceed via a β-elimination mechanism through a Schiff base intermediate. ttPolI is thought to be a major DNA polymerase that acts in DNA repair, and to have 5'-3' exonuclease activity (Auer *et al.*, 1995). RecJ from *T. thermophilus* HB8 (ttRecJ) has a ssDNA-specific 5'-3' exonuclease activity (Yamagata *et al.*, 2001). Although these enzymes have 5'-3' exonuclease activity, they were unable to remove 5'-dRP group under the condition examined here (Fig. 21B).

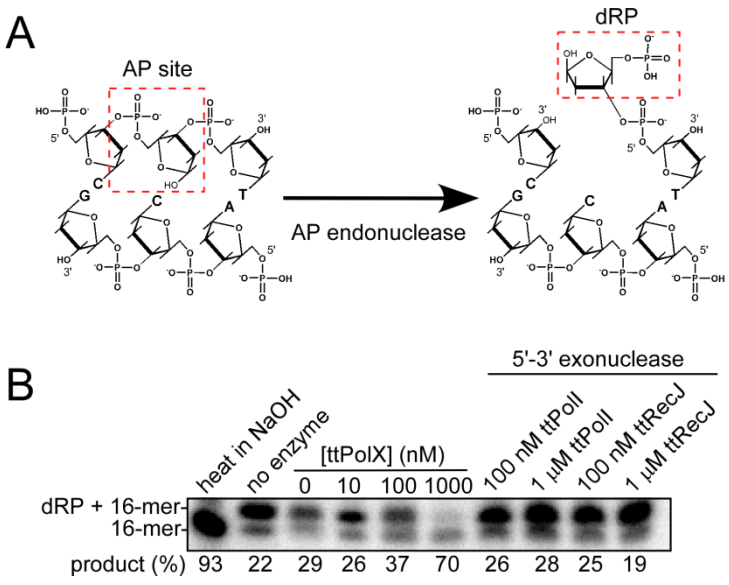

Figure 21. 5'-dRP lyase activity of ttPolX. (A) Structural formula of dRP. When AP site is incised by AP endonuclease, dRP is remained at 5'-end. AP site and 5'-dRP are surrounded by dotted red lines. (B) dRP lyase assay. Reaction mixtures comprising 50 mM HEPES-NaOH, 20 mM KCl, 1mM EDTA, 2 mM DTT, and 8 nM 3'-labeled 5'-dRP, pH 7.5, were incubated at 37°C for 30 min and analyzed by 15% denaturing PAGE (8 M urea) and autoradiography. Treatment with NaOH and heat was performed as a control of β-elimination reaction. When ttPolI and ttRecJ were used, $MgCl_2$ was added at final concentration of 5 mM. The percentage of dRP lyase product was indicated below the figure.

III. The molecular and functional analysis of the PHP domain

Exonuclease activity of ttPolX

ttPolX was demonstrated to have Mn^{2+}- and Co^{2+}-dependent 3'-5' exonuclease activities (Figs. 4A and 22). As shown in Fig. 22A, the 5'-labeled oligonucleotides became shorter in length in the presence of Mn^{2+} as time passed. This result indicated that the direction of the exonuclease activity was 3'-5'. This direction of exonuclease activity was further supported by the results of the FT-ICR MS analysis (Fig. 23 and Table 9), which showed that the ssDNA substrate was degraded one nucleotide at a time from the 3'-end. Figure 22A also shows that the ttPolX exonuclease activity for dsDNA was weaker than that for ssDNA. In addition to Mn^{2+}, ttPolX also exhibited exonuclease activity in the presence of Co^{2+} (Fig. 22B). The Co^{2+}-dependent 3'-5' exonuclease activity of ttPolX was weaker than its Mn^{2+}-dependent exonuclease activity, and a high concentration of $CoCl_2$ (5 mM) inhibited this activity. Furthermore, Co^{2+} ions inhibited the Mn^{2+}-dependent 3'-5' exonuclease activity of ttPolX (Fig. 22B). The Mn^{2+}-dependent 3'-5' exonuclease activity was the highest at 80-85°C (Fig. 22C). Interestingly, ttPolX was also shown to possess a Mn^{2+}-dependent 3'-5' exoribonuclease activity (Fig. 22D). Investigation of the substrate specificity of the 3'-5' exonuclease activity of ttPolX revealed that the activity was highest for the mismatched end and decreased in the following order of substrates: mismatched end > overhanging end > ssDNA > dsDNA > recessed end (Fig. 22E).

Since the POLXc (1-379) had no nuclease activity (Fig. 5A), I expected the PHP domain has nuclease activity. However, the PHP (339-575) exhibited no polymerase and no exonuclease activity with a cofactor of Mg^{2+} or Mn^{2+} (data not shown). The α subunit of *T. thermophilus* PolIII also has a PHP domain at its N-terminus, and has Zn^{2+}-dependent 3'-5' exonuclease activity (Stano *et al.*, 2006). I then performed the exonuclease assay with Zn^{2+} using the PHP (339-575), but observed no exonuclease activity (data not shown). CD spectra in the far-UV region indicated that the PHP (339-575) was highly structured with a high content of α-helix (data not shown). Therefore, I concluded that the PHP (339-575) has no 3'-5' exonuclease activity by itself, under the conditions tested here.

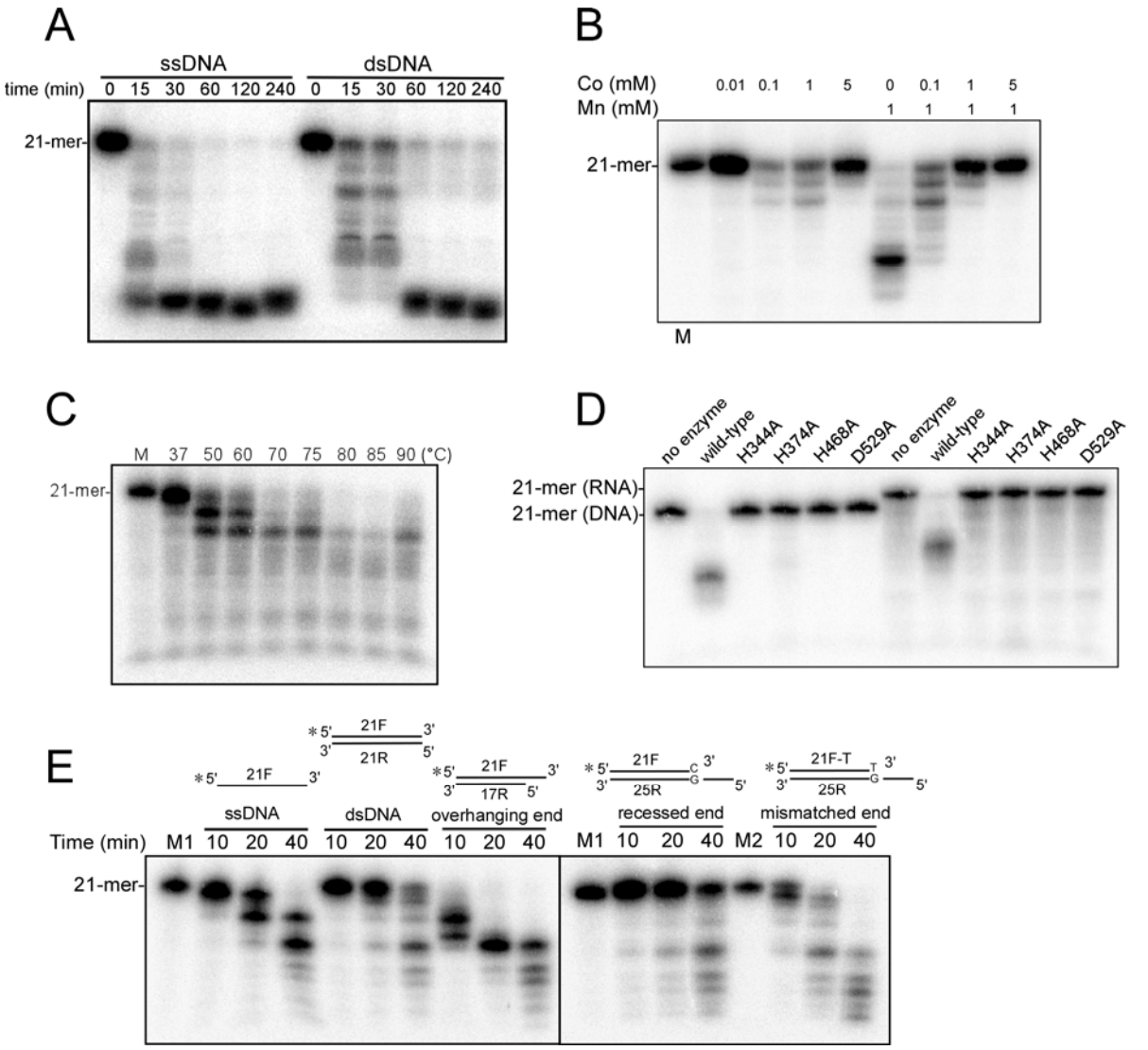

Figure 22. Exonuclease assays using ttPolX. (A) Time course analysis of 3'-5' exonuclease activity. Reaction mixtures containing 20 mM Tris-HCl, 20 mM KCl, 1 mM $MnCl_2$, 1 μM ttPolX and 10 nM 5'-labeled oligonucleotides, pH 8.1, were incubated at 37ºC for the indicated times. (B) The 3'-5' exonuclease activity in the presence of Co^{2+}. Reaction mixtures containing 20 mM Tris-HCl, 20 mM KCl, $CoCl_2$ and/or $MnCl_2$, 1 μM ttPolX, 10 μM EDTA and 10 nM 5'-labeled 21F, pH 8.1, were incubated at 37ºC for 30 min. (C) Temperature dependence of the 3'-5' exonuclease activity. Reaction mixtures containing 50 mM PIPES (pH 7.5 at 25°C), 100 mM KCl, 1 mM $MnCl_2$, 1 μM ttPolX and 10 nM 5'-labeled 21F were incubated at 37°C for 10 min. (D) RNase activity of ttPolX. Reaction mixtures containing 50 mM Tris (pH 8.5), 20 mM KCl, 1 mM $MnCl_2$, 1 μM ttPolX and 10 nM 5'-labeled DNA/RNA were incubated at 70°C for 1 min. (E) Substrate specificity of the 3'-5' exonuclease activity. Reaction mixtures containing 50 mM Tris (pH 7.5), 100 mM KCl, 1 mM $MnCl_2$, 1 μM ttPolX and 10 nM 5'-labeled DNA were incubated at 37°C for the indicated times. M and M1 represent 21F markers. M2 represents a 21F-T marker. The samples were analyzed on a 20% (panels A, C, and E) or 25% (panels B and D) denaturing gel with 8 M urea followed by autoradiography.

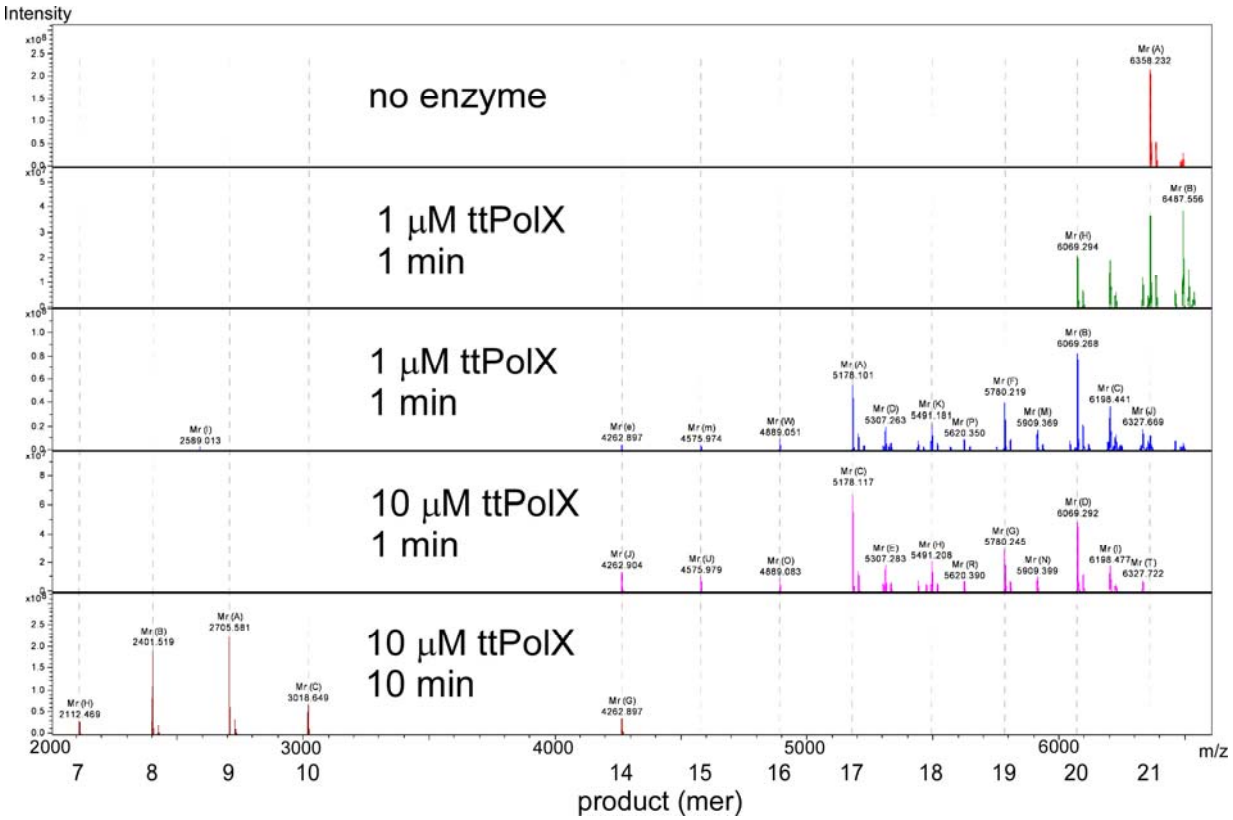

Figure 23. FT-ICR MS analysis of the 3'-5' exonuclease activity of ttPolX. ttPolX was reacted with 21F DNA substrate at 68°C in the presence of 1 mM $MnCl_2$. Purified reaction products were analyzed by solariX FT-ICR MS system (Bruker) with electrospray ionization under negative mode. Mass detection range was set from 200 to 3,000 *m/z*, and deconvoluted spectra were shown.

Table 9. Theoretical values of monoisotopic masses of the substrate and resultant products.

Oligonucleotide length	Sequence	Theoretical monoisotopic mass
21-mer substrate	5'OH-ATGACAACTAAAGCAACACCC-OH3'	6358.142
20-mer product	5'OH-ATGACAACTAAAGCAACACC-OH3'	6069.096
19-mer	5'OH-ATGACAACTAAAGCAACAC-OH3'	5780.049
18-mer	5'OH-ATGACAACTAAAGCAACA-OH3'	5491.000
17-mer	5'OH-ATGACAACTAAAGCAAC-OH3'	5177.950
16-mer	5'OH-ATGACAACTAAAGCAA-OH3'	4858.900
15-mer	5'OH-ATGACAACTAAAGCA-OH3'	4575.841
14-mer	5'OH-ATGACAACTAAAGC-OH3'	4262.784
10-mer	5'OH-ATGACAACTA-OH3'	3018.570
9-mer	5'OH-ATGACAACT-OH3'	2705.512
8-mer	5'OH-ATGACAAC-OH3'	2401.466
7-mer	5'OH-ATGACAA-OH3'	2112.420

The activities of a mixture of the POLXc (1-379) and PHP (339-575)

A mixture of the POLXc (1-379) and PHP (339-575) (domain mixture) had Mn^{2+}-dependent 3'-5' exonuclease activity as well as Mg^{2+}-dependent DNA polymerase activity (Fig. 24A). This metal ion selectivity of the activities was the same as that of ttPolX. These results suggest interaction between the POLXc (1-379) and PHP (339-575). Time course analysis of the exonuclease activity showed that the domain mixture was able to degrade both ssDNA and dsDNA but the activity for ssDNA was higher than that for dsDNA (Fig. 24B). Furthermore, I found that the exonuclease activity of the domain mixture increased in the presence of 0.1-10 μM dNTPs, whereas that of ttPolX did not change with dNTPs (Fig. 24C). I calculated steady-state kinetic parameters for the 3'-5' exonuclease activity of ttPolX and the domain mixture against 3'-labeled 21-mer ssDNA. The K_m values of ttPolX were 1,700 (without dNTPs) and 1,300 nM (with dNTPs), whereas those of the domain mixture were 770 (without dNTPs) and 530 nM (with dNTPs). The catalytic efficiencies (k_{cat}/K_m) of ttPolX were 2.8×10^4 (without dNTPs) and 3.8×10^4 $s^{-1}M^{-1}$ (with dNTPs), whereas those of the domain mixture were 3.5×10^2 (without dNTPs) and 1.5×10^3 $s^{-1}M^{-1}$ (with dNTPs). The catalytic efficiency of ttPolX was almost the same with and without dNTPs, whereas that of the domain mixture increased on the addition of dNTPs.

The interaction between the POLXc (1-379) and PHP (339-575)

To verify whether the POLXc (1-379) and PHP (339-575) interact with each other, I performed native PAGE. On the polyacrylamide gel, the ttPolX, POLXc (1-379) and PHP (339-575) showed mobility corresponding to their isoelectric points (Fig. 24D): 6.26, 8.40 and 6.04, respectively. It was confirmed by PMF analysis that all bands in the lane of the PHP (339-575) contained the PHP (339-575) (Fig. 24D, lane 3). In the lane of the domain mixture, the bands with the same mobility as ttPolX were apparently increased compared with the lanes of the POLXc (1-379) and PHP (339-575). This result suggests the two domains formed a complex with a similar surface charge and/or a similar overall shape to ttPolX. The smear band of ttPolX may be due to a non-uniform distribution of the surface charge or structural fluctuation of the ttPolX. I further examined this interaction by size exclusion chromatography (Fig. 24E and Table 10). The ttPolX, POLXc (1-379) and PHP (339-575) were eluted as single peaks at different elution volumes. When the POLXc (1-379) and PHP (339-575) were mixed, a new peak appeared at 9.7 ml, which was different from those of the POLXc (1-379) and PHP (339-575). Concomitantly with the appearance

of this peak, the peak of the PHP (339-575) (11.3 ml) decreased. Since the peak of the POLXc (1-379) partially overlapped with that of 9.7 ml, I could not observe a clear peak of the POLXc (1-379) in the elution profile of the domain mixture. The elution volume of 9.7 ml (50 kDa) was very similar to that of ttPolX (9.8 ml, 48 kDa), suggesting that the peak eluted at 9.7 ml corresponded to a complex between the POLXc (1-379) and PHP (339-575) in a 1:1 molar ratio. Based on the difference in the absorbance of the peaks corresponding to the PHP (339-575) between the PHP (339-575) alone and the domain mixture, approximately 40% of the PHP (339-575) was assumed to form the complex (Table 10). Furthermore, I changed the ratio of domains for the domain mixture to 2:1 or 10:1 (Fig. 25 and Table 11). When the domain ratio (POLXc (1-379):PHP (339-575)) was 10:1, most of the PHP (339-575) appeared to form the complex with the POLXc (1-379). SDS-PAGE analysis of the eluted fractions indicated that the early-eluting peak (10.0 ml) contained both POLXc (1-379) and PHP (339-575). In the presence of dNTPs, the peak absorbance of the complex of the domains was 1.1-fold increased, whereas the peak absorbance of the PHP (339-575) was 0.89-fold decreased (Fig. 24F and Table 10). These results suggest that the complex of the domains was stabilized in the presence of dNTPs.

Table 10. Comparison of the elution volumes in Figs. 24E and 24F.

	Elution volume (ml)	A_{280} (mAU)	MW[a]
ttPolX	9.8	32.5	48k (64k)
POLXc (1-379)	10.3	9.5	40k (44k)
PHP (339-575)	11.2	24.9	30k (29k)
domain mixture (1)	9.7	16.7	50k
domain mixture (2)	11.3	15.1	29k
domain mixture with dNTPs (1)	9.7	19.2	50k
domain mixture with dNTPs (2)	11.2	13.4	30k

[a]The apparent molecular weights were calculated using the following equation: log MW = −0.147 [elution volume (ml)] + 3.12. The MWs given in the parentheses are theoretical values calculated from amino acid sequences. The void volume of this Superdex 75 column measured using blue dextran was 7.8 ml.

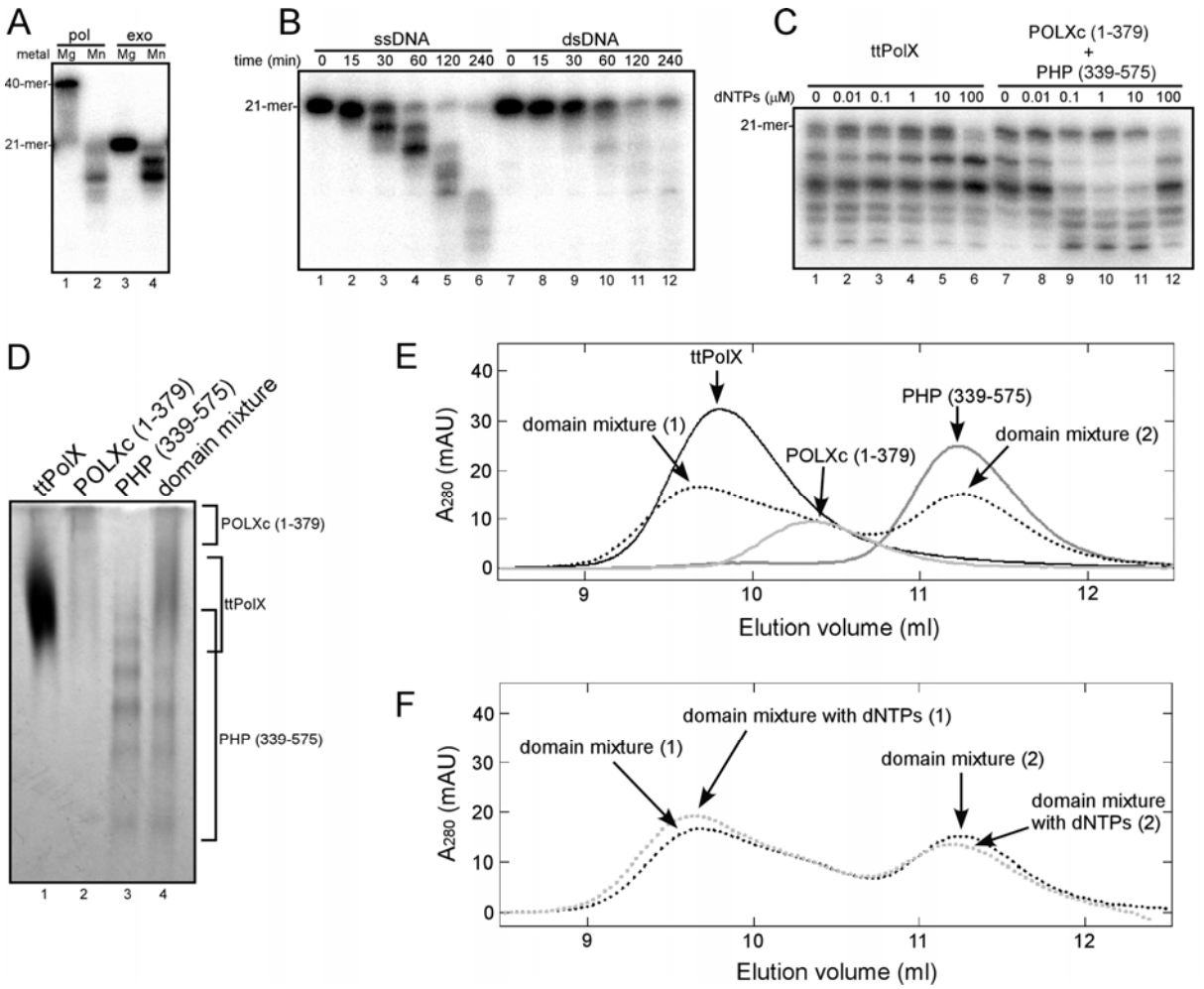

Figure 24. The analysis of the mixture of the POLXc (1-379) and PHP (339-575). The assay conditions of polymerase and exonuclease activities were the same as given in Fig. 4 except for the use of domain mixture (containing 1 μM POLXc (1-379) and 1 μM PHP (339-575)). (A) Metal ion dependence of polymerase and exonuclease activities. (B) Time course analysis of exonuclease activity against ssDNA and dsDNA. (C) Exonuclease assay with dNTPs. Reaction mixtures comprised 20 mM Tris-HCl, 20 mM KCl, 1 mM $MnCl_2$, 100 nM ttPolX or 1 μM domain mixture, 10 nM 5'-labeled 21F and indicated amount of dNTPs, pH 8.1, at 37ºC. The reaction mixtures were incubated for 30 min at 37ºC, and then analyzed by 20% denaturing PAGE (8 M urea), but the running time was longer than that in panel B. Note that the concentration of the domain mixture was higher than that of ttPolX. (D) The interaction between the POLXc (1-379) and PHP (339-575). Proteins were analyzed by 7.5% native PAGE and stained with CBB. The samples electrophoresed in the lanes were as follows: 1, 500 pmol ttPolX; 2, 500 pmol POLXc (1-379); 3, 500 pmol PHP (339-575); and 4, 500 pmol POLXc (1-379) and 500 pmol PHP (339-575). The positions of the proteins on the gel are indicated on right side of the figure. (E) Elution profiles of ttPolX (black line), the POLXc (1-379) (light gray line), the PHP (339-575) (dark gray line), and the domain mixture (dotted black line) on size exclusion chromatography. Proteins were incubated in buffer comprising 20 mM Tris-HCl and 100 mM KCl with or without 10 μM dNTPs, pH 8.1, at 37ºC. The mixtures were incubated for 30 min at 37 ºC and then applied to a Superdex 75 column and eluted with incubation buffer. The elution volume, absorbance values and MWs estimated from the elution volume of each peak are summarized in Table 10. Arrows in the graph indicate the peaks in each elution profile. In the profile of the domain mixture, there were two main peaks. I named their peaks 1 and 2 in elution order. (F) Elution profiles of the domain mixture in the presence (dotted light gray line) and absence (dotted black line) of 10 μM dNTPs. The eluted peaks were named as described above.

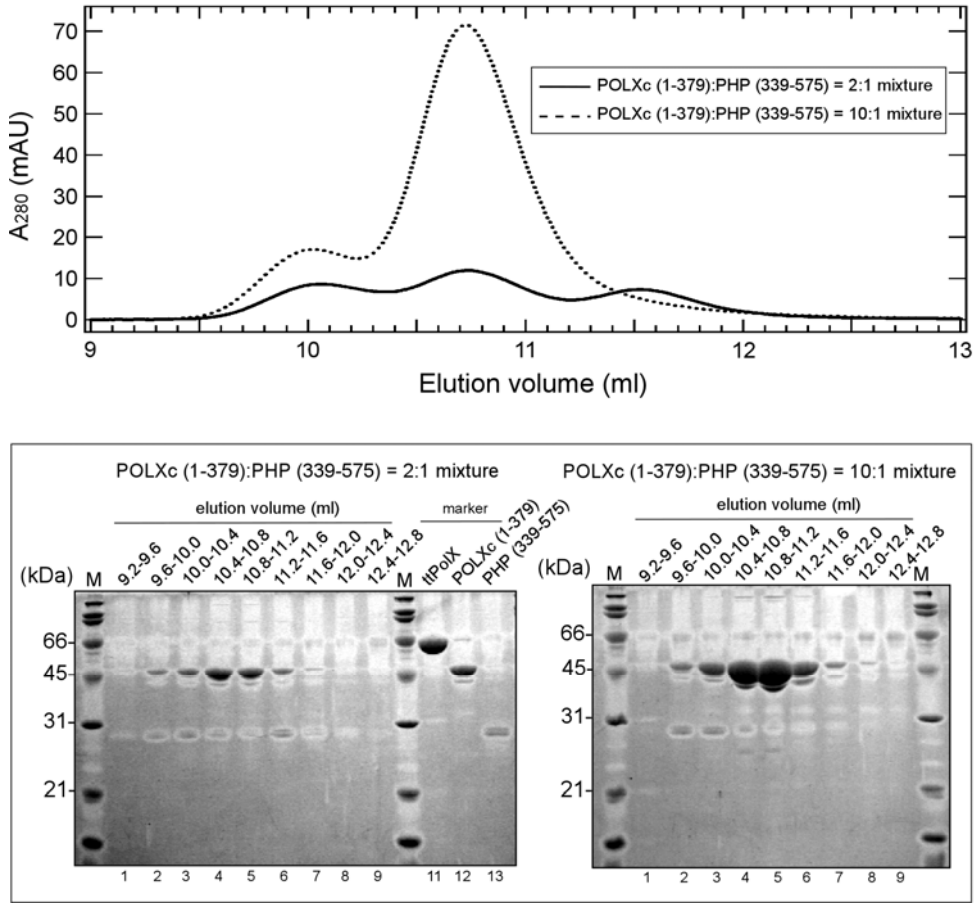

Figure 25. Elution profiles of the domain mixture at different ratios of the domains. The ratio (POLXc [1-379]:PHP [339-575]) was 0.5 nmol:0.25 nmol for a 2:1 mixture (black line) and 2.5 nmol:0.25 nmol for a 10:1 mixture (dotted black line). The collected fractions were precipitated with acetone and the proteins were analyzed by 12.5% SDS-PAGE and stained with CBB (lower panels). M represents molecular weight markers. In the "marker" lanes, ttPolX, POLXc (1-379) and PHP (339-575) were loaded in equimolar amounts. Note that the Superdex 75 column used in this experiment was different from the one used in Fig. 24.

Table 11. Comparison of the elution volumes in Fig. 25.

Elution volume (ml)	MW[a]
10.0 (domain complex)	51k
10.7 (POLXc (1-379))	38k
11.5 (PHP (339-575))	27k

[a]The apparent molecular weights were calculated using the following equation: log MW = −0.185 [elution volume (ml)] + 6.56. The void volume of this Superdex 75 column was 8.0 ml (measured using blue dextran).

Site-directed mutagenesis of the PHP domain

To investigate the involvement of the PHP domain in the exonuclease activity, the residues, Gln-342, His-344, Asp-349, His-374, Glu-413, His-440, His-468, Asp-529 and His-531, that were thought to bind to metal ions in the PHP domain, were substituted by alanine. The crystallographic analysis revealed that the PHP domain contained three metal ions (Fig. 11A). These metal ions were identified to be zinc ions by anomalous dispersion measurement (Fig.

26). Since crystallization reagent contained no zinc ions, ttPolX seemed to be purified with zinc ions derived from expression host, *E. coli*. ICP-AES measurement revealed that purified ttPolX actually contained zinc ions (Table 12). The zinc-binding residues of the PHP domain are well conserved among the PHP domains (Figs. 3C, 27 and Banos *et al.,* 2008b), indicating the importance of these residues for the activity of the PHP domain. Therefore, I produced nine mutants and mutations were confirmed by DNA sequencing and PMF with MALDI-TOF MS.

All nine mutations significantly decreased the Mn^{2+}-dependent 3'-5' exonuclease activity (Fig. 28A). In contrast, the Mg^{2+}-dependent DNA polymerase activity of all mutants was almost the same as that of wild-type ttPolX (Fig. 28B). The latter observation coincides with the notion that DNA polymerase activity resides in the POLXc domain. These results suggest that these residues are directly involved in the 3'-5' exonuclease activity but not in the DNA polymerase activity. The presence of dNTPs and of primer/template oligonucleotides promoted the Mn^{2+}-dependent 3'-5' exonuclease activity of Q342A, D349A, E413A and H531A (Figs. 28C and 28D). Since all mutants had weak or no 3'-5' exonuclease activity, I thought these mutants exhibit Mn^{2+}-dependent DNA polymerase activity like the POLXc (1-379) (Fig. 5A). Under the polymerase assay conditions in the presence of Mn^{2+}, however, Q342A, D349A, E413A and H531A exhibited stronger 3'-5' exonuclease activity (Fig. 28C) than under the exonuclease assay conditions (Fig. 28A). H344A, H374A, H440A, H468A and D529A exhibited Mn^{2+}-dependent DNA polymerase activity but no detectable Mn^{2+}-dependent 3'-5' exonuclease activity, therefore, these mutants hardly exhibited the exonuclease activity even in the presence of dNTPs and primer/template oligonucleotides. The effect of dNTPs on the Mn^{2+}-dependent 3'-5' exonuclease activity was further investigated (Fig. 28D). The Mn^{2+}-dependent 3'-5' exonuclease activities of Q342A, D349A and H531A were promoted more in the presence of dNTPs than in the absence of dNTPs but less than in the presence of dNTPs and primer/template oligonucleotides (Figs. 28A, 28C and 28D). Even when the reaction time was prolonged to 2 h in the exonuclease assay or the assay with dNTPs, the 3'-5' exonuclease activities of H344A, H374A, H468A and D529A were hardly observed, but that of H440A was observed (Figs. 28E and 28F). Therefore, I concluded that His-344, His-374, His-468 and Asp-529 of ttPolX are the most important residues for the 3'-5' exonuclease activity.

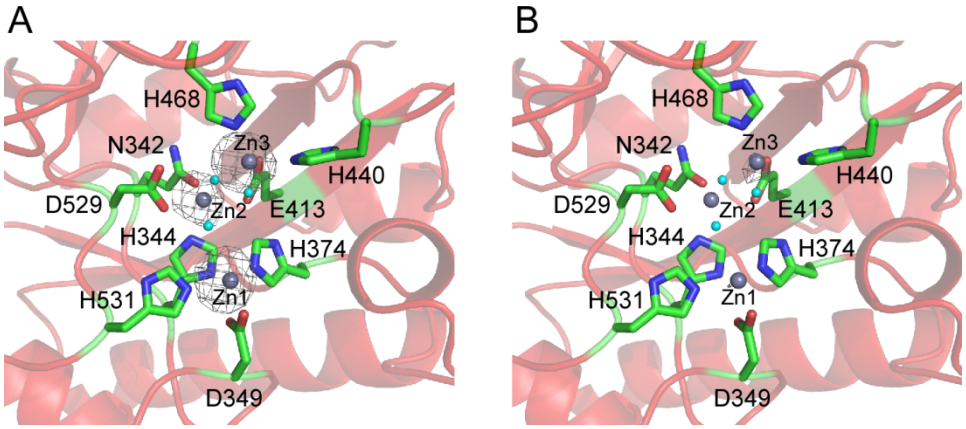

Figure 26. Zn ion-binding sites of the PHP domain. The active site of the PHP domain in the binary complex contains three Zn ions. Electron density maps (anomalous difference Fourier maps) were generated from the data collected at 1.281959 Å, the Zn anomalous peak wavelength (A), and at 1.309841 Å, a low remote wavelength (B). All electron densities are contoured at 3 σ. Gray and cyan spheres are Zn ions and water molecules, respectively.

Table 12. Metal contents of purified ttPolX determined by ICP-AES

Metal	Mg	Ca	Mn	Fe	Co	Ni	Zn
Content (/protein)	0.0067	0.063	0.0023	0.046 ± 0.023[a]	0.00058	0.10	0.15 ± 0.051[a]

[a]Data represent means for three samples ± standard deviation

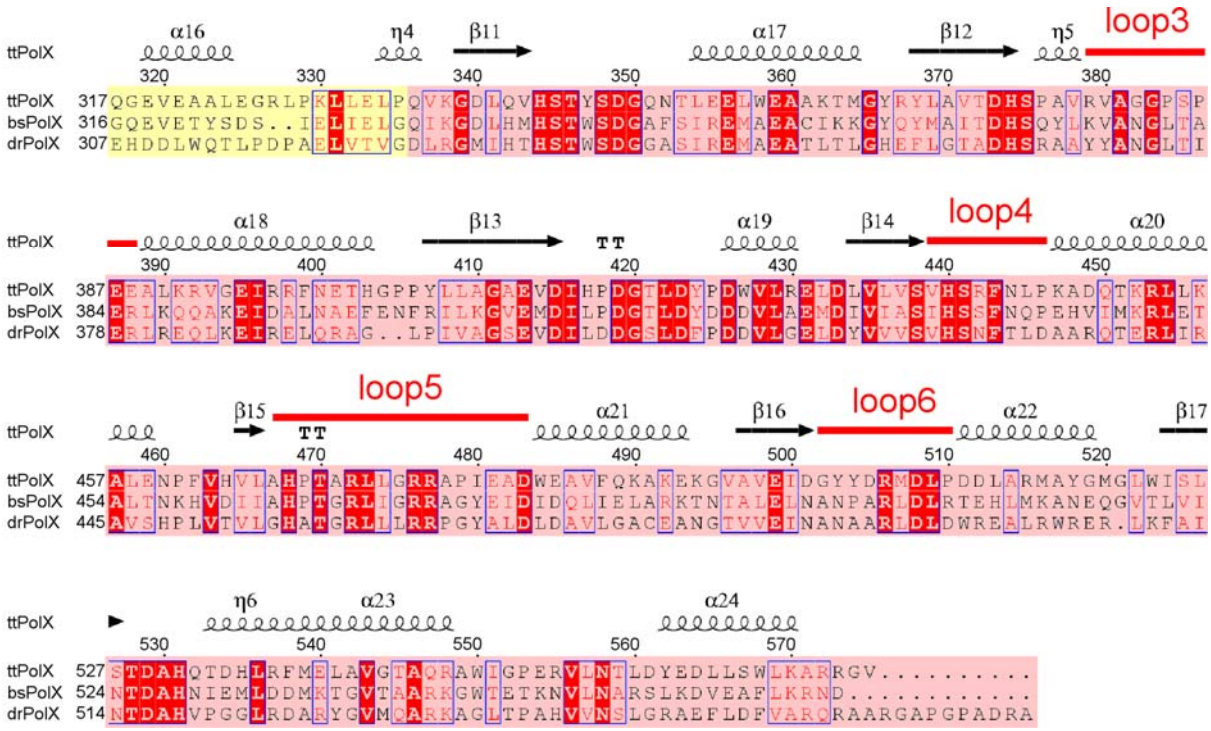

Figure 27. Sequence alignment of the PHP domain among representative bacterial PolXs. The abbreviations are as follows: ttPolX, *Thermus thermophilus* HB8 PolX; bsPolX, *B. subtilis* PolX and drPolX, *Deinococcus radiodurans* PolX. The sequence accession numbers are: YP_144416 for ttPolX, NP_390737 for bsPolX and NP_294190 for drPolX. The sequence domains are highlighted with the same color as in Fig. 11. Multiple alignments were calculated by ClustalW2 (Chenna *et al*., 2003) and displayed by ESPript (Gouet *et al*., 2003). The notations in the figure are as follows: α, α-helix, β, β-sheet, TT, strict β-turn, and η, 3_{10} helix.

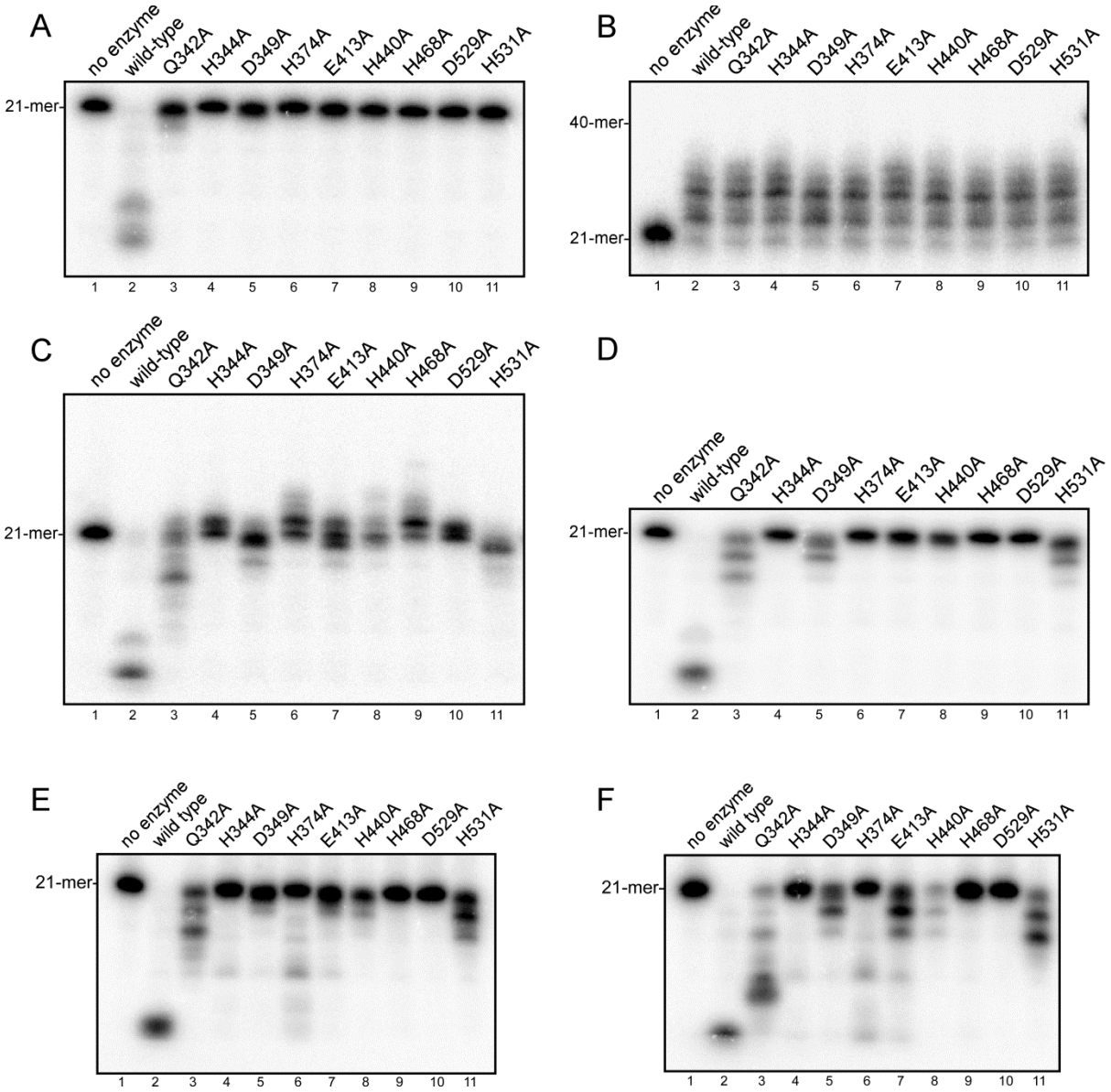

Figure 28. Site-directed mutagenesis of ttPolX. Reaction mixtures containing 1 μM wild-type ttPolX, a mutant or no enzyme were incubated for 30 min (panels A-D) or for 2 h (panels E and F) at 37ºC. (A) Exonuclease assays in the absence of dNTPs. (B) DNA polymerase assays using 21F/40T and 10 μM dNTPs in the presence of 5 mM Mg^{2+}. (C) DNA polymerase assays using 21F/40T and 10 μM dNTPs in the presence of 1 mM Mn^{2+}. (D) Exonuclease assays in the presence of 10 μM dNTPs. (E) Exonuclease assays for long time incubation in the absence of dNTPs. (F) Exonuclease assays for long time incubation in the presence of 10 μM dNTPs. The reaction mixtures were analyzed by 18% (panel B) or 20% (panels A, C, D, E and F) denaturing PAGE (8 M urea) and autoradiography.

ttPolX exhibits a 3'-phosphatase activity associated with the PHP domain

I found that ttPolX has a 3'-phosphatase activity that has not been reported for other PolXs (Fig. 29). The 3'-phosphate is generated in BER after the trifunctional DNA glycosylase removes a damaged base (see Fig. 48). To determine which metal ion activates ttPolX, pre-bound metal ions were removed by EDTA (Fig. 29, except for no metal lanes). The result showed that the 3'-phosphatase activity of ttPolX was strongly activated by Mn^{2+} and Co^{2+} ions. Additionally, ttPolX was also activated by Mg^{2+} ions and by a low concentration of Zn^{2+} ions. Because Tris buffer is known to chelate some metal ions (Fischer *et al*., 1979), the experiments were also performed with HEPES buffer. When HEPES buffer was used, ttPolX showed the 3'-phosphatase activity without the requirement of additional metal ions (Fig. 29B). This result can be attributed to metal ions that are prebound to the PHP domain of ttPolX (Fig. 26 and Table 12). However, none of the added metal ions exhibited the same degree of activity as the "no metal" condition. Therefore, I speculated that the intrinsically present mixture of metal ions may contribute to the higher 3'-phosphatase activity observed in the "no metal" condition (Fig. 29). D529A of ttPolX showed no 3'-phosphatase activity (Fig. 29B), indicating the involvement of the PHP domain in this activity. ttEndoIV also showed a 3'-phosphatase activity (Fig. 29B). This observation was consistent with the reports that EndoIVs of *E. coli* (Levin *et al*., 1988), *B. subtilis* (Salas-Pacheco *et al*., 2003), and *Thermotoga maritima* (Haas *et al.*, 1999) have a 3'-phosphatase activity.

To identify the domain in which the 3'-phosphatase activity of ttPolX was located, the POLXc (1-316) and PHP (336-575) domains were used for the 3'-phosphatase assay (Fig. 30). The POLXc (1-316) domain showed no activity for ssDNA, primer/template, and for 1-nt gapped DNA substrates containing 3'-phosphate (Fig. 30). The PHP (336-575) domain showed a 3'-phosphatase and a weak 3'-5' exonuclease activity in the presence of Mn^{2+} ions. The activity of the PHP (336-575) domain was highest for ssDNA and decreased in the following order of substrates: ssDNA > primer/template > 1-nt gap. ttPolX showed a strong 3'-5' exonuclease activity in the presence of Mn^{2+} after removing the 3'-phosphate. As per my expectations, based on the phosphoesterase activity of the PHP domain of ttPolX (Figs. 22 and 29), the 3'-phosphatase activity was also found to be located in the PHP domain of ttPolX.

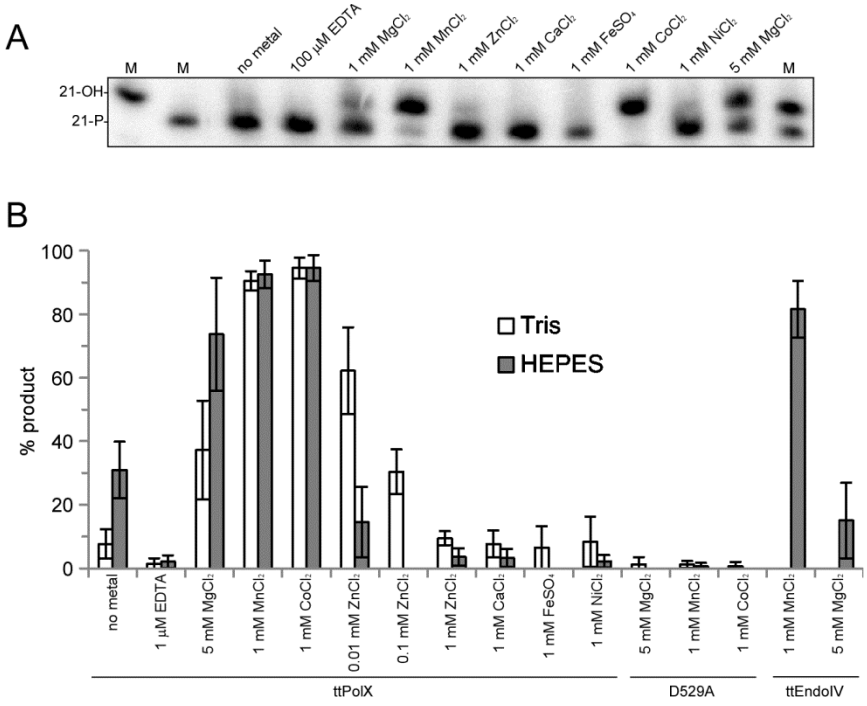

Figure 29. Metal ion selectivity of the 3'-phosphatase activity of ttPolX. (A) Autoradiographic image of the 3'-phosphatase activity. Pre-bound metal ions were removed by EDTA except for a "no metal" lane. M represents 21-mer markers with or without a 3'-phosphate. (B) 100 nM of ttPolX, D529A of ttPolX, or ttEndoIV were incubated with various divalent metal ions after removing pre-bound metal ions by 1 μM EDTA (except for a "no metal" lane) in a buffer containing 50 mM Tris-HCl or 50 mM HEPES-NaOH, 100 mM KCl, 10 nM 5'-labeled 1-nt gapped DNA with 3'-phosphate, pH 7.5 at 37°C for 10 min. The samples were analyzed by 15% denaturing PAGE (8 M urea) and autoradiography. The data represent the means of more than three experiments ± standard deviation. Note that the 3'-phosphatase activities of ttPolX, in the presence of Mn^{2+} or Co^{2+} ions, and of ttEndoIV, in the presence of Mn^{2+} ions were saturated under these conditions.

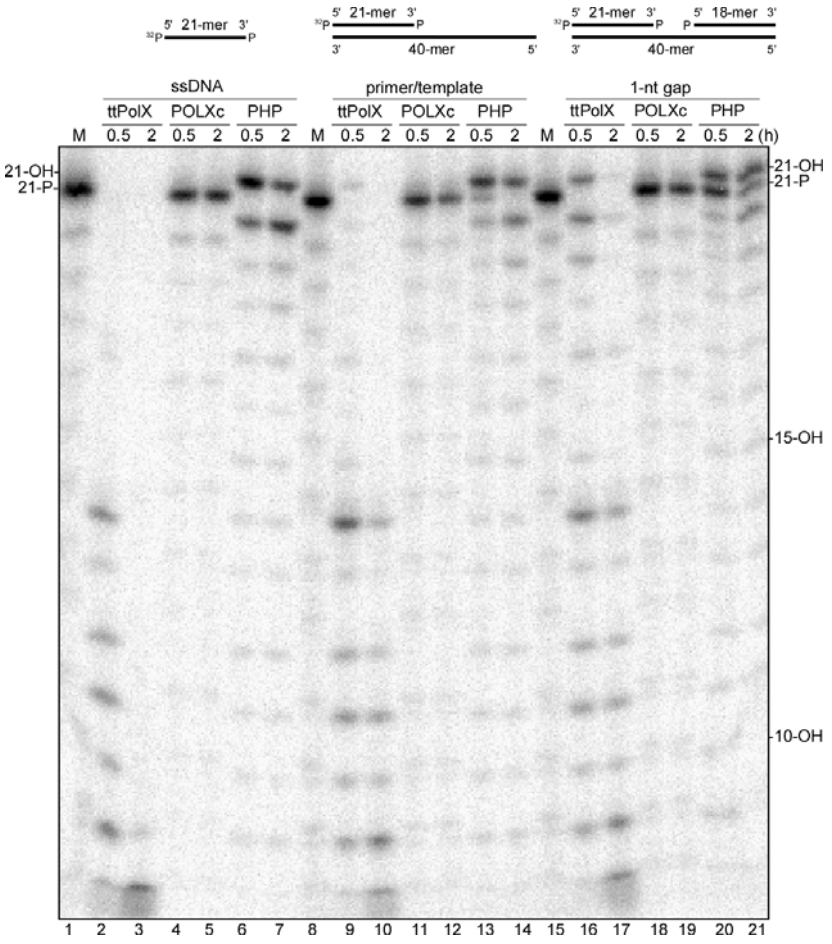

Figure 30. The 3'-phosphatase assay using ttPolX or its domains POLXc (1-316) and the PHP (336-575). Reaction mixtures containing 1 μM enzyme, 100 μg/ml BSA and 1 mM $MnCl_2$, pH 7.5 were incubated at 25°C for the indicated times. The samples were analyzed by 20% denaturing PAGE (8 M urea) and autoradiography. M represents marker lanes.

Kinetic study of the 3'-phosphatase activity of ttPolX and ttEndoIV

Kinetic experiments were performed to compare the mechanism of the 3'-phosphatase activity of ttPolX and ttEndoIV and their substrates in *T. thermophilus* (Fig. 31 and Table 13). ttPolX showed a higher k_{cat} for ssDNA (4.1 min^{-1}), but a much higher K_m for ssDNA (2.8 μM) than for other substrates (Table 13). The k_{cat} of ttPolX for the primer/template (0.51 min^{-1}) and for 1-nt gap (0.26 min^{-1}) were similar, but the K_m of ttPolX for 1-nt gap (15 nM) was lower than that for the primer/template (52 nM). Taken together, the catalytic efficiency (k_{cat}/K_m) of ttPolX was the highest for 1-nt gap (2.9×10^5 $s^{-1}M^{-1}$). Because wild-type ttPolX had too high a k_{cat} (0.26 min^{-1}) to perform pre-steady-state kinetics at 25°C manually (Fig. 31D, open inverted triangles), I searched for ttPolX mutants that had a moderate k_{cat} (Fig. 31E). One such mutant, H440A, showed a strong 3'-phosphatase activity, although it showed little 3'-5' exonuclease activity (Fig. 28E). Another mutant, H531A, showed a moderate 3'-phosphatase activity under single-turnover condition at 25°C (Fig. 31E). The k_{cat} of ttPolX for 1-nt gap was decreased from 0.26 min^{-1} to 0.047 min^{-1} by mutation of His-531 (Table 13). Therefore, I used H531A for pre-steady-state analysis (Fig. 31D, open diamonds). The amplitude and the rate constant of H531A for 1-nt gap under a single-turnover condition were A = 92 ± 0.58 and k = 0.54 ± 0.013 min^{-1}, respectively. The rate constant of H531A for 1-nt gap under a single-turnover condition (0.54 min^{-1}) was an order of magnitude higher than that under a multiple-turnover condition (0.047 min^{-1}), which may indicate the turnover of ttPolX was inhibited by the stable product complex between ttPolX and 1-nt gapped DNA without a 3'-phosphate, such as observed in many DNA glycosylases (Porello *et al*., 1998; Kosaka *et al*., 2007; Morgan *et al*., 2011). Kinetic analysis of the 3'-phosphatase activity of ttEndoIV showed that the k_{cat} (2.4 min^{-1}) and K_m (40 nM) values for 1-nt gapped DNA (Table 13). The k_{cat} value of ttEndoIV for 1-nt gapped DNA was an order of magnitude higher than that of ttPolX (Table 13). This difference in k_{cat} and K_m between ttPolX and ttEndoIV may reflect the difference in the function of the 3'-phosphatase activity.

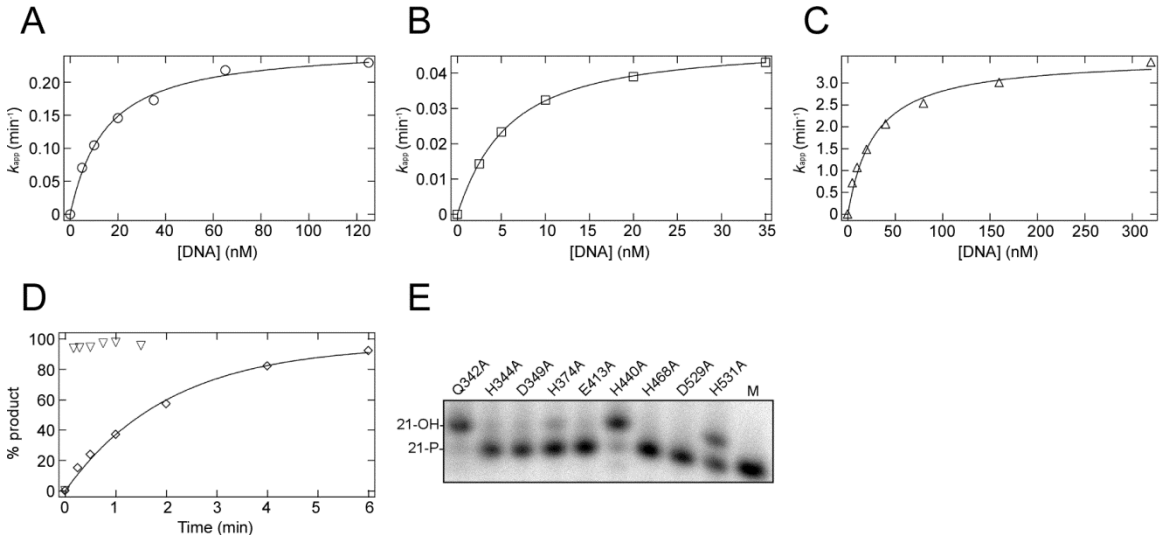

Figure 31. Multiple- and single-turnover assays for the 3'-phosphatase activity. (A) The 3'-phosphatase activity of wild-type ttPolX for 1-nt gapped DNA. The data was fitted with equation (14), as described in the *Materials and Methods*, to obtain the steady-state kinetic parameters, k_{cat} and K_m. (B) The same analysis as in panel A except H531A mutant was used. (C) The same analysis as in panel A except ttEndoIV was used. (D) Single-turnover analysis of the 3'-phosphatase activity of wild-type ttPolX (▽) or H531A mutant (◇). The data were fitted with equation (15), as described in the *Materials and Methods*. (E) The 3'-phosphatase activity of the PHP domain mutants. Reaction mixtures containing 5 μM mutant and 1 μM 1-nt gapped DNA containing 3'-phosphate, pH 7.5 were incubated at 25°C for 1 min. Note that the 3'-5' exonuclease activity of ttPolX was very weak under these conditions.

Table 13. Steady-state kinetic parameters of the 3'-phosphatase activity.[a,b]

	ssDNA			primer/template			1-nt gap		
	k_{cat} (min^{-1})	K_m (μM)	k_{cat}/K_m ($s^{-1}M^{-1}$)	k_{cat} (min^{-1})	K_m (nM)	k_{cat}/K_m ($s^{-1}M^{-1}$)	k_{cat} (min^{-1})	K_m (nM)	k_{cat}/K_m ($s^{-1}M^{-1}$)
ttPolX 1 mM $MnCl_2$	4.1 ± 1.0	2.8 ± 0.47	2.4×10^4	0.51 ± 0.038	52 ± 4.9	1.6×10^5	0.26 ± 0.023	15 ± 2.7	2.9×10^5
ttPolX 1 mM $MnCl_2$ + 10 mM $MgCl_2$							0.37 ± 0.050	55 ± 18	1.1×10^5
ttPolX 1 mM $MnCl_2$ + 10 mM $MgCl_2$ + 50 μM dGTP[c]							0.16 ± 0.015	17 ± 3.9	1.6×10^5
H531A 1 mM $MnCl_2$	0.17 ± 0.013	3.0 ± 0.46	9.5×10^2	0.21 ± 0.029	100 ± 31	3.4×10^4	0.047 ± 0.038	3.5 ± 1.1	2.2×10^5
ttEndoIV 1 mM $MnCl_2$							3.7 ± 0.12	27 ± 1.4	2.3×10^6
ttEndoIV 1 mM $MnCl_2$ + 10 mM $MgCl_2$							2.4 ± 0.034	40 ± 9.8	1.0×10^6

[a]The data represent the means of more than three experiments ± standard deviation.
[b]The 3'-5' exonuclease activity of ttPolX was very weak under these conditions.
[c]The extended 22-mer was also quantified as a product of the 3'-phosphatase activity.

The crystal structure of the PHP domain

Interestingly, I found that, in addition to the POLXc domain in one PolX (designated molecule 1) bound to a gapped DNA, the PHP domain in adjacent asymmetric unit in the crystal (designated molecule 2) also bound the same gapped DNA; i.e.; ttPolX forms a 2:1

ttPolX-DNA complex in the crystal (Fig. 32A). There are six loops that may contribute to formation of the 2:1 complex (Figs. 27, 32B and 32C): i.e., loops 1 and 2 from the POLXc domain of molecule 1 and loops 3-6 from the PHP domain of molecule 2. Loops 1 and 3 are close to each other. Loops 2 and 4 are also close and the gapped DNA appears to be partially surrounded by these four loops (Fig. 32B, loops 1-4 in top and bottom views). Loops 4-6 form hydrogen bonds with DNA (Fig. 32D). Loops 5 and 6 form positive and negative protrusions around the active site of the PHP domain for binding DNA, respectively (Figs. 32B, bottom view, and 32D). The interaction of the PHP domain of molecule 2 may be specific for gapped DNA and is concentrated upstream of the bend position (DNA residues 9-11 in Figs. 32C and 32D). Therefore, the observed 2:1 complex might be formed only when the substrate is gapped DNA.

To further investigate the possibility of 2:1 ttPolX-DNA complex formation, I carried out crosslinking reactions targeting primary amines (Fig. 34). Ternary complex of ttPolX, 1-nt gapped DNA and ddGTP was produced by the same method used to make the crystals for diffraction analysis (see Materials and Methods), but the ^{32}P labeled DNA was used. If DNA was not added, a self-crosslinked ttPolX band was observed by CBB staining slightly above 66.2 kDa (Fig. 33A, lane 2). When DNA was present, formation of this band was reduced and instead the bands indicated by arrows 1 and 2 were observed (Fig. 33A, lanes 3-8). As the DNA concentration increased, band 1 gradually increased whereas band 2 decreased. Band 2 was observed when the DNA concentration was lower than that of ttPolX. Therefore, bands 1 and 2 were suggested to be 1:1 and 2:1 ttPolX-DNA complexes, respectively. The 2:1 band should not be the result of crosslinking the POLXc domains of two PolXs bound to one DNA because the DNA length is too short to bind two ttPolX molecules (Fig. 32A). The size of band 1 was smaller than the expected size for a 1:1 complex (73 kDa), possibly because gapped DNA may have been in a stable compact state during electrophoresis and had negative charges. The apparent size of band 2 was larger than the expected size of 2:1 complex (137 kDa). This may have been due to the binding of crosslinker and Tris to make the apparent size larger or to fewer SDS being bound to the crosslinked product. Autoradiography showed three bands at about 180, 70 and 60 kDa in the cross-linked samples (Fig. 33A, lanes 9-16). Each CBB-stained band was cut out of the gel and analyzed by autoradiography. This showed that the upper band at ~180 kDa was near the position of band 2 in the CBB-stained gel, which may be the 2:1 ttPolX:DNA complex. The band at ~70 kDa was slightly above that of the self-crosslinked ttPolX band. There were no observable bands at this position in the CBB-stained image. The band at ~60

kDa was near the position of band 1, which may be the 1:1 ttPolX:DNA complex. However, the ~60 and ~70 kDa RI-bands were also observed when no crosslinker was added (data not shown), although the RI-level was lower than that of crosslinked lanes. Since there were no RI-bands in lanes 1 and 9 (DNA-only lanes), these RI-bands were not free DNA. The 1:1 ttPolX:DNA complex might be stable under SDS-PAGE conditions. These crosslinking assay might support the formation of a 2:1 ttPolX:gapped DNA complex shown by crystal structure (Fig. 32), but the content of 1:1 and 2:1 ttPolX:DNA complexes in the crosslinking assay (Fig. 33A) were very small. When I used glutaraldehyde as a crosslinker, the content of crosslinking product of ttPolX:DNA complex was still small (Fig. 33B). I concluded that crosslinking assay may not be suited to detect a ttPolX:DNA complex.

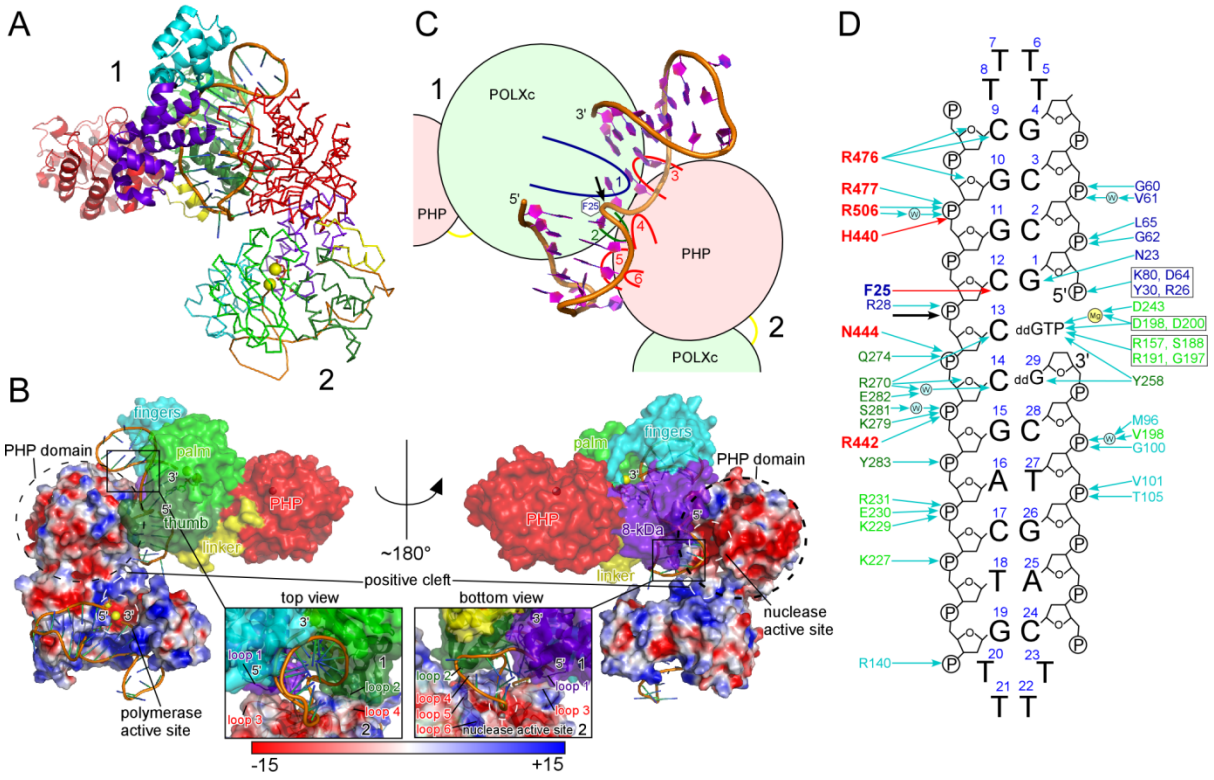

Figure 32. Possible model of 2:1 ttPolX:DNA complex. (A) The POLXc domain of molecule 1 and the PHP domain of molecule 2 both bound to a gapped DNA. Molecules 1 and 2 are different asymmetric units in the crystal. (B) DNA partially surrounded by two molecules of ttPolX (marked 1 and 2). Four loops (loop 1, residues 21-23; loop 2, 276-278; loop 3, 379-388 and loop 4, 439-456) involved in making a cavity and two loops (loop 5, residues 467-483 and loop 6, 502-510) interacting with DNA are shown. Molecule 2 is shown as an electrostatic potential surface model. The 8-kDa subdomain of molecule 2 has been removed to show the polymerase active site. Blue and red colors represent positive and negative charges, respectively. White arrows represent positive clefts between the polymerase and nuclease active sites. PyMOL plugin APBS was used for the calculation of electrostatic potential (Baker *et al.*, 2001). (C) Schematic diagram of the 2:1 ttPolX-DNA complex. The six loops possibly related to forming the 2:1 complex are shown. Loop 1 is drawn to include two α helices (α1 and α2, Fig. 12A). Black arrows indicate the template strand bend. (D) The DNA-binding residues of the PHP domain were added in Fig. 19A as red letters.

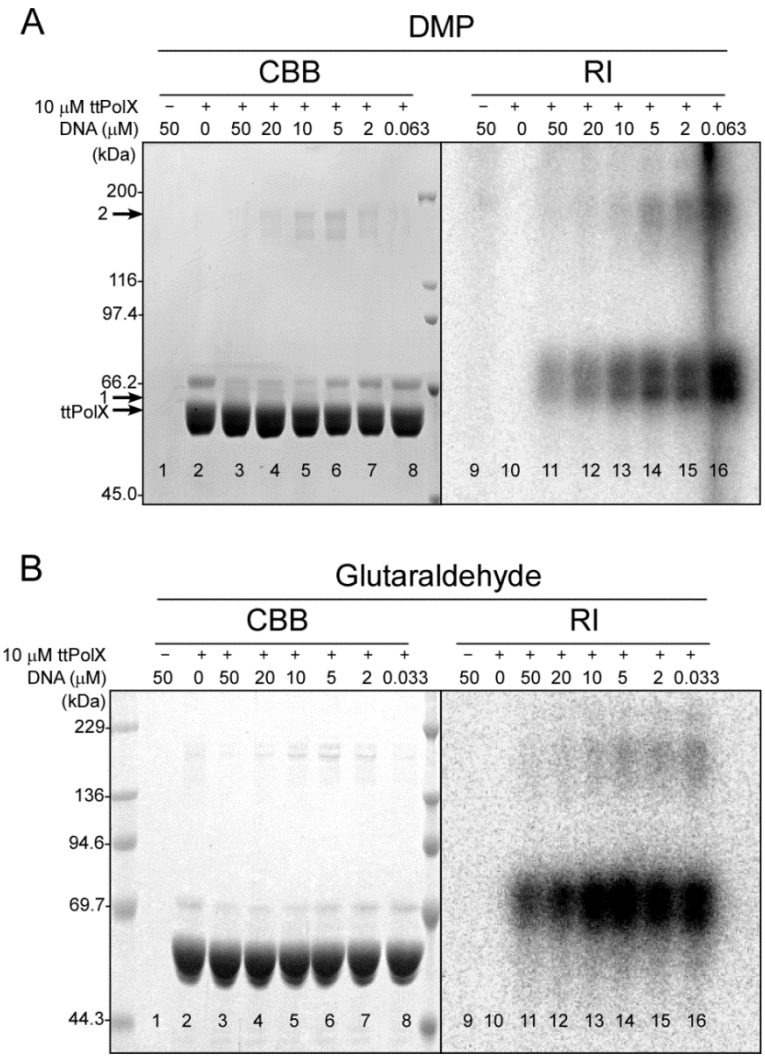

Figure 33. Crosslinking assay. Crosslinking reactions with the ttPolX, 1-nt gapped DNA, and ddGTP ternary complex in solution, showing an CBB-stained image (lanes 1-8) and autoradiograph (lanes 9-16) of the same gel. All samples except for lanes 1 and 9 contained 10 μM ttPolX. All lanes except lanes 2 and 10 contained 63 or 33 nM ^{32}P-labeled DNA. The DNA sequence is shown in Fig. 19A. ttPolX was incubated with or without DNA, followed by crosslinked with a 1250-fold molar excess of DMP at 25°C for 1 h (A) or with a 50-fold molar excess of glutaraldehyde at 25°C for 10 min (B). Crosslinked samples were analyzed by 7.5% SDS-PAGE and stained with CBB. The position of ttPolX (64 kDa) is indicated by an arrow. Arrows 1 and 2 indicate possible 1:1 and 2:1 ttPolX-gapped DNA complexes, respectively.

Stoichiometric analysis of the 3'-phosphatase activity

The proposed ttPolX:DNA 2:1 complex was investigated from a kinetic point of view by analyzing the 3'-phosphatase activity of ttPolX. The 3'-phosphatase assay was performed using a fixed concentration of DNA substrate and various concentrations of the H531A mutant (Fig. 34). These substrate and enzyme concentrations were set in large excess of the K_m value of the enzyme to facilitate maximally binding between the substrate and the input enzyme. The initial velocity (v) of such an enzyme reaction is k_{cat}[ES], and, therefore, the measured velocities increase proportionally with [ES] until the substrate is saturated with the enzyme at their stoichiometric ratios. The velocity of the H531A reaction remained constant at the H531A:DNA ratio of around 1:1 in the presence of $MnCl_2$, both for the primer/template and for the 1-nt gapped DNAs (Figs. 34A, open circles, and 34B, open triangles; Table 14). The determined crystal structure of ttPolX ternary complex contained incoming ddGTP (Fig.

32A), which suggested that an incoming nucleotide may be needed for the 2:1 complex. Based on this crystallographic information, I added an incoming dGTP and repeated the 3'-phosphatase assay (Figs. 34C, open rectangles, and 34D, open diamonds). The results indicated a slight increase in the stoichiometric ratio for 1-nt gapped DNA ($[E]_0/[S]_0 = 1.3$); however, the ratio was quite different from the 2:1 ratio of the complex (Table 14). The ratio for the primer/template and the maximum velocity, v_{max}, for the primer/template and for the 1-nt gap did not change regardless of the presence of dGTP (Table 14). Because the polymerase activity of ttPolX was stronger in the presence of Mg^{2+} than in the presence of Mn^{2+} ions (Fig. 5), and the 3'-phosphatase activity was stronger in the presence of Mn^{2+} than in the presence of Mg^{2+} ions (Fig. 29), I performed the assay using the H531A in the presence of Mg^{2+}, Mn^{2+} and dGTP (Figs. 34C, closed rectangles, and 34D, closed diamonds; Table 14). Surprisingly, the stoichiometry was increased to approximately $[E]_0/[S]_0 = 1.5$, and v_{max} was also increased to approximately 2.0 μM/min for both the primer/template and the 1-nt gapped DNA substrates (Table 14). However, similar assay results were obtained in the presence of Mg^{2+} and Mn^{2+} ions, but in the absence of dGTP (Figs. 34A, closed circles, and 34B, closed triangles; Table 14). Therefore, I concluded that the change in the 3'-phosphatase activity of the H531A was due to the coexistence of Mg^{2+} and Mn^{2+} ions. I further investigated the activation of the 3'-phosphatase activity by Mg^{2+} ion under a steady-state condition (Table 13). The k_{cat} of the 3'-phosphatase activity of ttPolX was higher in the presence of Mg^{2+} and Mn^{2+} than in the presence of Mn^{2+} alone, which was comparable to the results obtained from the stoichiometric analysis of H531A. In contrast, the k_{cat} was slightly decreased in the presence of Mg^{2+}, Mn^{2+} and dGTP (Table 13). This decrease in enzyme turnover was perhaps because of the POLXc domain strongly binding to the 1-nt gapped DNA in the presence of the incoming nucleotide. Based on the above results, I suggested that ttPolX may have at least two mechanisms for the 3'-phosphatase activity depending on the status of metal ions. In the case of ttEndoIV, the k_{cat} was slightly lower in the presence of Mg^{2+} and Mn^{2+} than that in the presence of Mn^{2+} alone (Table 13).

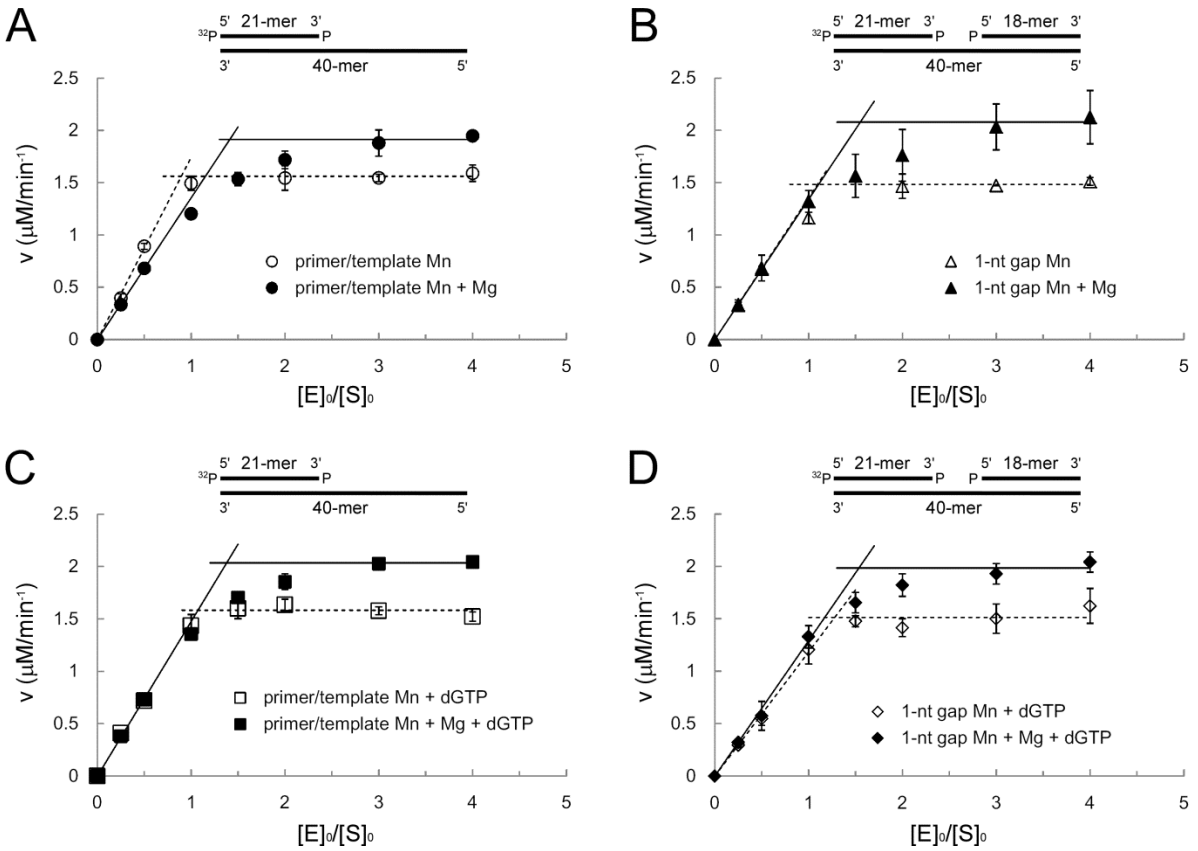

Figure 34. Stoichiometric analysis of the 3'-phosphatase activity of H531A using 2 μM of primer/template DNA or 1-nt gapped DNA. Initial velocities are plotted against the ratio of $[E]_0/[S]_0$, where $[E]_0$ and $[S]_0$ are the total concentration of H531A and the total concentration of substrate DNA (2 μM), respectively. (A) The reaction velocity for primer/template DNA in the presence of 1 mM $MnCl_2$ or in the presence of 1 mM $MnCl_2$ and 10 mM $MgCl_2$. (B) The reaction velocity for 1-nt gapped DNA in the presence of 1 mM $MnCl_2$ or 1 mM $MnCl_2$ and 10 mM $MgCl_2$. (C) The reaction velocity for primer/template DNA in the presence of 1 mM $MnCl_2$ and 50 μM dGTP, or in the presence of 1 mM $MnCl_2$, 10 mM $MgCl_2$ and 50 μM dGTP. (D) The reaction velocity for 1-nt gapped DNA with 1 mM $MnCl_2$ and 50 μM dGTP, or in the presence of 1 mM $MnCl_2$, 10 mM $MgCl_2$ and 50 μM dGTP. The data represent the means of more than three experiments ± standard deviation. The 3'-5' exonuclease activity was very weak under these conditions. The extended 22-mer was also quantified as a product of the 3'-phosphatase activity in the case of panels C and D.

Table 14. Summary of the stoichiometric analysis of the 3'-phosphatase activity of H531A.

	DNA substrate	$[E]_0/[S]_0$	v_{max} (μM/min)
1 mM $MnCl_2$	Primer/template	0.88	1.6
	1-nt gap	1.1	1.5
1 mM $MnCl_2$ + 10 mM $MgCl_2$	Primer/template	1.4	1.9
	1-nt gap	1.5	2.1
1 mM $MnCl_2$ + 50 μM dGTP	Primer/template	1.1	1.6
	1-nt gap	1.3	1.5
1 mM $MnCl_2$ + 10 mM $MgCl_2$ + 50 μM dGTP	Primer/template	1.4	2.0
	1-nt gap	1.5	2.0

AP endonuclease activity of the PHP domain

The PHP domain of ttPolX showed AP endonuclease activity (Fig. 35). The AP site is generated spontaneously and is an intermediate in DNA repair processes such as BER (see Fig. 48). The cellular AP endonuclease incises at the AP sites within DNA and thereby helps in the progression of the DNA repair process. Many bacteria have EndoIV as an AP endonuclease. In addition to EndoIV, bsPolX was reported to have an AP endonuclease activity in its PHP domain (Banos *et al.*, 2010). In the present study, ttPolX showed a Mn^{2+}-dependent AP endonuclease activity similar to bsPolX (Fig. 35B and 35C). This AP endonuclease activity was located in the PHP domain. Time course analysis demonstrated that ttPolX exhibits an AP endonuclease activity for both ssDNA and dsDNA (Fig 35B and 35C). In the case of ssDNA, the sudden appearance of a 9-mer product indicated the presence of an AP endonuclease activity, although ttPolX also showed a strong 3'-5' exonuclease activity (Fig. 35B). The AP endonuclease activity of ttPolX strongly suggests the involvement of ttPolX in the process of BER.

It is surprising that the PHP domain of ttPolX has both exonuclease and endonuclease activities. Here, I present the first structure of the PHP domain bound to DNA (Figs. 32 and 35E). The PHP domain was bound to an internal region of DNA, not to the 3'- or 5'-terminus, indicating the possibility that this binding state is similar to the one representing an intermediate states of an endonuclease reaction. It had been suggested that bsPolX had two important residues (Phe-440 and Arg-474) for the AP endonuclease activity based on a comparison with residues Arg-37 and Tyr-72 of *E. coli* EndoIV (ecEndoIV) (Banos *et al.*, 2010; Garcin *et al.*, 2008) (Fig. 35D). The possible functions of Arg-37 and Tyr-72 in ecEndoIV include the stabilization of the complex of ecEndoIV and DNA containing the AP site by stacking of a base, and shielding the active site of the enzyme from bulk solvent, respectively (Garcin *et al.*, 2008). Similar to ecEndoIV, ttPolX has Phe-443 and Arg-477 within the PHP domain (Fig. 35E). Although the spatial positions of the PHP hydrophobic (Phe-443) and stacking (Arg-477) residues are opposite to those of ecEndoIV (Arg-37 and Tyr-72), they are expected to have similar functions.

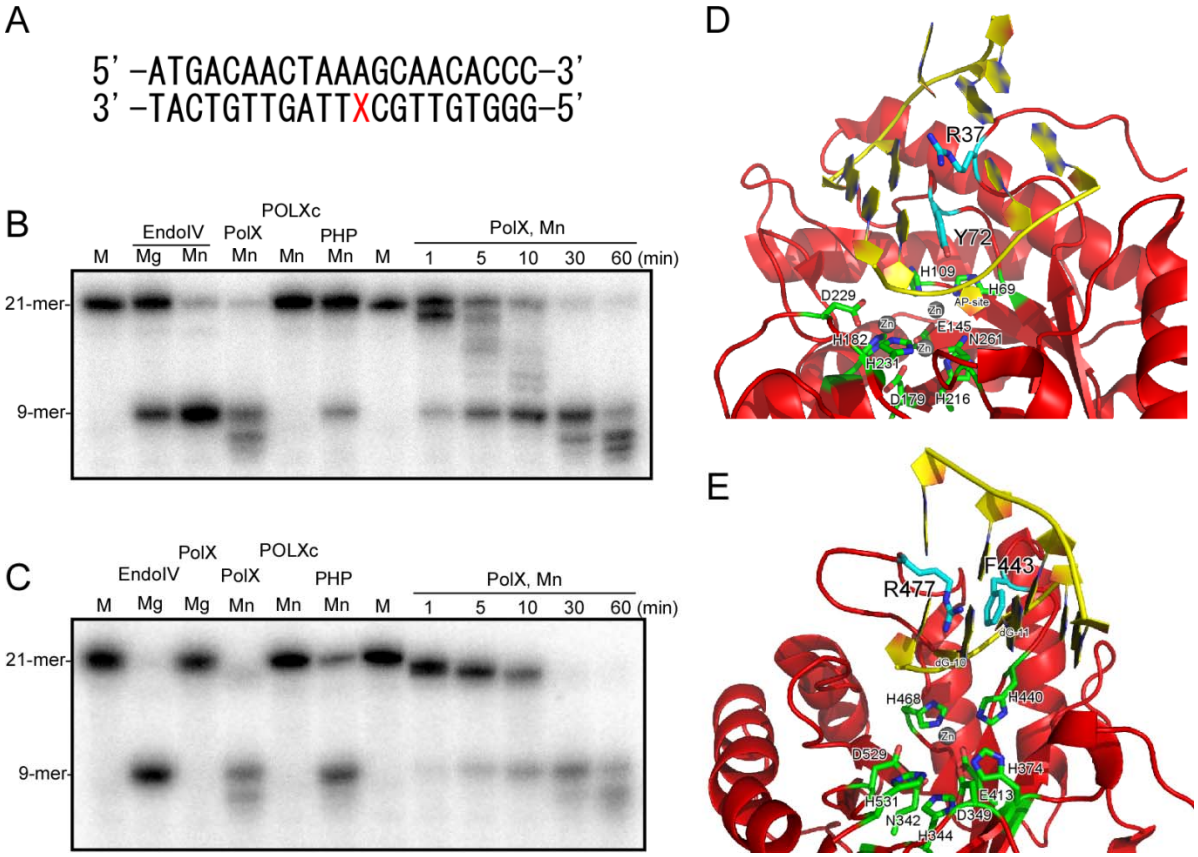

Figure 35. AP endonuclease activity of ttPolX. (A) The sequence used for AP endonuclease assay. X = tetrahydrofuran (THF), a stabilized AP-site analog. The oligonucleotide containing THF was 5'-labeled using [γ-^{32}P] ATP. (B) The AP endonuclease activity of ttPolX for ssDNA containing THF. (C) AP endonuclease activity of ttPolX for dsDNA containing THF. I used POLXc (1-316) and C-terminal His-tagged PHP (336-575) domains in these assays. ttEndoIV was used as a positive control for AP endonuclease activity. M represents the marker lanes. (D) Ribbon diagram showing the active site of the ecEndoIV E261Q mutant along with DNA containing the AP-site analog THF (Garcin *et al*., 2008). DNA around the AP-site analog is shown in yellow. Catalytic and stacking residues are shown in green and cyan, respectively. (E) Ribbon diagram showing active site within the PHP domain of ttPolX in a ternary complex with 1-nt gapped DNA and ddGTP (Figs. 11B and 32). DNA residues 1-4 and 9-12 are shown in yellow. Catalytic and possible stacking residues are shown in green and cyan, respectively. Although this structure contains one zinc ion, the PHP domain of ttPolX can contain up to three zinc ions (PDBID, 3AU2).

IV. Cellular Functions of ttPolX

The balance of 5'-3' DNA polymerase and 3'-5' exonuclease activities

To know how ttPolX controls polymerase and exonuclease activities, the activity was measured in the presence of Mg and Mn ions (Fig. 36). Many DNA polymerases have 3'-5' exonuclease activity as a proofreading activity. Bacterial PolXs also have 3'-5' exonuclease activity, but eukaryotic PolXs don't have. ttPolX also has 3'-5' exonuclease activity, however, Mg ions, which is the most popular cofactor of DNA polymerase activity, did not activate 3'-5' exonuclease activity (Fig. 4A). ttPolX showed strong 3'-5' exonuclease activity in the presence of Mn ions (Figs. 4A and 36), although ttPolX has Mn^{2+}-dependent DNA polymerase activity (Fig. 5). The assay was performed in a fixed concentration of Mg (10 mM) and varied concentrations of Mn (0-0.5 mM) (Fig. 36). The DNA polymerase activity was changed to the 3'-5' exonuclease activity between 0.1-0.2 mM Mn ions. The intracellular concentrations of metal ions in *T. thermophilus* HB8 was measured (Kondo *et al*., 2008); intracellular Mg and Mn concentrations were 1.5 < Mg < 35 and 0.00091 < Mn < 0.16 mM. (Fig. 36). In this condition, ttPolX is expected to have strong DNA polymerase activity with weak 3'-5' exonuclease activity. This means that the 3'-5' exonuclease activity of ttPolX may act as a proofreading function.

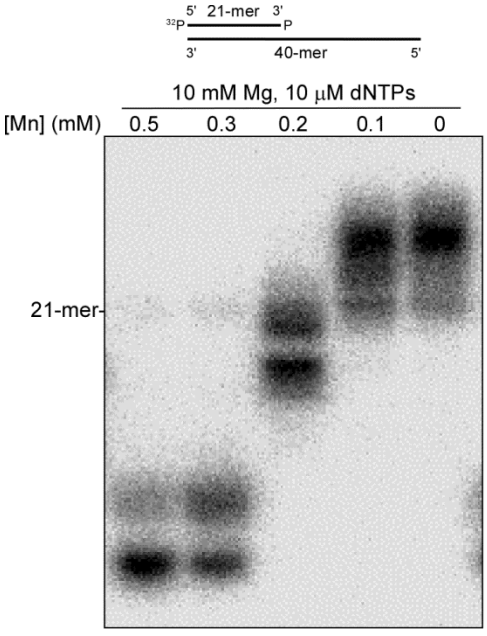

Intracellular concentration of metal ions in TTHB8

Metal	TR medium (mM)	Intracellular concentration (mM)	
		Acid treatment	Sonic treatment
Na	20	42.6 ± 1.8	21.6 ± 0.94
Mg	0.17	35.0 ± 2.7	1.53 ± 0.044
Si	0.19	0.343 ± 0.074	0.321 ± 0.0093
P	1.5	221 ± 8.2	32.1 ± 0.91
K	4.4	72.1 ± 2.9	43.5 ± 1.4
Ca	0.29	6.74 ± 0.57	0.130 ± 0.011
Mn	0.00014	0.163 ± 0.0057	0.000906 ± 0.000079
Fe	0.0034	1.77 ± 0.058	0.0034 ± 0.00042
Co	<0.000017[a]	<0.000624[a]	<0.000624[a]
Ni	<0.00016[a]	0.150 ± 0.000057	<0.00587[a]
Cu	<0.000031[a]	0.0548 ± 0.0038	<0.00113[a]
Zn	0.0050	0.584 ± 0.041	0.00255 ± 0.0010
Mo	<0.000058[a]	0.011 ± 0.0038	0.00504 ± 0.0019
Cd	<0.000018[a]	0.00657 ± 0.0011	<0.00066[a]

[a] Detections were under detectable level

Figure 36. Polymerase and exonuclease activities of ttPolX in the presence of Mg and Mn ions. Reaction mixture containing 20 mM Tris-HCl, 20 mM KCl, 10 nM 5'-^{32}P labeled DNA, 10 mM $MgCl_2$, $MnCl_2$ and 1 μM ttPolX, pH 8.1 was incubated at 37°C for 30 min. The samples were analyzed by 18% denaturing PAGE (8 M urea) and autoradiography. Table of "Intracellular concentration of metal ions in TTHB8" is cited from (Kondo *et al*., 2008).

Strand-displacement synthesis

ttPolX had little strand-displacement activity compared with ttPolI, the other DNA repair DNA polymerase in *T. thermophilus* (Figs. 7B and 37). After removal of dRP or 3'-phosphate, the resultant 1-nt gap should be filled by DNA polymerase to complete BER (see Fig. 48). The DNA polymerase activity of ttPolX was weak for primer/template DNA, but remarkably stimulated with 1-nt gapped DNA as a substrate (Figs. 7 and 37, lanes 2-5). On the contrary, DNA polymerase activity of ttPolI was high for primer/template DNA and inhibited by 1-nt gapped DNA (Fig. 37, lanes 6-9). Moreover, ttPolX came to halt after filling the 1-nt gaps (Fig. 37, lanes 4 and 5), whereas ttPolI extended the primer after filling gaps (Fig. 37, lanes 8 and 9). This coupled polymerase and dsDNA unwinding activity is called strand-displacement synthesis. Strand displacement generates an additional 5'-flap and needs a flap endonuclease activity in order for DNA ligase to seal the gap. Therefore, ttPolX appears to be a more suitable DNA polymerase for filling 1-nt gaps.

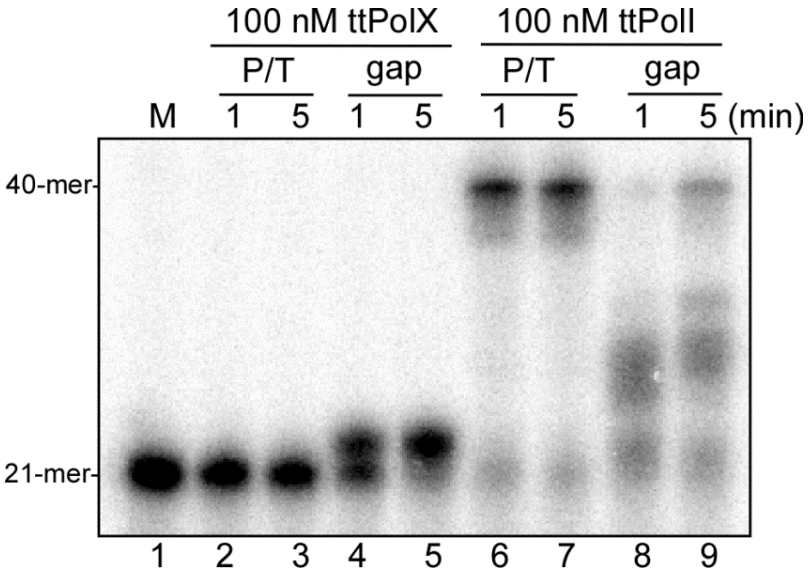

Figure 37. Strand-displacement synthesis by ttPolX and ttPolI. Reaction mixtures composed of 50 mM Tris-HCl, 100 mM KCl, 10 mM $MgCl_2$, 100 μM dNTPs, 10 nM 5'-^{32}P labeled DNA and 100 nM ttPolX or ttPolI, pH 7.5, were incubated for the indicated time at 37°C, and analyzed by 18% denaturing PAGE (8 M urea) and autoradiography. P/T and gap denote primer/template (21F/40T) and 1-nt gapped (21F/40T/P18G) DNA, respectively. M represents a 21-mer marker.

Transcriptomic analysis of ttPolX

The expression level of mRNA of ttPolX was increased as growth phase was shifted to stationary phase (Fig. 38, black line). The other DNA polymerases did not increased mRNA expression level at stationary phase. Because stationary phase is known that DNA damage is accumulated and required DNA repair in bacteria (Bridges, 1998; Nystrom, 2003; Finkel, 2006), ttPolX is expected to act for DNA repair in stationary phase.

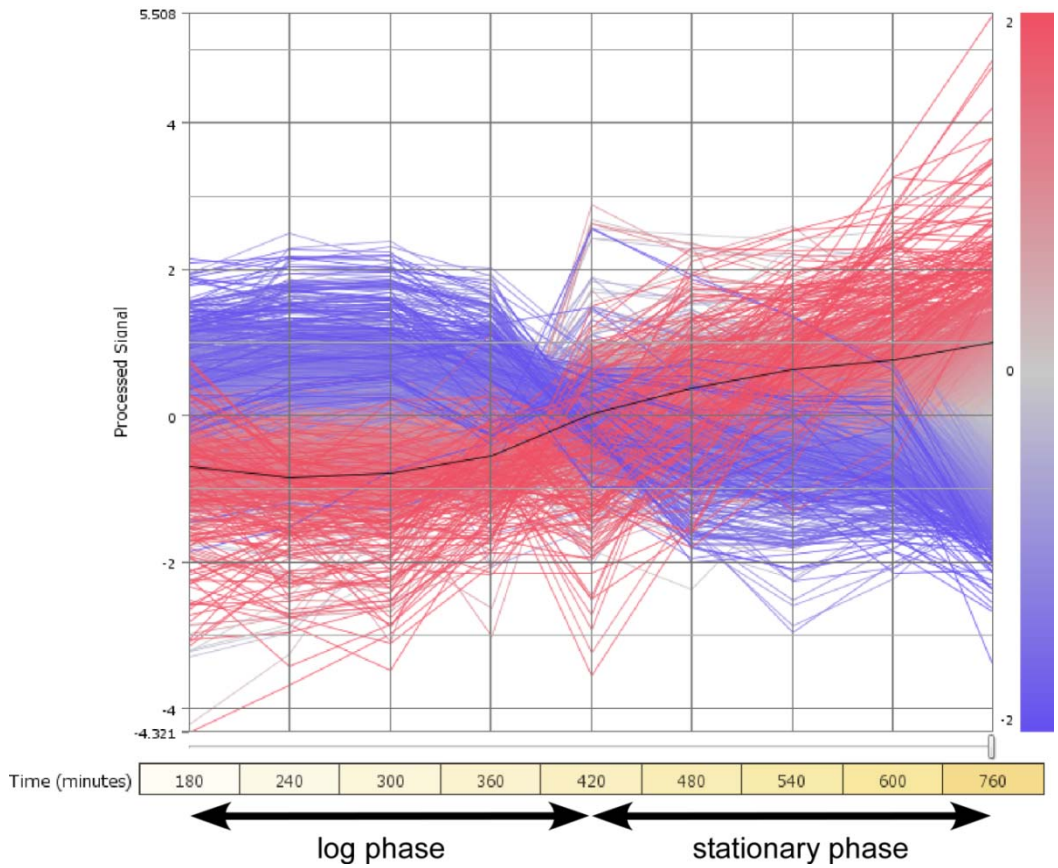

Figure 38. Expression profile of mRNA as a function of growth phase of *T. thermophilus* HB8. Overnight cultured cells were inoculated into fresh TT medium, and aliquots of cells were collected at each time points. mRNA expression level of ttPolX is represented as black line. Microarray data of *T. thermophilus* are available on GPL4902 platform at GEO web site (http://www.ncbi.nlm.nih.gov/geo/).

Gene disruption of DNA polymerases and 3'-phosphatases

I produced Δ*ttpolX*, Δ*ttpolI*, and Δ*ttendoIV* disruptants of *T. thermophilus* HB8 to investigate the function of ttPolX *in vivo*. ttPolI and ttPolX are both DNA repair polymerases. ttEndoIV is the only known 3'-phosphatase in *T. thermophilus* HB8 other than ttPolX. The disruption of genes was confirmed by PCR at the DNA level (Fig. 39) and by Western blotting at the protein level (Fig. 40). I successfully obtained the following six disruptants: Δ*ttpolX*, Δ*ttpolI*, Δ*ttendoIV*, Δ*ttpolI*/Δ*ttpolX*, Δ*ttpolX*/Δ*ttpolI*, and Δ*ttendoIV*/Δ*ttpolX*.

Disruptants showed no serious growth delay in rich medium (Fig. 41). The disruptants Δ*ttpolX*, Δ*ttpolI*, and Δ*ttpolI*/Δ*ttpolX* showed slightly slower growth than the wild-type, and the growth of disruptants Δ*ttendoIV*/Δ*ttpolX* was even further delayed than the wild-type; however, none of these differences were statistically significant (Figs. 41A and 41B). Δ*ttpolX*/Δ*ttpolI* showed much slower growth than the wild-type. This might be due to unexpected mutations in the gene regions other than *ttpolX* and *ttpolI* because

Δ*ttpolI*/Δ*ttpolX* showed a growth pattern similar to the wild-type.

The stress resistance of Δ*ttpolX* was evaluated at log phase (Figs. 41C-41E). The resistance of Δ*ttpolX* and the wild-type to UV-C radiation was similar (Fig. 41C), indicating that ttPolX is not involved in the DNA repair process elicited by UV-C damage. Hydrogen peroxide and sodium nitrite reduced the survival rate of Δ*ttpolX* approximately by one order of magnitude as compared to the wild-type (Figs. 41D and 41E). Hydrogen peroxide and sodium nitrite cause oxidative damage (Ward, 1998; Asad *et al*., 2004) and deamination (Schuster, 1960) of the genomic DNA, respectively. Damaged bases, generated as a result of these stresses, can be repaired by the BER, that is initiated by the corresponding DNA glycosylases. The reduction in the survival rate of Δ*ttpolX* after exposure to hydrogen peroxide and sodium nitrite (Figs. 41D and 41E) suggests the involvement of ttPolX in BER.

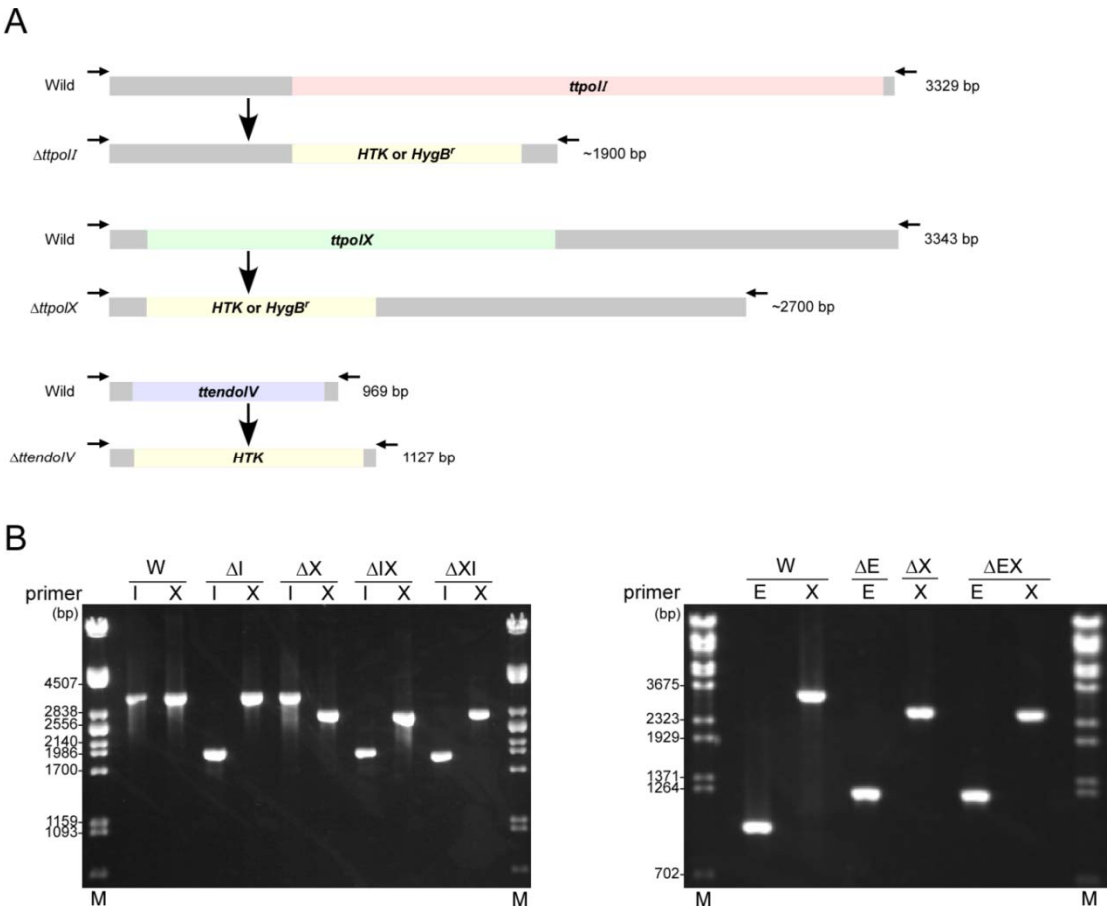

Figure 39. Disruptions of *ttpolI*, *ttpolX* and *ttendoIV* were confirmed by PCR. (A) A schematic representation of the amplified regions in the wild-type and disruptants genomes. Arrows represent primers used for PCR. Expected sizes of the PCR products are shown on the right side. (B) The amplified DNA fragments were analyzed by 0.7% or 1% agarose electrophoresis. The template genomes used for PCR were as follows: W, wild-type; ΔI, Δ*ttpolI* (Km^r); ΔX, Δ*ttpolX* (Km^r); ΔIX, Δ*ttpolI* (Km^r)/ Δ*ttpolX* (Hyg^r); ΔIX, Δ*ttpolX* (Km^r)/ Δ*ttpolI* (Hyg^r); ΔE, Δ*ttendoIV* (Km^r) and ΔEX, Δ*ttendoIV* (Km^r)/ Δ*ttpolX* (Hyg^r). Primer sets used for PCR were as follows: I, amplification for *ttpolI*; X, amplification for *ttpolX* and E, amplification for *ttendoIV*. The size of the amplified fragments showed good concordance with the theoretical size of the targeted regions, indicating that the genes were successfully disrupted.

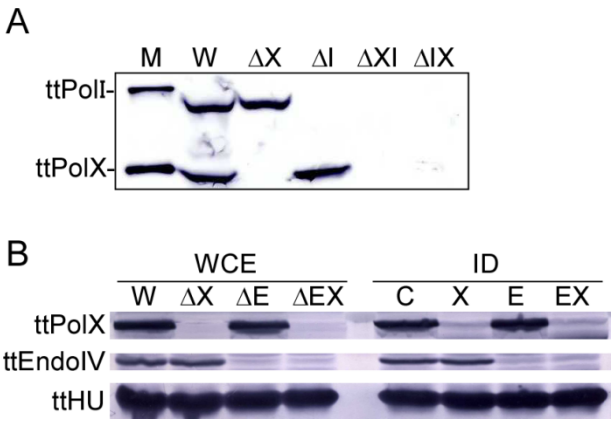

Figure 40. Disappearance of the expression of the targeted enzymes in the disruptants was confirmed by Western blotting. (A) Confirmation for ttPolX and ttPolI expression. M represents recombinant ttPolI and ttPolX markers. (B) Remaining of the ttPolX and ttEndoIV proteins in WCEs and ID cell lysates were confirmed. Anti-ttHU (TTHA 1349) antibody was used as a loading control. The cell lysates used for Western blotting were as follows: W, wild-type cells; ΔX, Δ*ttpolX* cells; ΔI, Δ*ttpolI* cells; ΔXI, Δ*ttpolX*/*ttpolI* cells; ΔIX, Δ*ttpolI*/*ttpolX* cells; ΔE, Δ*ttendoIV* cells; ΔEX, Δ*ttendoIV*/*ttpolX* cells; C, immunodepletion against no antibody; X, immunodepletion against anti-ttPolX antibody; E, immunodepletion against anti-ttEndoIV antibody and EX, immunodepletion against anti-ttEndoIV and anti-ttPolX antibodies.

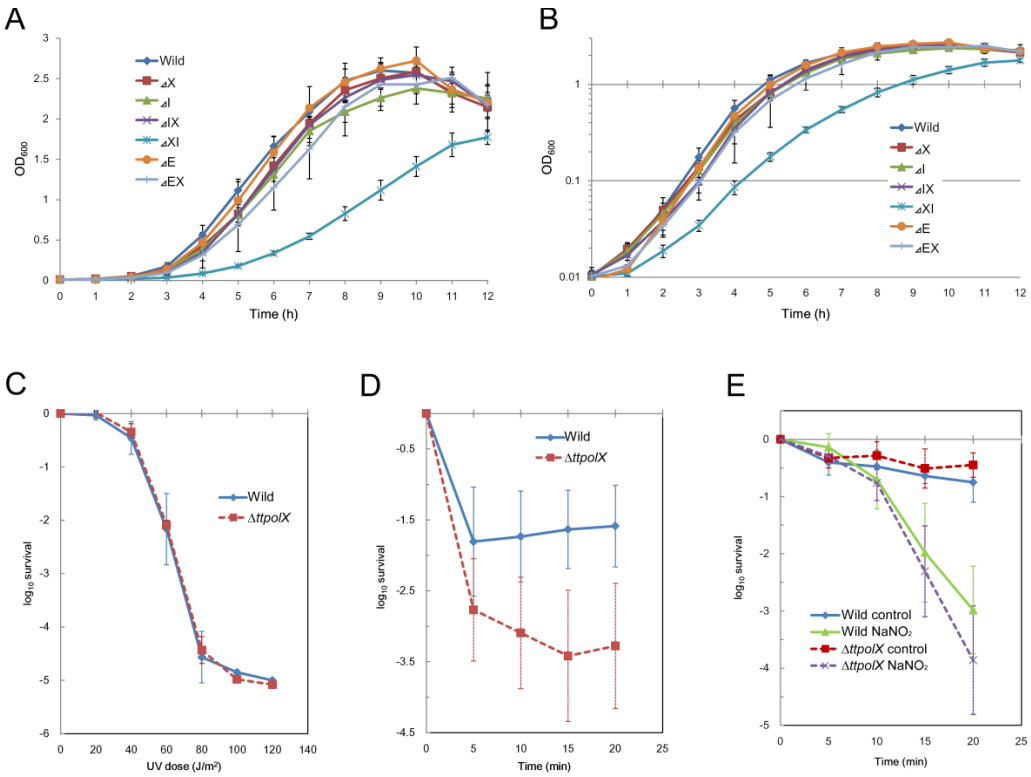

Figure 41. Growth curves and survival rates following exposure of wild-type and disruptant cells to various stresses. (A) Growth curves of wild-type, and single as well as double disruptant cells. (B) OD_{600} in panel A at each time point is represented as $\log_{10}$ value. (C) UV (254 nm) resistance of wild-type and Δ*ttpolX* cells at log phase. Cells (1×10^8/ml) cultured in TR medium were appropriately diluted and plated onto TT plates, after which the cells were irradiated with UV (254 nm) at the indicated levels. After incubation at 70°C for 24 h, the colonies were counted. The survival rate was defined as the ratio of the number of colonies of the treated sample to that of the non-treated sample (0 J/m^2). (D) Resistance against 20 mM hydrogen peroxide at log phase. Cells (1×10^8/ml) cultured in 3 ml TR medium were treated with 20 mM hydrogen peroxide, incubated at 70°C for the indicated times, and plated onto TT plates. The resulting colonies were counted, and the survival rate was calculated as described in (C). (E) Resistance against 10 mM sodium nitrite ($NaNO_2$) at log phase was measured using a modified method described by Cohen *et al.*, 1989. Log-phase cells (1×10^8/ml) were collected by centrifuging the cultures, resuspended in 500 µl of 0.1 M sodium acetate buffer (pH 4.6), and treated with 10 mM sodium nitrite (pH 7.2). Cells that were handled identically, but without adding sodium nitrite, served as a control. After incubation at 70°C for the indicated times, the cells were diluted 1:10 into McIlvaine's buffer (pH 7.0) (18.15 ml of 0.1 M citric acid + 81.85 ml of 0.2 M disodium phosphate) to neutralize the nitrous acid, and then further diluted appropriately with the medium, and plated as described above. Data represent means of at least three experiments ± standard deviation.

The 3’-phophatase and AP endonuclease activities of cell lysates

My hypothesis was that if *T. thermophilus* HB8 only has two 3’-phosphatases, namely ttPolX and ttEndoIV, the cell lysates lacking these enzymes should lack the 3’-phosphatase activity. To test this hypothesis, WCEs from wild-type and disruptants were used in a 3’-phosphatase assay (Fig. 42). The lysates obtained from wild-type cells showed a strong 3’-phosphatase activity (Fig. 42, lanes 2 and 10), and the lysates obtained from Δ*ttpolX* and Δ*ttendoIV* cells retained this activity (Fig. 42, lanes 3, 4, 11, and 12). As expected from the above hypothesis, the lysates obtained from the disruptant Δ*ttendoIV*/Δ*ttpolX* had no 3’-phosphatase activity (Fig. 42, lanes 5 and 13), indicating that the primary 3’-phosphatases in *T. thermophilus* HB8 were ttPolX and ttEndoIV. These results were also confirmed by using ID lysates (Figs. 40B and 42, lanes 6-9 and 14-17). The lysates that were depleted of ttPolX and ttEndoIV showed no 3’-phosphatase activity (Fig. 42, lanes 9 and 17), which is consistent with the results obtained from WCE assays. The temperature, incubation time, and protein concentration of the lysates were increased; nevertheless, the lysates depleted of ttPolX and ttEndoIV showed no 3’-phosphatase activity (Fig. 42, lanes 21-24). To evaluate whether the ttPolX or the ttEndoIV activity was more stronger in the lysate, a time course analysis was performed (Fig. 42B). After incubation for 30 min, the ttPolX and ttEndoIV activities were similar in the WCEs of wild-type, Δ*ttpolX*, and Δ*ttendoIV* (Figs. 42A, lanes 2-4 and 42B). Prior to the 30 min incubation, the WCE of Δ*ttendoIV* showed a weaker 3’-phosphatase activity than that of the wild-type (Fig. 42B), although that of Δ*ttpolX* showed a similar 3’-phosphatase activity as the wild-type. These results suggest that ttEndoIV is the major 3’-phosphatase in *T. thermophilus* HB8, and that ttPolX activity supports ttEndoIV activity.

The AP endonuclease activity, which is another common activity of ttPolX and ttEndoIV, was also investigated using cell lysates (Fig. 43). The dsDNA containing AP:G was derived by removing a uracil by uracil DNA glycosylases (Fig. 43A). Uracil is generated through the deamination of cytosine. The AP endonuclease activity of ttPolX was strongly inhibited by high salt (100 mM KCl) and phosphate (1 mM KPi) conditions (Fig. 43B) although that of ttEndoIV was not. The AP endonuclease assay of the cell lysates was performed under the condition that recombinant ttPolX had the AP endonuclease activity (Figs. 43C, lane 1 and 43E, lanes 1-3). The wild-type lysates had a strong AP endonuclease activity (Fig. 43C), and the 3’-5’ and/or 5’-3’ exonuclease activities were stimulated as time passed. The ttPolX-deficient lysates exhibited a similar activity as that of the wild-type (Fig.

43D). However, the ttEndoIV-deficient lysates had a very weak AP endonuclease activity (Fig. 43E). Double-deficient (ttEndoIV and ttPolX) lysates showed negligible AP endonuclease activity (Fig. 43F). Therefore, almost all the AP endonuclease activity of cell lysates was attributed to ttEndoIV.

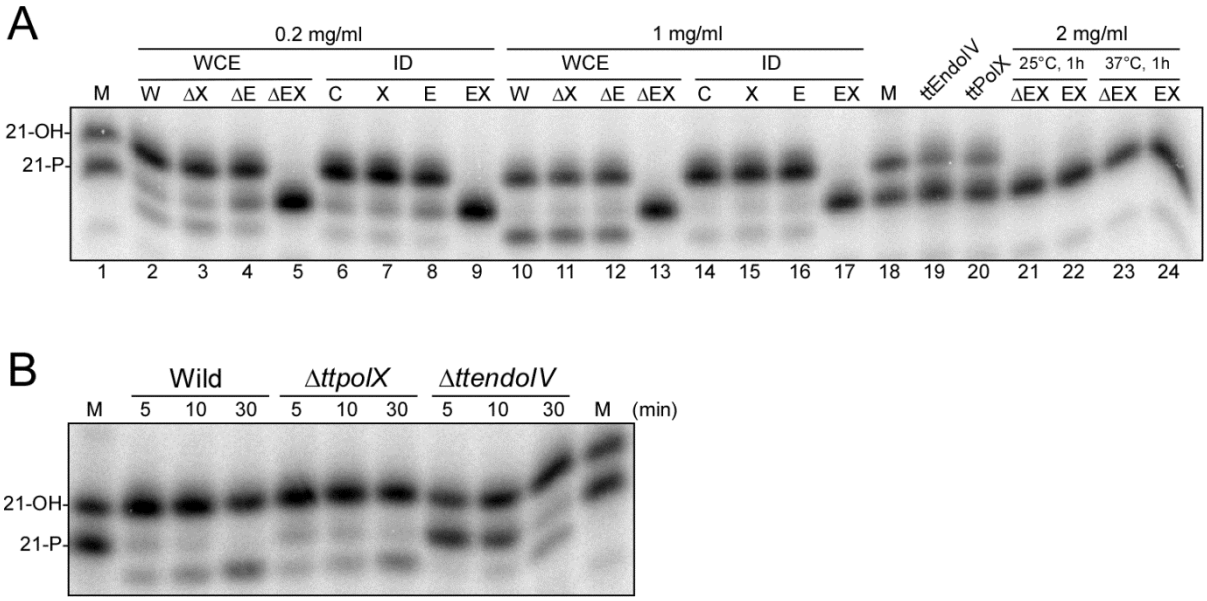

Figure 42. The 3'-phosphatase activity of WCE and ID lysates. The following WCEs were used: W, wild-type; ΔX, Δ*ttpolX*, ΔE, Δ*ttendoIV*; and ΔEX, Δ*ttendoIV* /Δ*ttpolX*. The following ID lysates were used: C, using nonimmune antibody; X, ttPolX depleted; E, ttEndoIV depleted; and EX, ttPolX and ttEndoIV depleted. (A) Reaction mixtures containing 50 mM Tris-HCl, 60 mM NaCl, 40 mM KCl, 1 mM $MnCl_2$, 100 μg/ml BSA, 10 nM DNA, 4 mM KPi and indicated concentrations of lysates, pH 7.5 were incubated at 25°C for 30 min, and analyzed by 15% denaturing PAGE (8 M urea) and autoradiography. Recombinant ttEndoIV (0.15 nM) and ttPolX (1 nM) were used as positive controls (lanes 19 and 20). The lysate concentration, temperature, and incubation time were increased (lanes 21-24). (B) Time-course analysis of the 3'-phosphatase assay using WCEs of wild-type, Δ*ttpolX*, and Δ*ttendoIV*. Reaction mixtures containing 50 mM Tris-HCl, 100 mM KCl, 1 mM $MnCl_2$, 100 μg/ml BSA, 10 nM DNA and 0.2 mg/ml lysates, pH 7.5 were incubated at 25°C for the indicated times, and analyzed by 15% denaturing PAGE (8 M urea) and autoradiography. M represents markers.

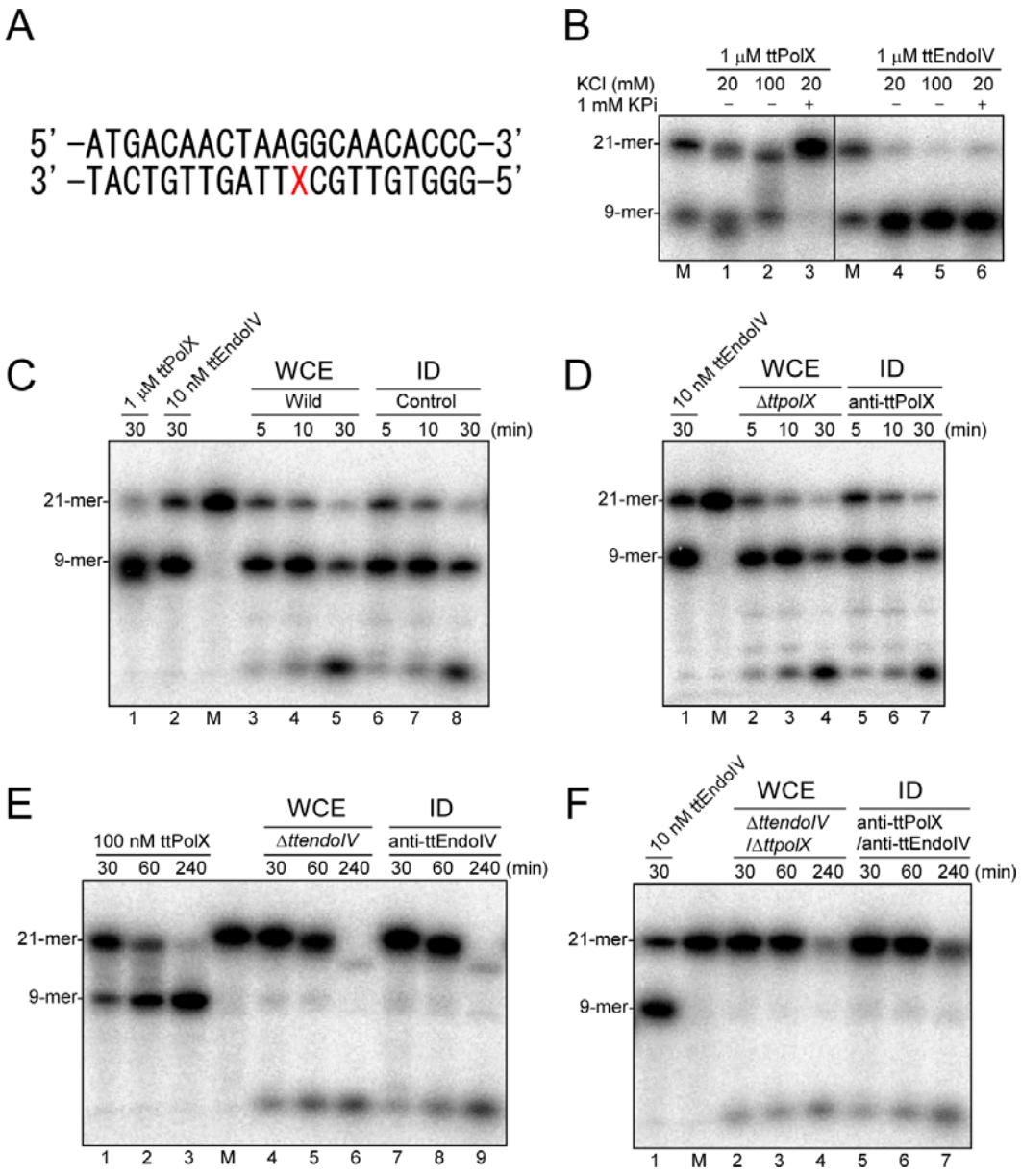

Figure 43. The AP endonuclease activity of WCEs and ID lysates. The WCEs of wild-type, Δ*ttpolX*, Δ*ttendoIV*, and Δ*ttendoIV* /Δ*ttpolX* as well as the ID lysates treated with using nonimmune (control), anti-ttPolX, anti-ttEndoIV, and anti-ttEndoIV/anti-ttPolX antibodies were used. Reaction mixtures containing 50 mM Tris-HCl, 20 mM KCl, 1 mM $MnCl_2$, and 0.2 mg/ml lysates, pH 7.5 were incubated at 37°C for the indicated times, and analyzed by 20% denaturing PAGE (8 M urea) and autoradiography. Recombinant ttEndoIV and ttPolX were used as positive controls. (A) Sequence used for AP endonuclease assay. X = tetrahydrofuran (THF), a stabilized AP-site analog. It should be noted that the AP lyase activity cannot incise at this stabilized AP site. An oligonucleotide containing THF was 5'-labeled using [γ-^{32}P] ATP. (B) Inhibition of the AP endonuclease activity. KCl and KPi were used as inhibitors. (C) The AP endonuclease activity of the lysate obtained from wild-type cells. (D) The AP endonuclease activity of the ttPolX-deficient lysates. (E) The AP endonuclease activity of the ttEndoIV deficient-lysates. (F) The AP endonuclease activity of the ttEndoIV and ttPolX double-deficient lysates. M represents markers.

Partial reconstitution of BER

Because ttPolX has 3'-phosphatase and gap-filling activities, partial reconstitution of BER from 3'-phosphorylated 1-nt gapped DNA (Fig. 44A) was attempted to examine whether the activities of ttPolX are sequentially stimulated in BER. I observed that ttPolI had no 3'-phosphatase activity and could not extend a 3'-phosphorylated primer (Fig. 44B, lane 1). If the 3'-phosphate was removed by ttEndoIV, ttPolI could extend the primer using its strand-displacement activity (Fig. 44B, lane 2). In contrast, ttPolX alone was able to remove the 3'-phosphate and fill 1-nt gaps (Fig. 44B, lane 5). Furthermore, DNA ligase A from *T. thermophilus* HB8 (ttLigA, TTHA1097), which is the only DNA ligase in *T. thermophilus* HB8 and needs NAD^+ as a cofactor, could seal nicked DNA after gap filling by ttPolX (Fig. 44B, lane 6). Therefore, partial reconstitution of BER from 3'-phosphorylated 1-nt gapped DNA could be achieved by only ttPolX and ttLigA.

Cell lysates from *T. thermophilus* HB8 also exhibited the repair of 3'-phosphorylated 1-nt gapped DNA (Figs. 44C and 44D). When dGTP was added, ttPolX and/or ttPolI extended the 3'-phosphate-removed primers to a 23-mer, after which DNA ligase sealed the resultant nicks to produce a 40-mer repaired product (Fig. 44C, lane 2). The appearance of a 40-mer product in the absence of NAD^+ indicates that ttLigA was partially adenylated in the cell. The amount of the repaired 40-mer product was increased when NAD^+ was added (Fig. 44C, lane 3). Strand-displacement activity was observed in the presence of dNTPs (Fig. 44C, lane 4), and the amount of 40-mer product was slightly increased with the addition of NAD^+ (Fig. 44C, lane 5). The repair activity, especially for gap-filling, was well retained in ttEndoIV-deficient lysates (Fig. 44C, lanes 11-15), although the 3'-phosphatase activity was slightly lower than that of the wild-type. In contrast, the ttPolX-deficient lysates showed a lower gap-filling activity (Fig. 44C, lane 7), and the amount of 40-mer repaired product was decreased (Fig. 44C, lane 8). These results suggest that ttPolX is responsible for the gap-filling activity in the cell. This finding was also supported by the results obtained from ttPolI-deficient lysates (Fig. 44D). ttPolI-deficient lysates retained a strong gap-filling activity (Fig. 44D, lane 2), but the strand-displacement activity was lost (Fig. 44D, lanes 2-5). This result was also consistent with the fact that ttPolI showed a strand-displacement activity, but that of ttPolX was very weak (Figs. 7B, 37 and 44B). Furthermore, the deficiency of ttPolI and ttPolX led to the loss of DNA polymerase activity (Fig. 44D, lanes 7-10). This result indicates that ttPolI and ttPolX are the only DNA polymerases involved in BER, although it is possible that the Pol III α subunit, which is a replicative DNA polymerase,

could not act on the 40-mer 1-nt gapped DNA because the DNA length was too short. Taken together, these results strongly suggest that ttPolX is capable of performing 3'-phosphatase as well as gap-filling activities in BER.

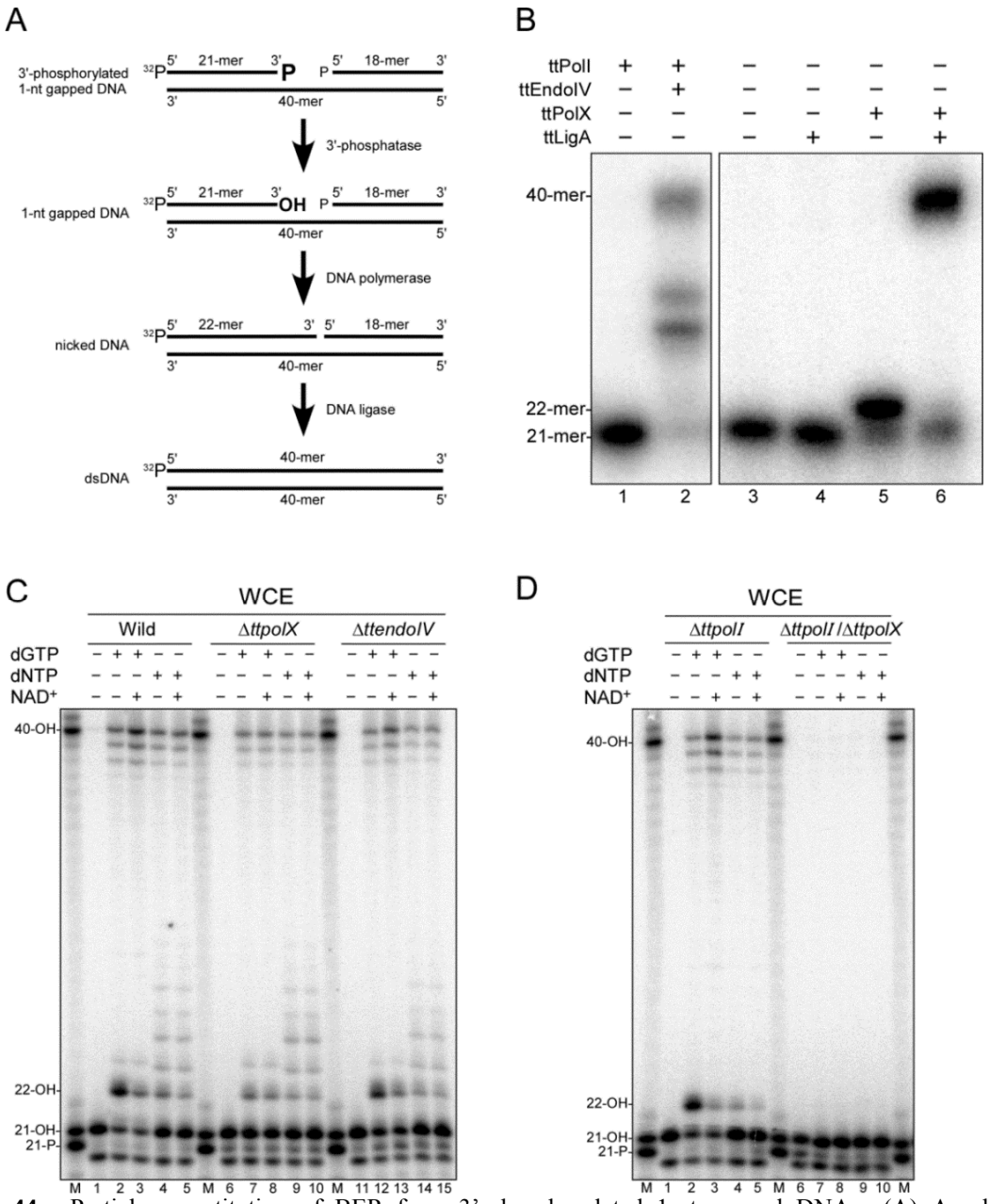

Figure 44. Partial reconstitution of BER from 3'-phosphorylated 1-nt gapped DNA. (A) A schematic representation of the repair of 3'-phosphorylated 1-nt gapped DNA by BER enzymes. The 3'-phosphatase removes the 3'-phosphate, after which a DNA polymerase fills the 1-nt gap, and the resultant nicked DNA is sealed by DNA ligase. (B) Partial reconstitution of BER using recombinant enzymes. Reaction mixtures containing 50 mM Tris-HCl, 100 mM KCl, 5 mM $MgCl_2$, 100 μM dNTPs, 10 nM DNA and 100 nM enzymes, pH 7.5 were incubated at 37°C for 10 min, and analyzed by 18% denaturing PAGE (8 M urea) and autoradiography. When ttLigA was added to the mixture, 100 μM NAD^+ was used as a cofactor. (C) Partial reconstitution of BER using WCEs of wild-type, Δ*ttpolX* and Δ*ttendoIV* cells. Reaction mixtures containing 50 mM Tris-HCl, 100 mM KCl, 10 mM $MgCl_2$, 1 mM $MnCl_2$, 50 μM dGTP, 50 μM dNTPs, 100 μM NAD^+, 10 nM DNA and 0.2 mg/ml WCE, pH 7.5 were incubated at 37°C for 30 min, and analyzed by 15% denaturing PAGE (8 M urea) and autoradiography. (D) Partial reconstitution of BER using WCEs of Δ*ttpolI* and Δ*ttpolI*/Δ*ttpolX* cells. M represents markers.

IP and pull down assay of ttPolX

Interaction partners of ttPolX were investigated by IP and pull down assay using ttPolX column (Fig. 45; Tables 15 and 16). BER enzymes are known to make interaction networks for efficiency and regulation of the repair (Fan *et al*., 2005; Cuneo *et al*., 2010). The combination of IP and nLC-ESI-MS/MS analysis revealed interaction candidates with ttPolX, ttPolI, and formamidopyrimidine DNA glycosylase from *T. thermophilus* HB8 (ttMutM, TTHA1806) (Figs. 45A and 45B; Table 15). ttMutM is a trifunctional DNA glycosylase, which removes a 8-oxoG from oxidatively damaged DNA (Sugahara *et al*., 2000; Mikawa *et al*., 1998). Several candidates of interaction partners with ttPolX, ttPolI, ttPolX were detected with significant MS/MS score by mascot search analysis (Table 15). Among them, nonspecific bindings were excluded. ttPolX was interacted with one of uracil DNA glycosylase in *T. thermophilus* HB8, UDGB, a nucleotide excision repair (NER)-related enzyme, UvrB, kinases, and some other DNA-related proteins. ttPolI was interacted with DNA-related proteins including replication-related ones. ttPolX was detected with high score as a result of IP of ttMutM. The interaction partners with ttPolX were also explored by pull down assay using ttPolX column and PMF (Figs. 45C and 45D; Table 16). Some interaction candidates were identified with high possibility and had good agreement between theoretical MW and mobility on SDS-PAGE gel (Table 16, bold and red letter). The interactions between ttPolX-ttMutM and ttPolX-ttUDGB were detected (Fig. 45; Table 15 and 16), implying coordinated reactions in BER. ttPolX was also interacted with NER proteins (UvrA and UvrB) and subunits of RNA polymerases (α, β and β') (Fig. 45; Tables 15 and 16), indicates that ttPolX is possibly involved in transcription coupled repair (TCR) and NER.

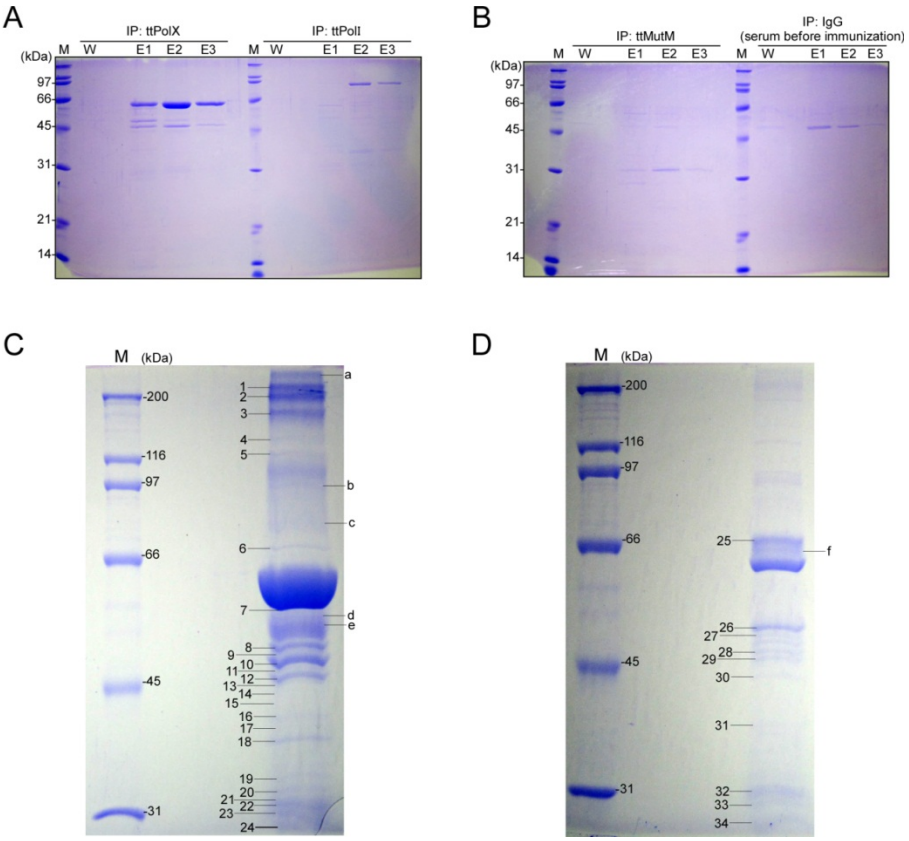

Figure 45. IP and pull down samples were analyzed by SDS-PAGE. (A, B) IP samples used for MS/MS analysis were analyzed by 12.5% SDS-PAGE. Antibodies of ttPolX, ttPolI, ttMutM and nonimmune IgG were used for IP. W and E mean wash and elute samples, respectively. (C, D) Pull down samples using ttPolX column used for PMF analysis were analyzed by 10% SDS-PAGE. ttPolX column was produced by binding antibody of ttPolX and recombinant ttPolX (C) and crosslinked by DMP (D).

Table 15. Possible interaction partners with ttPolX detected by MS/MS ion search by nLC-micrOTOF-QII MS.

IP	Detected protein		Total MS/MS score
	Gene ID	Product name	
ttPolX (TTHA1150)	TTHA0843	Serine protein kinase	119
	TTHA1812	DNA-directed RNA polymerase subunit beta' (RpoC)	50
	TTHA0027	potassium channel, beta subunit (oxidoreductase)	37
	TTHA1892	excinuclease ABC subunit B (UvrB)	33
	TTHA1149	uracil-DNA glycosylase (UDGB)	33
	TTHA1524	Serine hydroxymethyltransferase	30
	TTHA1645	DNA mismatch repair protein MutS2	28
	TTHA0701	transcription elongation factor NusA	26
	TTHA1266	ATP-dependent DNA helicase RecG	24
	TTHA0138	serine/threonine protein kinase	21
	TTHA1619	tRNA (guanine-N7-)-methyltransferase	21
	TTHA0074	DNA topoisomerase IA	20
	TTHA1097	DNA ligase [NAD+]	19
ttPolI (TTHA1054)	TTHA1097	DNA ligase [NAD+]	26
	TTHA1324	DNA mismatch repair protein MutS	24
	TTHA0889	transcription-repair coupling factor	22
	TTHA0180	DNA polymerase III subunit alpha	21
ttMutM (TTHA1806)	TTHA1150	DNA polymerase beta family protein	302
	TTHA0701	transcription elongation factor NusA	24
	TTHA1003	sensor histidine kinase	20
	TTHA1637	ribose-phosphate pyrophosphokinase	20

IP samples using MS/MS analysis are elute samples in Figs. 44A and 44B.
Listed proteins are only interesting and having significant score.
Bait proteins and nonspecific binding proteins detected in control samples are excluded from the list.

Table 16. Possible interaction partners with ttPolX detected by PMF analysis.

Band No.	Gene ID	Gene product	Theoretical MW	Mascot score
1	TTHA0133	short chain dehydrogenase/reductase family oxidoreductase	24,863.5	51
	TTHA0568	**hypothetical protein**	**284,631**	**72**
2	TTHA1150	PolX		
	TTHA0138	serine/threonine protein kinase	66,001.5	155
	TTHA0568	hypothetical protein	284,631	48
3	TTHA1150	PolX		
	TTHA1812	**DNA-directed RNA polymerase subunit beta' (RpoC)**	**170,756.4**	**117**
4	**TTHA1813**	**DNA-directed RNA polymerase subunit beta**	**125,264.4**	**185**
	TTHA1150	PolX		
5	**TTHA1440**	**excinuclease ABC subunit A (UvrA)**	**105,149.7**	**106**
	TTHA0950	DegV family protein	29,692.3	50
6	**TTHA1491**	**molecular chaperone DnaK**	**66,824.4**	**98**
	TTHA1150	PolX		
	TTHA0532	RNA polymerase pricipal sigma factor (RpoD)	48,524	49
7	TTHA1150	PolX		
	TTHA1210	**2-isopropylmalate synthase (EC:2.3.3.13)**	**57,440.4**	**138**
	TTHA1149	uracil-DNA glycosylase (UDGB)	24,286.1	51
8	TTHA1150	PolX		
	TTHA1329	**glutamine synthetase**	**50,556.8**	**151**
9	TTHA1150	PolX		
	TTHA1329	**glutamine synthetase**	**50,556.8**	**109**
	TTHA0722	**histidinol dehydrogenase**	**44,123.3**	**50**
10	**TTHA1150**	**PolX**		
	TTHA1411	**sulfite dehydrogenase SoxC precursor**	**48,140.9**	**60**
11	TTHA1150	PolX		
	TTHB198	**hypothetical protein**	**45,067.9**	**105**
	TTHA1664	DNA-directed RNA polymerase subunit alpha	35,013.2	112
	TTHA1089	cell division protein FtsZ	37,236.6	75
12	TTHA1150	PolX		
	TTHA1664	DNA-directed RNA polymerase subunit alpha	35,013.2	105
	TTHA1089	cell division protein FtsZ	37,236.6	97
	TTHB198	**hypothetical protein**	**45,067.9**	**73**
13	TTHA1150	PolX		
	TTHA0500	**glycerate dehydrogenase/hydroxypyruvate reductase**	**43,699.6**	**108**
	TTHA1149	uracil-DNA glycosylase (UDGB)	24,286.1	47
14	TTHA1150	PolX		
	TTHA0214	kinase	55,945.1	56
	TTHA1089	**cell division protein FtsZ**	**37,236.6**	**47**
15	**TTHA1089**	**cell division protein FtsZ**	**37,236.6**	**51**
	TTHA0950	DegV family protein	29,692.3	53
16	TTHA1150	PolX		
	TTHB190	**hypothetical protein**	**40,779.7**	**70**
	TTHA0706	cation-transporting ATPase	71,913.2	59
17	**TTHA0027**	**potassium channel, beta subunit (oxidoreductase)**	**35,882.1**	**144**
	TTHA1150	PolX		
	TTHA0214	kinase	55,945.1	47
18	**TTHA0027**	**potassium channel, beta subunit (oxidoreductase)**	**35,882.1**	**215**
19	TTHA0255	ferric uptake regulation protein	16,989.5	80
	TTHA1806	**formamidopyrimidine-DNA glycosylase (MutM)**	**29,915.4**	**69**
	TTHA0138	serine/threonine protein kinase	66,001.5	60
20	TTHA1150	PolX		
	TTHA0955	**mannosyl-3-phosphoglycerate phosphatase**	**28,191.3**	**161**
	TTHA1076	**S-adenosyl-methyltransferase MraW**	**31,171.1**	**48**
21	TTHA1150	PolX		
	TTHB149	**hypothetical protein**	**27,381.4**	**101**

22	TTHA1150	PolX		
	TTHA0852	**pyrroline-5-carboxylate reductase**	**27,763**	**83**
	TTHB198	hypothetical protein	45,067.9	55
	TTHA1347	endonuclease V	24,430.6	52
	TTHA0226	hypothetical protein	15,708	51
23	TTHA1150	PolX		
	TTHA1580	**GntR family transcriptional regulator**	**25,193.7**	**104**
	TTHB073	**transcriptional regulator**	**28,015.3**	**47**
	TTHA1704	**hypothetical protein**	**28,321.1**	**48**
24	**TTHA1149**	**uracil-DNA glycosylase (UDGB)**	**24,286.1**	**104**
	TTHA0802	**hypothetical protein**	**19,872.4**	**47**
25	TTHA1150	PolX		
	TTHA0448	**long-chain-fatty-acid--CoA ligase**	**73,424.1**	**47**
	TTHA1149	uracil-DNA glycosylase (UDGB)	24,286.1	47
26	**TTHA0614**	**trigger factor**	**46,287.7**	**152**
27	TTHA1150	PolX		
	TTHA1840	**SufD protein membrane protein**	**47,943.8**	**58**
	TTHB053	precorrin-6Y C5,15-methyltransferase [decarboxylating]	43,721.7	52
28	**TTHB198**	**hypothetical protein**	**45,067.9**	**161**
	TTHA1150	PolX		
	TTHA0579	**sugar ABC transportor, ATP-binding protein**	**42,133.7**	**61**
29	TTHA1150	PolX		
	TTHA1664	DNA-directed RNA polymerase subunit alpha	35,013.2	106
	TTHA1089	cell division protein FtsZ	37,236.6	115
	TTHB198	**hypothetical protein**	**45,067.9**	**109**
	TTHA1149	uracil-DNA glycosylase (UDGB)	24,286.1	47
30	**TTHA1378**	**homoisocitrate dehydrogenase**	**35,922.3**	**126**
	TTHA1149	uracil-DNA glycosylase (UDGB)	24,286.1	52
31	**TTHA0027**	**potassium channel, beta subunit (oxidoreductase)**	**35,882.1**	**182**
	TTHA0614	trigger factor	46,287.7	75
32	TTHA1150	PolX		
	TTHA1179	**fructosamine-3-kinase**	**29,324.6**	**68**
	TTHB198	hypothetical protein	45,067.9	68
33	TTHA1150	PolX		
	TTHA1580	**GntR family transcriptional regulator**	**25,193.7**	**66**
	TTHA0246	50S ribosomal protein L1		64
	TTHA1483	**hypothetical protein**	**25,667.4**	**53**
	TTHB073	**transcriptional regulator**	**28,015.3**	**54**
	TTHA0135	MutT/NUDIX family protein	17,353.1	47
34	**TTHA1149**	**uracil-DNA glycosylase (UDGB)**	**24,286.1**	**73**
	TTHA0022	glucose-1-phosphate adenylyltransferase	47,225	56
a	TTHA0950	DegV family protein	29,692.3	52
b	TTHA1149	uracil-DNA glycosylase (UDGB)	24,286.1	57
c	TTHA1150	PolX		
	TTHA0214	kinase	55,945.1	58
d	TTHA1150	PolX		
	TTHA0911	hypothetical protein	20,652.1	49
e	TTHA1150	PolX		
	TTHA0802	hypothetical protein	19,872.4	48
f	TTHA1150	PolX		
	TTHA1149	uracil-DNA glycosylase (UDGB)	24,286.1	48

IP samples were collected using anti-ttPolX antibody in Figs. 44C and 44D.
Bold letters in red represent proteins that theoretical MW were coincided with estimated MW by SDS-PAGE.
a-b are the bands which contain no coincided proteins of theoretical MW with estimated MW.

DISCUSSION

Domain organization of ttPolX

Sequence analysis has predicted that many bacterial PolXs including ttPolX consist of mainly two domains, the POLXc and PHP domains (Fig. 1B). The POLXc domain is a polymerase domain, whereas the PHP domain is confirmed to be a phosphoesterase domain in this study. The PHP domain is associated with other domains such as the polymerase domain (Lamers *et al.*, 2006; Bailey *et al.*, 2006) or exists as a stand-alone protein (Teplyakov *et al.*, 2003; Omi *et al.*, 2007). Multiple alignments showed the border of these domains and internal linker (Figs. 3C, 12 and 27) Although enzymes designed by these alignments (the POLXc (1-316) and PHP (336-575)) were stable (Fig. 2) and had activities (Figs. 6B, 30 and 35), limited proteolysis indicated the other border of the domains (Figs. 2 and 3). However, the POLXc (1-379) was unstable (Fig. 2A) and the C-terminal fragment (380-575) was failed to express. Proteases digested at exposed loop region on the PHP domain (Fig. 11A), but this region was not the true domain border. Linker region retains the POLXc and PHP domains close and the domains are interacted with each other at some regions (Figs. 11A, 11B and 14B). The crystal structure of drPolX also shows the interaction of the POLXc and PHP domains (Leulliot *et al*., 2009). ttPolX seemed to have sophisticated activity with full length more than simply combining the POLXc and PHP domains (Figs. 4, 5, 20, 28 and 30).

The biochemical activities of ttPolX

This study revealed ttPolX has Mg^{2+}-, Mn^{2+}- and Zn^{2+}-dependent DNA/RNA polymerase (Figs. 4-6) and dRP lyase (Fig. 21) activities with the POLXc domain, and Mn^{2+}- and Co^{2+}-dependent 3'-5' exonuclease (Figs. 22 and 23), Mn^{2+}-dependent 3'-5' exoribonuclease (Fig. 22D), Mn^{2+}-dependent AP endonuclease (Fig. 35) and Mg^{2+}-, Mn^{2+}-, Co^{2+}- and Zn^{2+}-dependent 3'-phosphatase (Fig. 30) activities with the PHP domain. My results indicate that the 3'-5' exonuclease activity of ttPolX is much stronger than its polymerase activity in the presence of Mn^{2+}, however, the possibility of proofreading activity is raised by consideration of intracellular metal ion concentrations (Fig. 36) and substrate specificity of the 3'-5' exonuclease activity (Fig. 22E).

ttPolX had both ssDNA- and dsDNA-binding abilities (Fig. 20 and Table 8). EMSA analysis suggested that more than two molecules of ttPolX bind to a 40-mer DNA with or without a 1-nt gap (Table 8). It was reported that rat Polβ formed a 2:1 Polβ-DNA complex in solution against 1-nt gapped 16-mer DNA when Polβ was in excess of DNA (Tang *et al.*,

2008a). Tang *et al.* also reported that more than two Polβ molecules bind to 45-mer 1-nt gapped DNA under the lower salt (~0.1 M KCl) conditions. This observation is in agreement with that for ttPolX. The POLXc domain showed the same property to ttPolX (Fig. 20), indicating a contribution to the binding to DNA. Indeed, the subdomains, which exhibit binding activity as to ssDNA or dsDNA, both belong to the POLXc domain in Polβ (Beard *et al.*, 2006a). However, the POLXc domain exhibited lower affinity to DNA than ttPolX. The PHP domain may stabilize the ttPolX-DNA complex without affecting the DNA-binding manner. Since DNA-binding activity was not detected for the PHP domain (Fig. 20), the contribution of the PHP domain to the affinity to DNA is probably auxiliary. Although ttPolX has an additional domain, a PHP domain, the DNA-binding model of ttPolX is assumed to be the same as that of Polβ; this is confirmed by the crystal structure of ttPolX in ternary complex with 1-nt gapped DNA and ddGTP (Fig. 11B).

ttPolX preferred gapped DNA over non-gapped DNA, but did not recognize a 5'-phosphate group in the 1-nt gap (Fig. 20 and Table 8). Some DNA polymerases involved in BER and DSBR prefer gapped DNA, especially 5'-phosphorylated gapped DNA, because these DNAs are some of the intermediates in these repair processes (Hegde *et al.*, 2008; Pitcher *et al.*, 2007; Moon *et al.*, 2007). The crystal structures of the complex of 5'-phosphorylated gapped DNA and Polβ (Batra *et al.*, 2006), Polλ (Garcia *et al.*, 2005) or Polμ (Moon *et al.*, 2007) revealed putative basic residues which recognize 5'-phosphate groups. Multiple sequence alignment of the POLXc domain regions of PolXs shows that three residues (B1-B3) are partially conserved (Fig. 20C). It was reported that Polβ, Polλ, Polμ and spPolIV had higher gap filling activity against a substrate containing 5'-phosphate group in the gap than a substrate without 5'-phosphate group (Garcia *et al.*, 2002;,Nick *et al.*, 2003; Alonso *et al.*, 2006; Gonzalez *et al.*, 2005) but scPolIV did not (Bebenek *et al.*, 2005). ttPolX had little or no ability to recognize a 5'-phosphate group in the gap (Fig. 20 and Table 8). Interestingly, ttPolX and scPolIV have Asp and Ser at the B2 position, respectively, whereas the other four PolXs have basic residues at the same position (Fig. 20C). The distances between the oxygen atom of 5'-phosphate and nitrogen atoms of B1-B3 residues are as follows: Polβ, 2.73 (Lys-35), 2.60 (Lys-68), and 4.20 Å (Lys-72); Polλ, 2.95 (Arg-275), 2.84 (Arg-308), and 3.43 Å (Lys-312); Polμ, 3.65 (Arg-175) and 2.77 Å (His-208); ttPolX, 3.3 (Arg-26), 2.9 (Asp-64) and 3.8 Å (Lys-68) (Figs. 20C and 32D). Although ttPolX has one more base residue, Lys-80 at a distance of 3.4 Å from 5'-phosphate, B2 is the closest residue to the 5'-phosphate group in the three crystal structures and B2 is considered to be the

critical residue for recognition of the 5'-phosphate group. Therefore, these results suggest that it is due to the lack of a basic residue at the B2 position that ttPolX and scPolIV cannot recognize a 5'-phosphate group (Fig. 20C).

As seen in the assay of single nucleotide insertion, ttPolX inserted dGMP, GMP and 8-oxo-dGMP, and slightly inserted dIMP and IMP opposite dC (Fig. 4C). Such an ability of ttPolX to discriminate base-pairing is similar to those of Polβ, Polλ and Polμ of the mammalian PolXs on single nucleotide insertion when the frameshift DNA synthesis is not taken into consideration (Brown *et al.*, 2007; Fiala *et al.*, 2006; Zhang *et al.*, 2001). ttPolX exhibited no detectable TLS against xanthine or inosine, or RT activity in the presence of Mg^{2+} (Fig. 4D). Note that ttPolX exhibited no 3'-5' exonuclease activity in these assays because it exhibited no exonuclease activity with Mg^{2+}. Although the POLXc (1-379) inserted dGMP, GMP, dIMP, IMP and 8-oxo-dGMP opposite dC (Fig. 5C), the incorporation rate of damaged bases with the POLXc (1-379) was higher than that in the case of ttPolX. This enhancement of the rate cannot be explained only by the higher polymerase activity than that of ttPolX. Moreover, the POLXc (1-379) differed from ttPolX in that this domain exhibited TLS activity opposite dI (Fig. 5D). It is probable that the PHP domain represses the incorporation of NTPs, especially damaged bases, directly or indirectly. The PHP domain may improve the stringency of base paring. Several X-family DNA polymerases such as Polλ and Polμ are called translesion or error-prone DNA polymerases because they insert incorrect bases including damaged ones or carrying out TLS against a damaged base or a mismatched base (Brown *et al.*, 2007; Zhang *et al.*, 2001; Covo *et al.*, 2004). However, ttPolX is unlikely to be a translesion DNA polymerase.

The RNA polymerase activity of ttPolX may help to repair DNA. ttPolX is able to insert NMPs opposite a DNA template and also can degrade (Figs. 4B and 22D). Some PolXs such as Polβ and Polμ are also capable of incorporating NMPs (Gonzalez *et al.*, 2005). It was reported that the intracellular NTPs concentration was much higher than that of dNTPs in human cell lines (Huang *et al.*, 2003) and in *E. coli* cells (Buckstein *et al.*, 2008). It is perhaps an advantage for repairing DNA that ttPolX can use NTPs, which exist at high concentrations in the cell, especially when the intracellular dNTP concentration is low. The nucleotide concentration is known to decrease in the stationary phase, but even in such a phase, the NTP concentration is still higher than that of dNTP (Buckstein *et al.*, 2008). *T. thermophilus* HB8 has a junction ribonuclease, which recognizes the RNA-DNA junction of an RNA-DNA/DNA heteroduplex and cleaves it leaving a mono-ribonucleotide at the 5'

terminus of the RNA-DNA junction (Ohtani *et al.*, 2008). Incorporated NMP in DNA could serve as a "flag waver" and be recognized by enzymes such as a junction ribonuclease and induce an additional DNA repair system or DNA-damage-checkpoint pathways (Larkin *et al.*, 2007).

Single-nucleotide gap filling of ttPolX

The observation that both *syn* and *anti* conformations of dGTP can occur in the binary complex (Fig. 11E) suggests that the bound nucleotide can change its conformation even in ttPolX. The ability to switch its nucleotide-binding property may depend on Lys-263 (Figs. 11, 15 and 16). This ability may be advantageous from an entropic point of view and contribute to strong nucleotide binding in the absence of DNA (Table 1). Furthermore, the *syn-anti* equilibrium also allows DNA to be bound without release of Mg^{2+}-dNTPs since the *anti*-dNTPs can base pair directly with a template base (Fig 11D and Table 2). NMR analysis showed that Mg-dATP and Mg-TTP bound to bacterial PolI had the *anti* conformation (Ferrin *et al*., 1985). At the location corresponding to Lys-263 of ttPolX, PolIs have aromatic residues that stack with incoming *anti*-dNTPs but not with *syn*-dNTPs (Li *et al*., 1998; Golosov *et al*., 2010). Since the PolI-dNTP binary complex is thought to be nonproductive (Bryant *et al*., 1983), the two binary complexes with *syn*-dNTP and *anti*-dNTP achieved by Lys-263 may be important for a strong and productive complex in the absence of DNA. However, K263A and K263D mutants still retained the dNTP-first binding order (Tables 6 and 7). As described earlier, residues other than Lys-263 may also be involved in substrate-binding order.

This study has identified the important role played by the *syn-anti* conformational change of the incoming nucleotide in the active site of ttPolX. Spectroscopic analysis showed that nucleosides rapidly achieve a *syn-anti* equilibrium in solution (Danyluk *et al*., 1968; Schweize *et al*., 1968; Son *et al*., 1972; Stolarski *et al*., 1984). This *syn-anti* equilibrium is affected by sugar puckering and modifications (Miles *et al*., 1969; Miles *et al*., 1971; Saran *et al*., 1973). The phosphorylation of O5' increases the interaction between O5' and a base, which increases C3'-*endo* in sugar puckering, followed by an increase of the *anti* conformation (Tso *et al*., 1969; Ikehara *et al*., 1972). In guanine nucleotides, the interaction between the amino group at the C2-position and the 5'-phosphate stabilizes the *syn* conformation (Son *et al*., 1972). Interaction with the protein can also influence the *syn-anti* equilibrium. Our study showed that a single amino acid can affect the *syn-anti* equilibrium

of the nucleotide (Fig. 15). Since nucleotides are usually in the *anti* conformation during base paring, template-dependent polymerases require a conformational change in the incoming nucleotide from *syn* to *anti* for catalysis (Kapuler *et al*., 1971). The biased conformation of *syn*-dGTP in K263D may have inhibited *syn-anti* conversion and resulted in a lower k_{cat} value compared to the wild-type (Tables 2 and 7).

NTPs, which are more abundant in the cell than dNTPs, are thought to be potential inhibitors of dNTP-ttPolX binding. However, comparison of the results of our binding study and intracellular concentrations of NTPs may exclude this possibility. The binding affinity of ttPolX for Mg-GTP was approximately two orders lower than that for Mg^{2+}-dGTP (Table 1). A slightly hydrophobic region around 2'-H of the ribose may contribute to rejection of the NTP (Fig. 11F). This difference in binding affinities may be consistent with the fact that ttPolX can incorporate NTPs in addition to dNTPs, although the polymerase activity for NTPs is lower than for dNTPs (Fig. 4B) (Nakane *et al*., 2009). In mammalian cells, the intracellular concentration of dNTPs is 5.2-37 μM and of NTPs is 278-3152 μM (Traut *et al*., 1994). In other organisms, nucleotide concentrations have been determined by various methods and found to be similar (Bochner *et al*., 1982; Soga *et al*., 2002; Buchstein *et al*., 2008). The ratio of NTP/dNTP in *T. thermophilus* cultured in synthetic medium was estimated at approximately 10.6:1 for CTP/dCTP and 154:1 for ATP/dATP from metabolomics data (Ooga *et al*., 2009); these values are again similar to those of other organisms (Traut *et al*., 1994; Bochner *et al*., 1982; Buckstein *et al*., 2008). The ratio of the K_d of GTP/dGTP of ttPolX is ~100:1 (Table 1); therefore, I conclude that ttPolX is mainly bound to metal ion-dNTP and not NTP in cells.

This study has identified the strategy used by ttPolX for filling 1-nt gaps (summarized in Fig. 46). Biochemical and crystallographic studies revealed that Lys-263 in ttPolX contributed to the strong binding affinity for Mg^{2+}-dNTP in the absence of DNA with binding to both *syn*- and *anti*-dNTPs (Figs. 11, 15 and 16; Table 1). Steady-state kinetic approach and inhibition assays showed that ttPolX followed a dNTP-first Theorell-Chance mechanism for filling 1-nt gaps (Fig. 9 and Table 2). This mechanism is thought to be a special case of an ordered Bi Bi mechanism with low concentration of the ternary complex under steady-state conditions. It was reported that the reaction mechanism of mouse DNA polymerase α, a replicative polymerase with moderate processivity, was close to a Theorell-Chance mechanism with DNA as the first substrate (Tanabe *et al*., 1980). Theorell-Chance mechanisms may be a common strategy for the efficient catalysis of

template-dependent polymerases, regardless of whether the first substrate is dNTP or DNA. Our observations here raise the question of how dNTP-bound ttPolX fills 1-nt gaps with the four template bases. In the case of ASFV PolX, dNTP-bound PolX had low affinity against primer/template DNA with mismatched template (Kumar *et al.*, 2008). The dNTP-first binding of ttPolX indicates that it has the same mechanism for gapped DNA. ttPolX may form four dNTP-ttPolX binary complexes for 1-nt gaps with different templates in the cell.

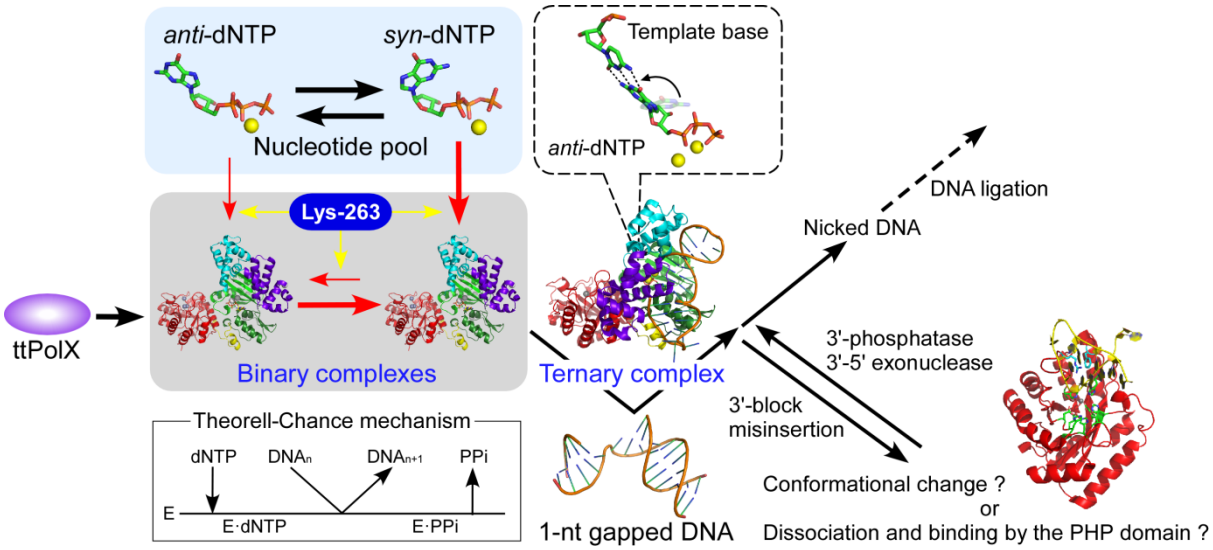

Figure. 46. A model for efficient repair of 1-nt gaps by ttPolX. In solution, dNTPs are in equilibrium between the *syn* and *anti* conformations. ttPolX can bind both Mg-*syn*-dNTP and Mg-*anti*-dNTP in the absence of DNA. The dNTP bound to ttPolX may change its conformation between *syn* and *anti* but the proportion with an *anti*-conformation is small (see Fig. 11E). This *syn-anti* equilibrium may be modulated by Lys-263 and may contribute to the stability of the binary complex in the absence of DNA. In the presence of DNA, the bound *syn*-dNTP changes its conformation to *anti* and base pairs with the DNA. dNTP-bound ttPolX reacts with 1-nt gapped DNA in a "hit-and-run" fashion via a Theorell-Chance mechanism. When a 3'-end of the primer is blocked by such as 3'-phosphate, or mismatched by misinsertion, conformational change or the DNA re-binding may be occurred and the PHP domain removes 3'-blocks. After filling a 1-nt gap, ttPolX is dissociated from nicked DNA, and DNA ligation by DNA ligase A subsequently seals a nick.

The PHP domain associated with the DNA polymerase

My study demonstrated that the PHP domain provide the several phosphoesterase activities to ttPolX. The PHP domain is present in organisms ranging from archaea and bacteria to fungi. The conserved residues in the PHP family are similar to those in the metal-dependent amidohydrolase superfamily, which includes the TatD-related DNase and phosphotriesterase families (Aravind *et al.*, 1998). The enzymes belonging to this superfamily have a metal-binding site where a metal-activated water molecule acts as a nucleophile for hydrolysis of the substrate. Site-directed mutagenesis revealed that Gln-342, His-344,

Asp-349, His-374, Glu-413, His-440, His-468, Asp-529 and His-531 in ttPolX are important residues for the nuclease activity (Figs. 28 and 29). Among these residues, His-344, His-374, His-468 and Asp-529 are essential for the activity. These residues are coordinated to bound Zn 2, Zn 1, Zn 3 and Zn 2 in a trinuclear zinc cluster, respectively (Fig. 26). It supposes that the mechanism underlying the nuclease activity is similar to that of ecEndoIV, which utilizes a three-metal-ion catalytic mechanism (Ivanov *et al.*, 2007).

The active sites of the POLXc and PHP domains are separated, and the 1-nt gapped DNA is bound to the side of the POLXc domain in the crystal (Fig. 11B). This observation raises the question, "How does the PHP domain bind to the 3'-end (or AP site) and exert its activity ?" There are roughly three possibilities (Fig. 47): the first possibility is that another ttPolX molecule, different from the one binding the 1-nt gapped DNA to the POLXc domain, exerts a nuclease activity via the PHP domain (i.e., ttPolX forms a 2:1 ttPolX-DNA complex). The crystal structure of ttPolX in ternary complex with the 1-nt gapped DNA and ddGTP suggests that ttPolX is bound to the 1-nt gapped DNA in a 2:1 ratio in the crystal, with the DNA substrate binding to the POLXc domain of one PolX molecule and to the PHP domain of another PolX molecule (Fig. 32A). Formation of this 2:1 complex in solution was also shown by crosslinking reactions (Fig. 33), although the amounts of the crosslinking products of the 1:1 and 2:1 ttPolX:DNA complexes were small. A 2:1 complex may be needed for the 3' processing activity of the PHP domain because the primer terminus would be closer to the active site of the molecule 2 PHP domain than to the molecule 1 PHP domain (Fig. 32). If this is the case, the primer terminus might reach the nuclease active site with minimal movement. However, stoichiometric kinetic analysis showed the stoichiometry of the 3'-phosphatase activity of $[E]_0/[S]_0$ to be ~1 in the presence of $MnCl_2$ and ~1.5 in the presence of $MnCl_2$ and $MgCl_2$, irrespective of whether the substrate DNA was primer/template or 1-nt gapped DNA (Fig. 34 and Table 14). Therefore, at least the formation of the 2:1 ttPolX:DNA complex is not the main mechanism of the 3'-phosphatase activity; however, the ratio of ~1.5 and increase in the v_{max} in the presence of Mn^{2+} and Mg^{2+} may indicate a structural change rather than dissociation and re-binding of the substrate DNA with the PHP domain. The second possibility is that ttPolX dissociates from DNA and re-binds to the PHP domain (Fig. 47). This possibility includes a case that the PHP domain firstly binds to the 1-nt gapped DNA and performs 3'-end processing before the POLXc domain binds to the DNA. The third possibility is that the DNA-binding mode is switched between the "pol mode" and the "exo mode" (Fig. 47). In the case of the 3'-5' exonuclease activity of *E. coli* PolI, it has been suggested that the primer terminus is moved from its

polymerase domain to the 3'-5' exonuclease domain within the same molecule (Kukreti *et al*., 2008; Datta *et al*., 2009). This strategy could be available when DNA is bound between the polymerase and the 3'-5' exonuclease domains. ttPolX cannot use this strategy because DNA is bound to ttPolX, not between the POLXc and PHP domain active sites, but on the side of the POLXc domain active site (Fig. 11B). To use this strategy, the primer terminus, for example, may move along the positive cleft from the polymerase active site to the nuclease active site (Fig. 32B, positive cleft). In the case of the 5'-3' exonuclease activity of *E. coli* PolI, it has been suggested the another "exo mode", which needs large conformational change of the 5'-3' exonuclease domain without releasing the bound DNA substrate (Xie *et al*., 2011) ttPolX may be able to use this strategy; however, I observed no conformational change of the PHP domain or the linker between the POLXc and the PHP domain in the three different crystal structures of ttPolX (Figs. 11 and 14). Taken together, the first and second possibilities are thought to be realistic for processing the 3'-end of the primer in the case of ttPolX because of the great distance between the 3' end of the primer and the active site of the PHP domain (Figs. 32, 46, and 47).

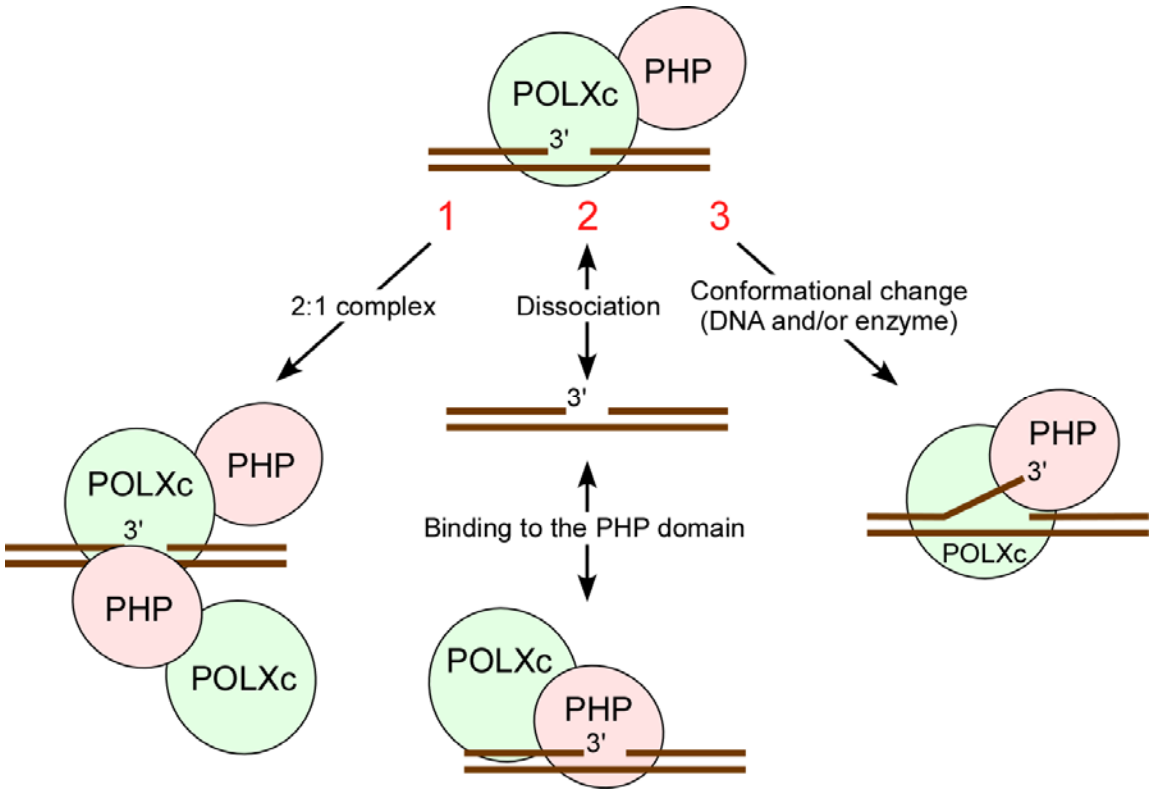

Figure 47. Three possibilities of 3'-end processing in 1-nt gapped DNA by the PHP domain of ttPolX. ttPolX forms 2:1 complex (1) (Fig. 32). ttPolX dissociates from the DNA and binds with the PHP domain, or ttPolX binds to the DNA with the PHP domain firstly (2). ttPolX and/or DNA undergo a conformational change without dissociation (3).

The functions of ttPolX in BER

This study clearly indicates that ttPolX is involved in several pathways in BER (Fig. 48). The pathways in BER are branched at several points. Damaged bases are recognized by various DNA glycosylases and determined which pathway will proceed. UDGA and UDGB, which are monofunctional DNA glycosylases, remove uracil from DNA and generate AP sites. AP sites are also generated spontaneously *in vivo*. These AP sites are generally incised by AP endonucleases, such as EndoIV. ttPolX also exhibits an AP endonuclease activity (Fig. 35). However, the loss of AP endonuclease activity in ttEndoIV-deficient cell lysates (Fig. 43) indicates that ttEndoIV is a major AP endonuclease in *T. thermophilus* HB8 cells. Not only does ttPolX have a lower AP endonuclease activity, but this activity is also easily inhibited by salt concentration and inorganic monophosphates (Fig. 43B). In *E. coli*, exonuclease III (ExoIII, also called as XthA), the AP endonuclease besides EndoIV, accounts for 90% of the total AP endonuclease activity in normal cell extracts (Ljungquist *et al*., 1976). EndoIV in *E. coli* is thought to recognize substrates different than those recognized by ExoIII because only EndoIV recognizes α-deoxyadenosine (Ide *et al*., 1994), and Δ*endoIV* is more sensitive to *tert*-butyl hydroperoxide and bleomycin than is Δ*exoIII* (Cunningh *et al*., 1986). Because *T. thermophilus* HB8 lacks the ExoIII gene, ttEndoIV is thought to be a major AP endonuclease in the cell with ttPolX playing an auxiliary role. Alternatively, the endonuclease activity of ttPolX may be put to work only in special cases or only for certain substrates by consideration of the relation between ExoIII and EndoIV in *E. coli*. It is also possible that the AP endonuclease activity of ttPolX is activated in a sequential reaction in BER because ttPolX also possesses a dRP lyase activity, which can remove the 5'-block after the AP endonuclease incises at the 5'-end of the AP site (Figs. 21 and 48).

Bifunctional DNA glycosylases, with glycosylase and lyase activities, initiate other pathways (Fig. 48). MutM removes 8-oxoG from oxidatively damaged DNA and generates a 3'-phosphate (Mikawa *et al*., 1998; Sugahara *et al*., 2000). This remaining 3'-phosphate can be removed by ttPolX and ttEndoIV (Fig. 42 and Table 13) for subsequent repair by DNA polymerases. Other bifunctional DNA glycosylases such as adenine DNA glycosylase, MutY (TTHA1898), and EndoIII (Nth, TTHA0112) leave a 3'-phospho-α,β-unsaturated aldehyde (3'-PUA) after removing damaged bases (Fig. 48). I did not investigate whether ttPolX can remove 3'-PUA. However, many enzymes with a 3'-phosphatase activity also have a 3'-phosphodiesterase activity for removing 3'-PUA or 3'-phosphoglycolate (Levin *et al*., 1988; Suh *et al*., 1997; Haas *et al*., 1999; Unk *et al*., 2001; Karumbati *et al*., 2003),

suggesting that ttPolX also can remove 3'-PUA. The 3'-5' exonuclease activity of ttPolX may support this suggestion because exonuclease is a kind of phosphodiesterase, and the direction of its activity (from the 3' end) is consistent with the mechanism of 3'-PUA removal. A combination of the DNA glycosylase, lyase, and nuclease activities typically produces the 1-nt gapped DNA (Fig. 48).

ttPolX is specialized in filling 1-nt gaps (Figs. 37 and 44; Table 2). The Theorell-Chance mechanism with nucleotide binding first may contribute to this ability (Fig. 46). The strong nucleotide binding of ttPolX with Lys-263 in the absence of DNA is thought to be involved in this mechanism (Fig. 46). By virtue of this ability, 1-nt gapped DNA is repaired by incorporating only a single nucleotide and by sealing through DNA ligase; this sub-pathway is called single-nucleotide BER (SN-BER) (Fig. 48). This efficient repair pathway is the main pathway in mammalian BER (Fortini *et al*., 1998; Podlutsky *et al*., 2001). In contrast, the other pathway is selected when dRP is oxidized or reduced because dRP lyase cannot remove oxidized and reduced dRPs, and DNA ligase cannot seal the filled gaps. In this case, strand-displacement synthesis is performed by certain DNA polymerases, and the generated 5'-flap is removed by a flap endonuclease. This pathway is called long-patch BER (LP-BER) (Fig. 48), and the patch size is generally 2-12 nucleotides (Sattler *et al*., 2003; Balakrishnan, *et al*., 2009). These two BER pathways also occur in bacterial and archaeal cells (Sung *et al*., 2003; Moen, *et al*., 2011; Kumar, *et al*., 2011). ttPolI exhibits strand-displacement (Figs. 37 and 44) and flap endonuclease (also called structure-specific 5'-nuclease) activities (Lyamichev, *et al*., 1993; Kaiser *et al*., 1999), but ttPolX does not (Figs. 37 and 44). These findings strongly suggest that ttPolX and ttPolI are involved in SN-BER and LP-BER, respectively (Fig. 48).

It is known that the BER enzymes interact with each other for efficiency and regulation of the repair (Fan *et al*., 2005; Cuneo *et al*., 2010). The interactions of ttPolX-ttUDGB and ttPolX-ttMutM (Fig. 45; Tables 15 and 16) imply coordinated reactions between DNA glycosylase, AP endonuclease, dRP lyase, and gap filling, or between DNA glycosylase, 3'-phosphatse, and gap filling. It has been reported that the N-terminal PHP domain of the α subunit of *E. coli* PolIII binds to the ε proofreading subunit during replication (Wieczorek *et al*., 2006). The PHP domain of ttPolX may also act as a scaffold with its interacting partners. In the case of mammalian SN-BER, the DNA is sequentially channeled from APE1 to Polβ, and then to DNA ligase (Prasad *et al*., 2010). The sensitivity of Δ*ttpolX* to sodium nitrite and hydrogen peroxide (Fig. 41) is consistent with this suggestion because

sodium nitrite induces the deamination of cytosine which result in uracil, and hydrogen peroxide generates oxidized, damaged base, such as 8-oxoguanine, indicating the involvement of ttPolX in different pathways initiated by ttUDGB and ttMutM (Fig. 48).

In the present study, I demonstrated the strong involvement of ttPolX in BER (Fig. 48). The PHP domain of ttPolX, which is not present in eukaryotic PolXs, was revealed to have many functions in BER. PolI has been thought to be the major DNA repair polymerase in bacteria; however, the involvement of ttPolX in all the sub-pathways in BER (Fig. 48) indicates that ttPolX is the major DNA polymerase at least in BER. In fact, the assay of cell lysates showed that Δ*ttpolI* had a stronger repair activity for 3'-phosphorylated 1-nt gapped DNA than exhibited by Δ*ttpolX* (Figs. 44C and 44D). Furthermore, ttPolX may be able to participate in other DNA repair systems, such as single- and double-strand break repairs, TCR, and NER. The lesions of single- and double-strand breaks arise from reactive oxygen species and ionizing radiations and contain non-ligatable 3'-ends like 3'-phosphate and 3'-phosphoglycolate (Caldecott *et al*., 2007; Mahaney *et al*., 2009; Ayora *et al*., 2011). The PHP domain of ttPolX can potentially remove these 3'-blocks. The interaction between ttPolX, RNA polymerase subunits, and NER proteins (Fig. 45, Tables 15 and 16) implies the involvement of ttPolX in TCR and NER. This is just the beginning of the research on bacterial PolXs. I expect that additional functions of bacterial PolXs will be revealed in the future.

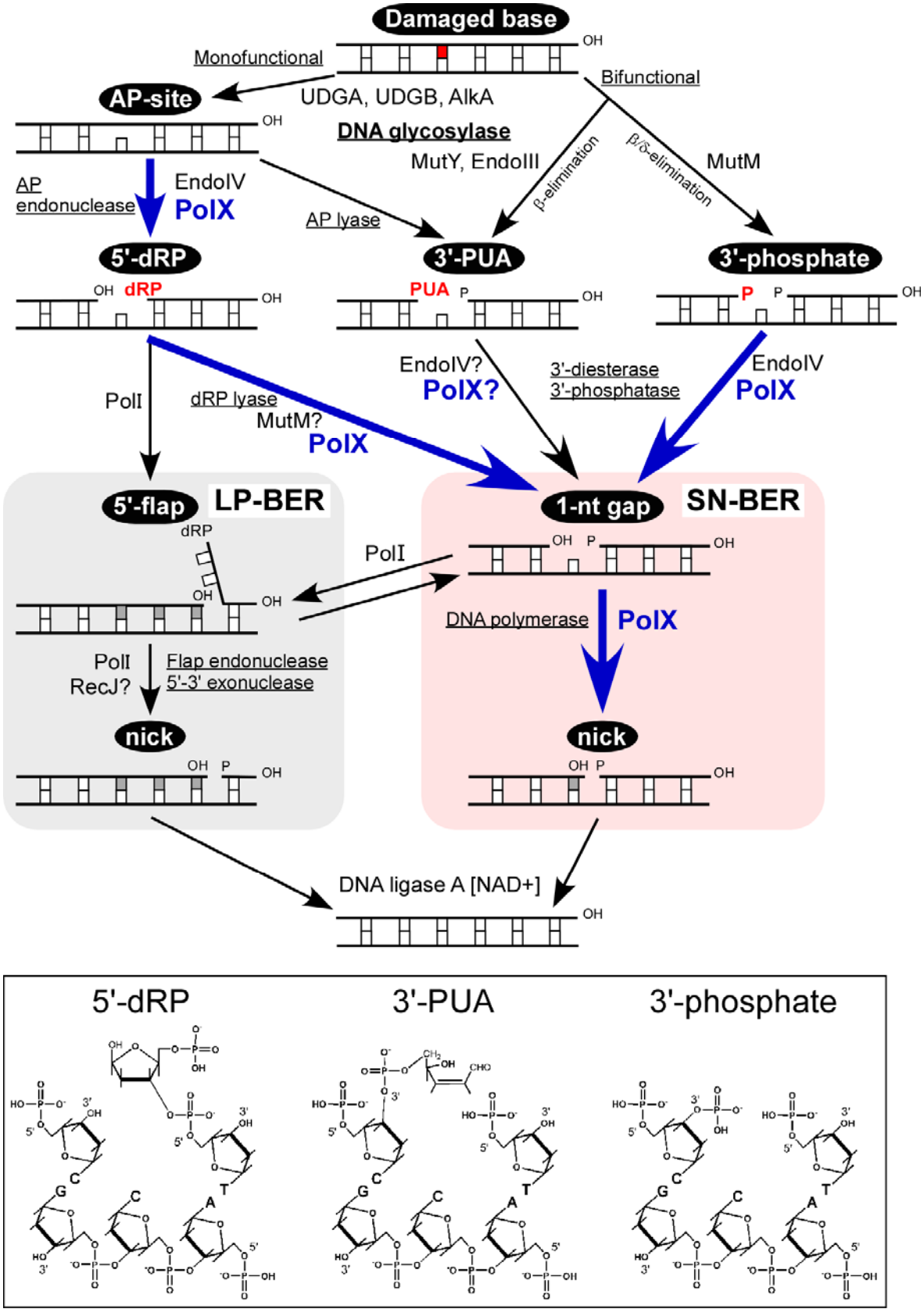

Figure 48. A model of multiple BER pathways in *T. thermophilus* HB8 (modified from Hedge *et al.*, 2008). Arrows in blue indicate the steps in which ttPolX is involved, as revealed in this study. AP, dRP, PUA, LP and SN stand for apurinic/apyrimidinic, deoxyribose phosphate, 3'-phospho-α,β-unsaturated aldehyde, long patch and single nucleotide, respectively. Structural formulae of 5'-dRP, 3'-PUA, and 3'-phosphate are depicted at the bottom.

REFERENCES

Adams, P.D., *et al*. (2010) PHENIX: a comprehensive Python-based system for macromolecular structure solution. *Acta Crystallogr. D Biol. Crystallogr.* **66**, 213-221.

Alonso, A., Terrados, G., Picher, A.J., Giraldo, R., Blanco, L. and Larraga, V. (2006) An intrinsic 5'-deoxyribose-5-phosphate lyase activity in DNA polymerase beta from *Leishmania infantum* supports a role in DNA repair. *DNA Repair (Amst)*, **5**, 89-101.

Aravind, L. and Koonin, E.V. (1998) Phosphoesterase domains associated with DNA polymerases of diverse origins. *Nucleic Acids Res.*, **26**, 3746-3752.

Aravind, L. and Koonin, E.V. (1999) DNA polymerase β-like nucleotidyltransferase superfamily: identification of three new families, classification and evolutionary history. *Nucleic Acids Res.*, **27**, 1609-1618.

Asad, N.R., Arad, L.M.B., de Almeida, C.E.B., Felzenszwalb, I., Cabral-Neto, J.B. and Leitao, A.C. (2004) Several pathways of hydrogen peroxide action that damage the *E. coli* genome., *Genet. Mol. Biol*., **27**, 291-303.

Auer, T., Landre, A.P. and Myers, W.T. (1995) Properties of the 5'-3' exonuclease/ribonuclease H activity of *Thermus thermophilus* DNA polymerase. *Biochemistry*, **34**, 4994-5002.

Ayora, S., Carrasco, B., Cardenas, P.P., Cesar, C.E., Canas, C., Yadav, T., Marchisone, C. and Alonso, J.C. (2011) Double-strand break repair in bacteria: a view from Bacillus subtilis. *FEMS Microbiol. Rev.*, **35**, 1055-1081.

Bailey, S. (1994) The Ccp4 Suite: Programs for protein crystallography. *Acta Crystallogr. D Biol. Crystallogr.* **50**, 760-763.

Bailey, S., Wing, R.A. and Steitz, T.A. (2006) The structure of *T. aquaticus* DNA polymerase III is distinct from eukaryotic replicative DNA polymerases. *Cell*, **126**, 893-904.

Baker, N.A., Sept, D., Joseph, S., Holst, M.J. and McCammon, J.A. (2001) *Proc. Natl. Acad. Sci. USA*, **98**, 10037-10041.

Balakrishnan, L., Brandt, P.D., Lindsey-Boltz, L.A., Sancar, A. and Bambara, R.A. (2009) Long patch base excision repair proceeds via coordinated stimulation of the multienzyme DNA repair complex. *J. Biol. Chem*., **284**, 15158-15172.

Banos, B., Lazaro, J.M., Villar, L., Salas, M. and de Vega, M. (2008a) Characterization of a Bacillus subtilis 64-kDa DNA polymerase X potentially involved in DNA repair. *J. Mol. Biol.*, **384**, 1019-1028.

Banos, B., Lazaro, J.M., Villar, L., Salas, M. and de Vega, M. (2008b) Editing of misaligned 3'-termini by an intrinsic 3'-5' exonuclease activity residing in the PHP domain of a family X DNA polymerase. *Nucleic Acids Res.*, **36**, 5736-5749.

Banos, B., Villar, L., Salas, M. and de Vega, M. (2010) Intrinsic apurinic/apyrimidinic (AP) endonuclease activity enables Bacillus subtilis DNA polymerase X to recognize, incise, and further repair abasic sites. *Proc. Natl. Acad. Sci. USA*, **107**, 19219-19224.

Batra, V.K., Beard, W.A., Shock, D.D., Krahn, J.M., Pedersen, L.C. and Wilson, S.H. (2006) Magnesium-induced assembly of a complete DNA polymerase catalytic complex. *Structure*, **14**, 757-766.

Beard, W.A. and Wilson, S.H. (2006a) Structure and mechanism of DNA polymerase β. *Chem. Rev.*, **106**, 361-382.

Beard, W.A., Prasad, R. and Wilson, S.H. (2006b) Activities and mechanisms of DNA polymerase β. *Methods*

Enzymol., **408**, 91-107.

Bebenek, K., Garcia-Diaz, M., Patishall, S.R. and Kunkel, T.A. (2005) Biochemical properties of *Saccharomyces cerevisiae* DNA polymerase IV. *J. Biol. Chem.*, **280**, 20051-20058.

Beese, L.S., Friedman, J.M. and Steitz, T.A. (1993) Crystal structures of the Klenow fragment of DNA polymerase I complexed with deoxynucleoside triphosphate and pyrophosphate. *Biochemistry,* **32**, 14095-14101.

Bentchikou, E., Servant, P., Coste, G. and Sommer, S. (2007) Additive effects of SbcCD and PolX deficiencies in the in vivo repair of DNA double-strand breaks in Deinococcus radiodurans. *J. Bacteriol.*, **189**, 4784-4790.

Berg, B.J.V, Beard, W.A. and Wilson, S.H. (2001) DNA structure and aspartate 276 influence nucleotide binding to human DNA polymerase β: Implication of the identity of the rate-limiting conformational change. *J. Biol. Chem.,* **276**, 3408-3416.

Bergoglio, V., Ferrari, E., Hubscher, U., Cazaux, C. and Hoffmann, J.S. (2003) DNA polymerase β can incorporate ribonucleotides during DNA synthesis of undamaged and CPD-damaged DNA. *J. Mol. Biol.*, **331**, 1017-1023.

Berti, P.J. and McCann, J.A., (2006) Toward a detailed understanding of base excision repair enzymes: transition state and mechanistic analysis of N-glycoside hydrolysis and N-glycoside transfer. *Chem. Rev.*, **106**, 506-555.

Bertocci, B., De Smet, A., Berek, C., Weill, J.C. and Reynaud, C.A. (2003) Immunoglobulin κ light chain gene rearrangement is impaired in mice deficient for DNA polymerase Mu. *Immunity*, **19**, 203-211.

Blasius, M., Shevelev, I., Jolivet, E., Sommer, S. and Hubscher, U. (2006) DNA polymerase X from *Deinococcus radiodurans* possesses a structure-modulated 3'-->5' exonuclease activity involved in radioresistance. *Mol. Microbiol.*, **60**, 165-176.

Bochner, B.R. and Ames, B.N. (1982) Complete analysis of cellular nucleotides by two-dimensional thin-layer chromatography. *J. Biol. Chem.,* **257**, 9759-9769.

Bork, P., Hofmann, K., Bucher, P., Neuwald, A.F., Altschul, S.F. and Koonin, E.V. (1997) A superfamily of conserved domains in DNA damage-responsive cell cycle checkpoint proteins. *FASEB J.*, **11**, 68-76.

Boule, J.B., Rougeon, F. and Papanicolaou, C. (2001) Terminal deoxynucleotidyl transferase indiscriminately incorporates ribonucleotides and deoxyribonucleotides. *J. Biol. Chem.*, **276**, 31388-31393.

Bridges, B.A. (1998) The role of DNA damage in stationary phase ('adaptive') mutation. *Mut. Res./DNA repair*, **408**, 1-9.

Brown, J.A., Duym, W.W., Fowler, J.D. and Suo, Z. (2007) Single-turnover kinetic analysis of the mutagenic potential of 8-oxo-7,8-dihydro-2'-deoxyguanosine during gap-filling synthesis catalyzed by human DNA polymerases λ and β. *J. Mol. Biol.*, **367**, 1258-1269.

Brunger, A.T., *et al*. (1998) Crystallography & NMR system: A new software suite for macromolecular structure determination. *Acta Crystallogr. D Biol. Crystallogr.* **54**, 905-921.

Brunger, A.T. (2007) Version 1.2 of the Crystallography and NMR system. *Nat. Protoc.* **2**, 2728-2733.

Bryant, F.R., Johnson, K.A. and Benkovic, S.J. (1983) Elementary steps in the DNA polymerase I reaction pathway. *Biochemistry,* **22**, 3537-3546.

Buckstein, M.H., He, J. and Rubin, H. (2008) Characterization of nucleotide pools as a function of physiological

state in *Escherichia coli*. *J. Bacteriol.*, **190**, 718-726.

Caldecott, K.W. (2007) Mammalian single-strand break repair: Mechanisms and links with chromatin. *DNA Repair*, **6**, 443-453.

Capp, J.P., Boudsocq, F., Bertrand, P., Laroche-Clary, A., Pourquier, P., Lopez, B.S., Cazaux, C., Hoffmann, J.S. and Canitrot, Y. (2006) The DNA polymerase λ is required for the repair of non-compatible DNA double strand breaks by NHEJ in mammalian cells. *Nucleic Acids Res.*, **34**, 2998-3007.

Capp, J.P., Boudsocq, F., Besnard, A.G., Lopez,B.S., Cazaux, C., Hoffmann, J.S. and Canitrot,Y. (2007) Involvement of DNA polymerase μ in the repair of a specific subset of DNA double-strand breaks in mammalian cells. *Nucleic Acids Res.*, **35**, 3551-3560.

Carson, D.R. and Christman, M.F. (2001) Evidence that replication fork components catalyze establishment of cohesion between sister chromatids. *Proc. Natl. Acad. Sci. USA*, **98**, 8270-8275.

Chenna, R., *et al*. (2003) Multiple sequence alignment with the Clustal series of programs. *Nucleic Acids Res.,* **31**, 3497-3500.

Cleland, W.W. (1963a) The kinetics of enzyme-catalyzed reactions with two or more substrates or products. I. Nomenclature and rate equations. *Biochim Biophys Acta,* **67**, 104-137.

Cleland, W.W. (1963b) The kinetics of enzyme-catalyzed reactions with two or more substrates or products. III. Prediction of initial velocity and inhibition patterns by inspection. *Biochim Biophys Acta,* **67**, 188-196.

Cohen, A.J., Williamson, D.L. and Brink, P.R. (1989) A motility mutant of Spiroplasma melliferum induced with nitrous acid. *Current Mocrobiol.*, **18**, 219-222.

Covo, S., Blanco, L. and Livneh, Z. (2004) Lesion bypass by human DNA polymerase μ reveals a template-dependent, sequence-independent nucleotidyl transferase activity. *J. Biol. Chem.*, **279**, 859-865.

Cuneo, M.J. and London, R.E. (2010) Oxidation state of the XRCC1 N-terminal domain regulates DNA polymerase beta binding affinity. *Proc. Natl Acad. Sci. USA*, **107**, 6805-6810.

Cunningham, R.P., Saporito, S.M., Spitzer, S.G. and Weiss, B (1986) Endonuclease IV (*nfo*) mutant of *Escherichia coli*. *J. Bacteriol.*, **168**, 1120-1127.

Daly, M.J., Gaidamakova, E.K., Matrosova, V.Y., Vasilenko, A., Zhai, M., Venkateswaran, A., Hess, M., Omelchenko, M.V., Kostandarithes, H.M., Makarova, K.S., Wackett, L.P., Fredrickson, J.K. and Ghosal, D. (2004) Accumulation of Mn(II) in *Deinococcus radiodurans* facilitates gamma-radiation resistance. *Science*, **306**, 1025-1028.

Danyluk, S.S. and Hruska, F.E. (1968) Effect of ph upon nuclear magnetic resonance spectra of nucleosides and nucleotides. *Biochemistry,* **7**, 1038-1043.

Datta, K., Johnson, N.P., LiCata, V.J. and von Hippel P.H. (2009) Local conformations and competitive binding affinities of single- and double-stranded primer-template DNA at the polymerization and editing active sites of DNA polymerases. *J. Biol. Chem.*, **284**, 17180-17193.

Delarue, M., Boule, J.B., Lescar, J., Expert-Bezancon, N., Jourdan, N., Sukumar, N., Rougeon, F. and Papanicolaou, C. (2002) Crystal structures of a template-independent DNA polymerase: murine terminal deoxynucleotidyltransferase. *EMBO J.,* **21**, 427-439.

Deibel, M.R. and Coleman, M.S. (1980) Biochemical-properties of purified human terminal deoxynucleotidyltransferase. *J. Biol. Chem.*, **255**, 4206-4212.

Deterding, L.J., Prasad, R., Mullen, G.P., Wilson, S.H. and Tomer, K.B. (2000) Mapping of the

5'-2-deoxyribose-5-phosphate lyase active site in DNA polymerase β by mass spectrometry. *J. Biol. Chem.* **275**, 10463-10471.

Dominguez, O., Ruiz, J.F., Lain de Lera, T., Garcia-Diaz, M., Gonzalez, M.A., Kirchhoff, T., Martinez-A.C., Bernad, A. and Blanco, L. (2000) DNA polymerase mu (Pol μ), homologous to TdT, could act as a DNA mutator in eukaryotic cells. *EMBO J.*, **19**, 1731-1742.

Eisenberg, D., Schwarz, E., Komaromy, M. and Wall, R. (1984) Analysis of membrane and surface protein sequences with the hydrophobic moment plot. *J. Mol. Biol.,* **179**, 125-142.

Emsley, P. and Cowtan, K. (2004) Coot: model-building tools for molecular graphics. *Acta Crystallogr. D Biol. Crystallogr.* **60**, 2126-2132.

Fan, J.S. and Wilson D.M. (2005) Protein-protein interactions and posttranslational modifications in mammalian base excision repair. *Free Radic. Biol. Med*., **38**, 1121-1138.

Ferrin, L.J. and Mildvan, A.S. (1985) Nuclear overhauser effect studies of the conformations and binding site environments of deoxynucleoside triphosphate substrates bound to DNA polymerase I and its large fragment. *Biochemistry*, **24**, 6904-6913.

Fiala, K.A., Duym, W.W., Zhang, J. and Suo, Z. (2006) Up-regulation of the fidelity of human DNA polymerase λ by its non-enzymatic proline-rich domain. *J. Biol. Chem.*, **281**, 19038-19044.

Finkel, S.E. (2006) Long-term survival during stationary phase: evolution and the GASP phenotype. *Nat. Rev. Microbiol*., **4**, 113-120.

Fischer, B.E., Haring, U.K., Tribolet, R. and Sigel, H. (1979) Metal ion/buffer interactions. Stability of binary and ternary complexes containing 2-amino-2(hydroxymethyl)-1,3-propanediol (Tris) and adenosine 5'-triphosphate (ATP). *Eur. J. Biochem.*, **94**, 523-530.

Fortini, P., Pascucci, B., Parlanti, E., Sobol, R.W., Wilson, S.H. and Dogliotti, E. (1998) Different DNA polymerases are involved in the short- and long-patch base excision repair in mammalian cells. *Biochemistry*, **37**, 3575-3580.

Garcia-Diaz, M., Bebenek, K., Sabariegos, R., Dominguez, O., Rodriguez, J., Kirchhoff, T., Garcia-Palomero, E., Picher, A.J., Juarez, R. and Ruiz, J.F., Kunkel, T.A. and Blanco, L. (2002) DNA polymerase λ, a novel DNA repair enzyme in human cells. *J. Biol. Chem.*, **277**, 13184-13191.

Garcia-Diaz, M., Bebenek, K., Krahn, J.M., Kunkel, T.A. and Pedersen, L.C. (2005) A closed conformation for the Pol λ catalytic cycle. *Nat. Struct. Mol. Biol.*, **12**, 97-98.

Garcia-Diaz, M., *et al*. (2009) Template strand scrunching during DNA gap repair synthesis by human polymerase λ. *Nat. Struct. Mol. Biol.,* **16**, 967-972.

Garcin, E.D., Hosfield, D.J., Desai, S.A., Haas, B.J., Bjoras, M., Cunningham, R P. and Tainer, J.A. (2008) DNA apurinic-apyrimidinic site binding and excision by endonuclease IV. *Nat. Struct. Mol. Biol.,* **15**, 515-522

Gates, K.S. (2009) An overview of chemical processes that damage cellular DNA: Spontaneous hydrolysis, alkylation, and reactions with radicals. *Chemical Res. Toxicol.*, **22**, 1747-1760.

Golosov, A.A., Warren, J.J., Beese, L.S. and Karplus, M. (2010) The mechanism of the translocation step in DNA replication by DNA polymerase I: a computer simulation analysis. *Structure,* **18**, 83-93.

Gonzalez-Barrera, S., Sanchez, A., Ruiz, J.F., Juarez, R., Picher, A.J., Terrados, G., Andrade, P. and Blanco, L. (2005) Characterization of SpPol4, a unique X-family DNA polymerase in *Schizosaccharomyces pombe*. *Nucleic Acids Res.*, **33**, 4762-4774.

Gouet, P., Robert, X. and Courcelle, E. (2003) ESPript/ENDscript: extracting and rendering sequence and 3D information from atomic structures of proteins. *Nucleic Acids Res.,* **31**, 3320-3323.

Haas, B.J., Sandigursky, M., Tainer, J.A., Franklin, W.A. and Cunningham, R.P. (1999) Purification and characterization of Thermotoga maritima endonuclease IV, a thermostable apurinic apyrimidinic endonuclease and 3'-repair diesterase. *J. Bacteriol.*, **181**, 2834-2839.

Hegde, M.L., Hazra, T.K. and Mitra, S. (2008) Early steps in the DNA base excision/single-strand interruption repair pathway in mammalian cells. *Cell Res.*, **18**, 27-47.

Holm, L. and Park, J. (2000) DaliLite workbench for protein structure comparison. *Bioinformatics,* **16**, 566-567.

Hashimoto, Y., Yano, T., Kuramitsu, S. and Kagamiyama, H. (2001) *FEBS Lett.*, **506**, 231-234.

Hoseki, J., Yano, T., Koyama, Y., Kuramitsu, S. and Kagamiyama, H. (1999) *J. Biochem*., **126**, 951-956.

Huang, D., Zhang, Y. and Chen, X. (2003) Analysis of intracellular nucleoside triphosphate levels in normal and tumor cell lines by high-performance liquid chromatography. *J. Chromatog. B,* **784**, 101-109.

Ide, H., Tedzuka, K., Shimizu, H., Kimura, Y., Purmal, A.A., Wallace, S.S. and Kow, Y.W. (1994) α-Deoxyadenosine, a major anoxic radiolysis product of adenine in DNA, is a substrate for Escherichia coli endonuclease IV. *Biochemistry*, **33**, 7842-7847.

Iino, H., Naitow, H., Nakamura, Y., Nakagawa, N., Agari, Y., Kanagawa, M., Ebihara, A., Shinkai, A., Sugahara, M., Miyano, M., Kamiya, N., Yokoyama, S., Hirotsu, K. and Kuramitsu, S. (2008) Crystallization screening test for the whole-cell project on *Thermus thermophilus* HB8. *Acta Crystallogr. F Struct. Biol. Cryst. Commun.* **64**, 487-491.

Ikehara, M., Uesugi, S. and Yoshida, K. (1972) Studies on conformation of purine nucleosides and their 5'-phosphates. *Biochemistry,* **11**, 830-836.

Ivanov, I., Tainer, J.A. and McCammon, J.A. (2007) Unraveling the three-metal-ion catalytic mechanism of the DNA repair enzyme endonuclease IV. *Proc. Natl Acad. Sci. USA*, **104**, 1465-1470.

Kaiser, M.W., Lyamicheva, N., Ma, W., Miller, C., Neri, B., Fors, L. and Lyamichev, V.I. (1999) A comparison of eubacterial and archaeal structure-specific 5'-exonucleases. *J Biol Chem*., **274**, 21387-21394.

Kapuler, A.M. and Reich, E. (1971) Some stereochemical requirements of Escherichia coli ribonucleic acid polymerase. Interaction with conformationally restricted ribonucleoside 5'-triphosphates: 8-bromoguanosine, 8-ketoguanosine, and 6-methylcytidine triphosphates. *Biochemistry,* **10**, 4050-4061.

Karumbati, A.S., Deshpande, R.A., Jilani, A., Vance, J.R., Ramotar, D. and Wilson, T.E. (2003) The role of yeast DNA 3'-phosphatase Tpp1 and Rad1/Rad10 endonuclease in processing spontaneous and induced base lesions. *J. Biol. Chem.*, **278**, 31434-31443.

Khairnar, N.P. and Misra, H.S. (2009) DNA polymerase X from Deinococcus radiodurans implicated in bacterial tolerance to DNA damage is characterized as a short patch base excision repair polymerase. *Microbiol*., **155**, 3005-3014.

Kondo, N., Nishikubo, T., Wakamatsu, T., Ishikawa, H., Nakagawa, N., Kuramitsu, S. and Masui, R. (2008) Insights into different dependence of dNTP triphosphohydrolase on metal ion species from intracellular ion concentrations in Thermus thermophilus. *Extremophiles*, **12**, 217-223.

Kosaka, H., Hoseki, J., Nakagawa, N., Kuramitsu, S. and Masui, R. (2007) Crystal structure of family 5 uracil-DNA glycosylase bound to DNA. *J. Mol. Biol.*, **373**, 839-850.

Kukreti, P., Singh, K., Ketkar, A and Modak, M.J. (2008) Identification of a new motif required for the 3'-5'

exonuclease activity of Escherichia coli DNA polymerase I (Klenow fragment)-The RRRY motif is necessary for the binding of single-stranded DNA substrate and the template strand of the mismatched duplex. *J. Biol. Chem*., **283**, 17979-17990.

Kumar, S., Bakhtina, M. and Tsai, M.D. (2008) Altered order of substrate binding by DNA polymerase X from African swine fever virus. *Biochemistry*, **47**, 7875-7887

Kumar, P., Bharti, S.K. and Varshney, U. (2011) Uracil excision repair in Mycobacterium tuberculosis cell-free extracts. *Tuberculosis*, **91**, 212-218.

Kuramitsu, S., Hiromi, K., Hayashi, H., Morino, Y. and Kagamiyama, H. (1990) Pre-steady-state kinetics of *Escherichia coli* aspartate aminotransferase catalyzed reactions and thermodynamic aspects of its substrate specificity. *Biochemistry*, **29**, 5469-5476.

Lamers, M.H., Georgescu, R.E., Lee, S.G., O'Donnell, M. and Kuriyan, J. (2006) Crystal structure of the catalytic α subunit of E. coli replicative DNA polymerase III. *Cell*, **126**, 881-892.

Langer, G., Cohen, S.X., Lamzin, V.S. and Perrakis, A. (2008) Automated macromolecular model building for X-ray crystallography using ARP/wARP version 7. *Nat. Protoc.* **3**, 1171-1179.

Larkin, M.A., Blackshields, G., Brown, N.P., Chenna, R., McGettigan, P.A., McWilliam, H., Valentin, F., Wallace, I.M., Wilm, A., Lopez, R., Thompson, J.D., Gibson, T.J. and Higgins, D.G. (2007) Clustal W and Clustal X version 2.0. *Bioinformatics*, **23**, 2947-2948.

Laskowski, R.A., Macarthur, M.W., Moss, D.S. and Thornton, J.M. (1993) PROCHECK: a program to check the stereochemical quality of protein structures. *J. Appl. Crystallogr.* **26**, 283-291.

le Coq, D., Fillinger, S. and Aymerich, S. (1999) Histidinol phosphate phosphatase, catalyzing the penultimate step of the histidine biosynthesis pathway, is encoded by *ytvP* (*hisJ*) in *Bacillus subtilis*. *J. Bacteriol.*, **181**, 3277-3280.

Lecointe, F., Shevelev, I.V., Bailone, A., Sommer, S. and Hubscher, U. (2004) Involvement of an X family DNA polymerase in double-stranded break repair in the radioresistant organism *Deinococcus radiodurans*. *Mol. Microbiol.*, **53**, 1721-1730.

LeMaster, D.M. and Richards, F.M. (1985) ^{1}H-^{15}N heteronuclear NMR studies of Escherichia coli thioredoxin in samples isotopically labeled by residue type. *Biochemistry,* **24**, 7263-7268.

Leulliot, N., Cladiere, L., Lecointe, F., Durand, D., Hubscher, U. and van Tibeurgh, H. (2009) The family X DNA polymerase from Deinococcus radiodurans adopts a non-standard extended conformation. *J. Biol. Chem.*, **284**, 11992-11999.

Levin J.D., Johnson A.W. and Demple, B. (1988) Homogeneous Escherichia coli endonuclease IV. Characterization of an enzyme that recognizes oxidative damage in DNA. *J. Biol. Chem.*, **263**, 8066-8071.

Li, Y., Kong, Y., Korolev, S. and Waksman, G. (1998) Crystal structures of the Klenow fragment of Thermus aquaticus DNA polymerase I complexed with deoxyribonucleoside triphosphates. *Protein Science,* **7**, 1116-1123.

Li, Y., Korolwv, S. and Waksman, G. (1998) Crystal structures of open and closed forms of binary and ternary complexes of the large fragment of Thermus aquaticus DNA polymerase I: structural basis for nucleotide incorporation. *EMBO J*., **17**, 7514-7525.

Ljungquist, S., Lindahl, T. and Howard-flanders, P. (1976) Methyl methane sulfonate-sensitive mutant of Escherichia coli deficient in an endonuclease specific for apurinic sites in deoxyribonucleic acid. *J.*

Bacteriol., **126**, 646-653.

Lyamichev, V., Brow, M.A. and Dahlberg, J.E. (1993) Structure-specific endonucleolytic cleavage of nucleic acids by eubacterial DNA polymerases. *Science*, **260**, 778-783.

Ma, Y., Lu, H., Tippin, B., Goodman, M.F., Shimazaki, N., Koiwai, O., Hsieh, C.L., Schwarz, K. and Lieber, M.R. (2004) A biochemically defined system for mammalian nonhomologous DNA end joining. *Mol. Cell*, **16**, 701-713.

Mahaney, B.L., Meek, K. and Lees-Miller, S.P. (2009) Repair of ionizing radiation-induced DNA double strand breaks by non-homologous end-joining. *Biochem. J.*, **417**, 639-650.

McClure, W.R. and Jovin, T.M. (1975) Steady state kinetic parameters and non-processivity of Escherichia coli deoxyribonucleic acid polymerase I. *J. Biol. Chem.,* **250**, 4073-4080.

McRee, D.E. (1999) XtalView Xfit-A versatile program for manipulating atomic coordinates and electron density. *J. Struc. Biol.* **125**, 156-165.

Mikawa, T., Kato, M., Sugahara, M. and Kuramitsu, S. (1998) Thermostable repair enzyme for oxidative DNA damage from extremely thermophilic bacterium, *Thermus thermophilus* HB8. *Nucleic Acids Res.*, **26**, 903-910.

Miles, D.W., Robins, M.J., Robins, R.K., Winkley, M.W. and Eyring, H. (1969) Circular dichroism of nucleoside derivatives. V. Cytosine derivatives. *J. Am. Chem. Soc.,* **91**, 831-838.

Miles, D.W., et al. (1971) Circular dichroism of nucleoside derivatives. X. Influence of solvents and substituents upon Cotton effects of guanosine derivatives. *J. Am. Chem. Soc.,* **93**, 1600-1608.

Moen, M.N., Knaevelsrud, I., Haugland, G.T., Grosvik, K., Birkeland, N.K., Klungland, A. and Bjelland, S. (2011) Uracil-DNA glycosylase of Thermoplasma acidophilum directs long-patch base excision repair, which is promoted by deoxynucleoside triphosphates and ATP/ADP, into short-patch repair. *J. Bacteriol*., **193**, 4495-4508.

Moon, A.F., Garcia-Diaz, M., Bebenek, K., Davis, B.J., Zhong, X., Ramsden, D.A., Kunkel, T.A. and Pedersen, L.C. (2007) Structural insight into the substrate specificity of DNA Polymerase μ. *Nat. Struct. Mol. Biol.*, **14**, 45-53.

Moon, A.F., Garcia-Diaz, M., Batra, V.K., Beard, W.A., Bebenek, K., Kunkel, T.A., Wilson, S.H. and Pedersen, L.C. (2007) The X family portrait: structural insights into biological functions of X family polymerases. *DNA Repair (Amst)*, **6**, 1709-1725.

Morgan, M.T., Maiti, A., Fitzgerald, M.E. and Drohat, A.C. (2011) Stoichiometry and affinity for thymine DNA glycosylase binding to specific and nonspecific DNA. *Nucleic Acids Res.*, **39**, 2319-2329.

Morita, R., Nakane, S., Shimada, A., Inoue, M., Iino, H., Wakamatsu, T., Fukui, K., Nakagawa, N., Masui, R. and Kuramitsu, S. (2010) Molecular mechanisms of the whole DNA repair system: A comparison of bacterial and eukaryotic systems. *J. Nucleic Acids*, **2010**, 179594.

Muise, O. and Holler, E. (1985) Interaction of DNA polymerase I of Escherichia coli with nucleotides antagonistic effects of single-stranded polynucleotide homopolymers. *Biochemistry,* **24**, 3618-3622.

Nakane, S., Nakagawa, N., Kuramitsu, S., Masui, R. (2009) Characterization of DNA polymerase X from Thermus thermophilus HB8 reveals the POLXc and PHP domains are both required for 3'-5' exonuclease activity. *Nucleic Acids Res.,* **37**, 2037-2052.

Nick McElhinny, S.A. and Ramsden, D.A. (2003) Polymerase Mu is a DNA-directed DNA/RNA polymerase.

Mol. Cell. Biol., **23**, 2309-2315.

Nystrom, T. (2003) Conditional senescence in bacteria: death of the immortals. *Mol. Microbiol.*, **48**, 17-23.

Ohtani, N., Tomita, M. and Itaya, M. (2008) Junction ribonuclease: a ribonuclease HII orthologue from *Thermus thermophilus* HB8 prefers the RNA-DNA junction to the RNA/DNA heteroduplex. *Biochem. J.*, **412**, 517-526.

Okazaki, N., *et al.* (2008) Mail-in data collection at SPring-8 protein crystallography beamlines. *J. Synchrotron Rad.* **15**, 288-291.

Oliveros, M., Yanez, R.J., Salas, M.L., Salas, J., Vinuela, E. and Blance, L. (1997) Characterization of an African swine fever virus 20-kDa DNA polymerase involved in DNA repair. *J. Biol. Chem.*, **272**, 30899-30910.

Omi, R., Goto, M., Miyahara, I., Manzoku, M., Ebihara, A. and Hirotsu, K. (2007) Crystal structure of monofunctional histidinol phosphate phosphatase from *Thermus thermophilus* HB8. *Biochemistry*, **46**, 12618-12627.

Ooga, T., Ohashi, Y., Kuramitsu, S., Koyama, Y., Tomita, M., Soga, T. and Masui, R. (2009) Degradation of ppGpp by nudix pyrophosphatase modulates the transition of growth phase in the bacterium Thermus thermophilus. *J. Biol. Chem.*, **284**, 15549-15556.

Oshima, T., Imahori, K. (1974) Description of *Thermus thermophilus* (Yoshida and Oshima) comb. nov., a nonsporulating thermophilic bacterium from a Japanese thermal spa. *Inter. J. System. Bacteriol.* **24**: 102-112

Otwinowski, Z. and Minor, W. (1997) Processing of X-ray diffraction data collected in oscillation mode. *Methods Enzymol., Pt A* **276**, 307-326.

Pitcher, R.S., Brissett, N.C. and Doherty, A.J. (2007) Nonhomologous end-joining in bacteria: a microbial perspective. *Annu. Rev. Microbiol.*, **61**, 259-282.

Podlutsky, A.J., Dianova, I.I., Wilson, S.H., Bohr, V.A. and Dianov, G.L. (2001) DNA synthesis and dRPase activities of polymerase β are both essential for single-nucleotide patch base excision repair in mammalian cell extracts. *Biochemistry*, **40**, 809-813.

Prabhudas, R.P. and Maxwell, L.E. (1978) Specific effect of zinc ions on DNA polymerase activity of avian myeloblastosis virus. *Mol. Cell. Biochem.*, **21**, 67-69.

Prasad, R., Shock, D.D., Beard, W.A. and Wilson, S.H. (2010) Substrate channeling in mammalian base excision repair pathways: passing the baton. *J. Biol. Chem.*, **285**, 40479-40488.

Ramadan, K., Maga, G., Shevelev, I.V., Villani, G., Blanco, L. and Hubscher, U. (2003) Human DNA polymerase λ possesses terminal deoxyribonucleotidyl transferase activity and can elongate RNA primers: implications for novel functions. *J. Mol. Biol.*, **328**, 63-72.

Ramadan, K., Shevelev, I. and Hubscher, U. (2004) The DNA-polymerase-X family: controllers of DNA quality? *Nat. Rev. Mol. Cell Biol.*, **5**, 1038-1043.

Rothwell, P.J. and Waksman, G. (2005) Structure and mechanism of DNA polymerases. *Adv. Protein Chem.*, **71**, 401-440.

Salas-Pacheco, J.M., Urtiz-Estrada, N., Martinez-Cadena, G., Yasbin R.E. and Pedraza-Reyes, M. (2003) YqfS from Bacillus subtilis is a spore protein and a new functional member of the type IV apurinic/apyrimidinic-endonuclease family. *J. Bacteriol.*, **185**, 5380-5390.

Saran, A., Perahia, D. and Pullman, B. (1973) Molecular orbital calculations on conformation of nucleic-acids

and their constituents. VII. Conformation of sugar ring in β-nucleosides pseudorotational representation. *Theor. Chim. Acta,* **30**, 31-44.

Sattler, U., Frit, P., Salles, B. and Calsou, P. (2003) Long-patch DNA repair synthesis during base excision repair in mammalian cells. *EMBO Rep.*, **4**, 363-367.

Sawaya, M.R., Pelletier, H., Kumar, A., Wilson, S.H. and Kraut, J. (1994) Crystal structure of rat DNA polymerase β: evidence for a common polymerase mechanism. *Science,* **264**, 1930-1935.

Schuster, H. (1960) The reaction of nitrous acid with deoxyribonucleic acid. *Biochem. Biophys. Res. Commun.*, 2, 320-323.

Schweize, M.P., Broom, A.D., Tso, P.O.P. and Hollis, D.P. (1968) Studies of inter- and intramolecular interaction in mononucleotides by proton magnetic resonance. *J. Am. Chem. Soc.,* **90**, 1042-1055.

Soga, T., et al. (2002) Pressure-assisted capillary electrophoresis electrospray ionization mass spectrometry for analysis of multivalent anions. *Anal. Chem.,* **74**, 6224-6229.

Son, T.D., Gueron, M. and Guschlba, W. (1972) Flexibility and conformations of guanosine monophosphates by overhauser effect. *J. Am. Chem. Soc.,* **94**, 7903-7911.

Stolarski, R., Hagberg, C.E. and Shugar, D. (1984) Studies on the dynamic *syn-anti* equilibrium in purine nucleosides and nucleotides with the aid of H-1 and C-13 NMR spectroscopy. *Eur. J. Biochem.,* **138**, 187-192.

Sucato, C.A., *et al*. (2007) Modifying the β, γ leaving-group bridging oxygen alters nucleotide incorporation efficiency, fidelity, and the catalytic mechanism of DNA polymerase β. *Biochemistry,* **46**, 461-471.

Sugahara, M. *et al*. (2000) Crystallization and preliminary X-ray crystallographic studies of *Thermus thermophilus* HB8 MutM protein involved in repairs of oxidative DNA damage. *J. Biochem.* **127**, 9-11.

Sung J.S. and Mosbaugh, D.W. (2003) Escherichia coli uracil- and ethenocytosine-initiated base excision DNA repair: Rate-limiting step and patch size distribution. *Biochemistry*, **42**, 4613-4625.

Srivastava, D.K., Berg, B.J., Prasad, R., Molina, J.T., Beard, W.A., Tomkinson, A.E. and Wilson, S.H. (1998) Mammalian abasic site base excision repair. Identification of the reaction sequence and rate-determining steps. *J. Biol. Chem.*, **273**, 21203-21209.

Stano, N.M., Chen, J. and McHenry, C.S. (2006) A coproofreading Zn^{2+}-dependent exonuclease within a bacterial replicase. *Nat. Struct. Mol. Biol.*, **13**, 458-459.

Struhl, K. (2001) Reagents and radioisotopes used to manipulate nucleic acids. *Curr. Protoc. Mol. Biol.* Chapter 3: Unit3.4.

Suh, D., Wilson III, D.M. and Povirk, L.F. (1997) 3'-Phosphodiesterase activity of human apurinic/apyrimidinic endonuclease at DNA double-strand break ends. *Nucleic Acids Res.*, **25**, 2495-2500.

Tanabe, K., Bohn, E.W., Wilson, S.H. (1979) Steady state kinetics of mouse DNA polymerase β. *Biochemistry,* **18**, 3401-3406.

Tanabe, K., Taguchi, Y.N., Matsukage A and Takahashi T (1980) Steady-state kinetics of mouse DNA polymerase α. *J. Biochem.,* **88**, 35-38.

Tang, K.H., Niebuhr, M., Aulabaugh, A. and Tsai, M.D. (2008a) Solution structures of 2 : 1 and 1 : 1 DNA polymerase-DNA complexes probed by ultracentrifugation and small-angle X-ray scattering. *Nucleic Acids Res.*, **36**, 849-860.

Tang, K.H. and Tsai, M.D. (2008b) Structure and function of 2:1 DNA polymerase-DNA complexes. *J. Cell.*

Physiol., **216**, 315-320.

Traut, T.W. (1994) Physiological concentrations of purines and pyrimidines. *Mol. Cell Biochem.,* **140**, 1-22.

Teplyakov, A., Obmolova, G., Khil, P.P., Howard, A.J., Camerini-Otero, R.D. and Gilliland, G.L. (2003) Crystal structure of the *Escherichia coli* YcdX protein reveals a trinuclear zinc active site. *Proteins*, **51**, 315-318.

Terwilliger, T.C. and Berendzen, J. (1999) Automated MAD and MIR structure solution. *Acta Crystallogr. D Biol. Crystallogr.* **55**, 849-861.

Terwilliger, T.C. (2000) Maximum-likelihood density modification. *Acta Crystallogr. D Biol. Crystallogr.* **56**, 965-972.

Terwilliger, T.C. (2003) Automated main-chain model building by template matching and iterative fragment extension. *Acta Crystallogr. D Biol. Crystallogr.* **59**, 38-44.

Tso, P.O.P., Kondo, N.S., Schweize, Mp. and Hollis, D.P. (1969) Studies of conformation and interaction in dinucleoside mono- and diphosphates by proton magnetic resonance. *Biochemistry,* **8**, 997-1029.

Ueno, G., Hirose, R., Ida, K., Kumasaka, T. and Yamamoto, M. (2004) Sample management system for a vast amount of frozen crystals at SPring-8. *J. Appl. Crystallogr.* **37**, 867-873.

Ueno, G., Kanda, H., Kumasaka, T. and Yamamoto, M. (2005) Beamline Scheduling Software: administration software for automatic operation of the RIKEN structural genomics beamlines at SPring-8. *J. Synchrotron Rad.* **12**, 380-384.

Ueno, G., *et al.* (2006) RIKEN structural genomics beamlines at the SPring-8; high throughput protein crystallography with automated beamline operation. *J. Struct. Funct. Genomics* **7**, 15-22.

Unk, I., Haracska, L., Prakash, S. and Prakash, L. (2001) 3'-Phosphodiesterase and 3'-5' exonuclease activities of yeast Apn2 protein and requirement of these activities for repair of oxidative DNA damage. *Mol. Cell. Biol*., **21**, 1656-1661.

Vagin, A.A., *et al*. (2004) REFMAC5 dictionary: organization of prior chemical knowledge and guidelines for its use. *Acta Crystallogr. D Biol. Crystallogr.* **60**, 2184-2195.

Wang, T.S.F., Korn, D. (1982) Specificity of the catalytic interaction of human DNA polymerase β with nucleic acid substrates. *Biochemistry,* **21**, 1597-1608.

Ward, J.F. (1998) DNA damage produced by ionizing radiation in mammalian cells: identities, mechanisms of formation and reparability. *Prog. Nucleic Acid Res. Mol. Biol.*, **35**, 95-125.

Wieczorek, A. and McHenry, C.S. (2006) The NH2-terminal php domain of the α subunit of the *Escherichia coli* replicase binds the epsilon proofreading subunit. *J. Biol. Chem.*, **281**, 12561-12567.

Xie, P. and Sayers, J.R. (2011) A model for transition of 5'-nuclease domain of DNA polymerase I from insert to active modes. *PLoS One*, **6**, e16213.

Yamagata, A., Masui, R., Kakuta, Y., Kuramitsu, S., and Fukuyama, K. (2001) Overexpression, purification and characterization of RecJ protein from *Thermus thermophilus* HB8 and its core domain. *Nucleic Acids Res.* **29**, 4617-4624.

Yokoyama, S., Hirota, H., Kigawa, T., Yabuki, T., Shirouzu, M., Terada, T., Ito, Y., Matsuo, Y., Kuroda, Y., Nishimura, Y., Kyogoku, Y., Miki, K., Masui, R. and Kuramitsu, S. (2000) Structural genomics projects in Japan. *Nat. Struct. Biol*., **7**, 943-945.

Zahradka, K., Slade, D., Bailone, A., Sommer, S., Averbeck, D., Petranovic, M., Lindner, A.B. and Radman,M.

(2006) Reassembly of shattered chromosomes in *Deinococcus radiodurans*. *Nature*, **443**, 569-573.

Zhang, Y., Wu, X., Yuan, F., Xie, Z. and Wang, Z. (2001) Highly frequent frameshift DNA synthesis by human DNA polymerase μ. *Mol. Cell. Biol.*, **21**, 7995-8006.

ACKNOWLEDGMENTS

I would like to express my great appreciation to Professor Seiki Kuramitsu, Associate professor Ryoji Masui and Assistant professor Noriko Nakagawa for their guidance and many valuable discussions. I also thank Dr. KIM Kwang for the MS analysis, Yumiko Inoue for the technical assistance in the peptide sequencing and Hirofumi Omori for the technical assistance in the DNA sequencing. I thank my colleagues in Kuramitsu laboratory, my friends for their kind help and encouragement.